



UNIVERSIDAD
DE MÁLAGA

ESCUELA DE INGENIERÍAS INDUSTRIALES

Departamento Ingeniería Mecánica, Térmica y de Fluidos

Área de Mecánica de Fluidos

TRABAJO FIN DE MASTER

**ESTUDIO EXPERIMENTAL DE LA EXTINCIÓN DE UNA
LLAMA DE DIFUSIÓN SOPLANDO UN ÚNICO CHORRO DE
AIRE EN CONFIGURACIÓN CRUZADA**

**EXPERIMENTAL STUDY OF THE EXTINCTION OF A
DIFFUSION FLAME BY BLOWING A SINGLE AIR JET IN
CROSS CONFIGURATION**

Máster en Ingeniería Industrial

Author: Stefano Murrieri

Tutor: Paloma Gutiérrez Castillo

Co-tutor: Stefano D'Ambrosio



DECLARACIÓN DE ORIGINALIDAD DEL PROYECTO/TRABAJO FIN DE MÁSTER

D./ Dña.: STEFANO MURRIERI

DNI/Pasaporte:CA60929CC. Correo electrónico: s280286@studenti.polito.it

Titulación: Máster en Ingeniería Industrial.

Título del Proyecto/Trabajo: ESTUDIO EXPERIMENTAL DE LA EXTINCIÓN DE UNA LLAMA DE DIFUSIÓN SOPLANDO UN ÚNICO CHORRO DE AIRE EN CONFIGURACIÓN CRUZADA.

DECLARA BAJO SU RESPONSABILIDAD

Ser autor/a del texto entregado y que no ha sido presentado con anterioridad, ni total ni parcialmente, para superar materias previamente cursadas en esta u otras titulaciones de la Universidad de Málaga o cualquier otra institución de educación superior u otro tipo de fin.

Así mismo, declara no haber trasgredido ninguna norma universitaria con respecto al plagio ni a las leyes establecidas que protegen la propiedad intelectual, así como que las fuentes utilizadas han sido citadas adecuadamente.

En Málaga, a 16 de Febrero de 2022

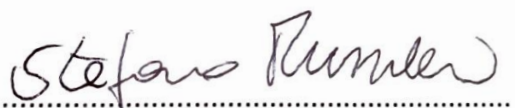
Fdo.: 

TABLE OF CONTENTS

RESUMEN.....	9
ABSTRACT.....	10
Chapter 1. INTRODUCTION	11
1.1. BACKGROUND.....	11
1.2. BRIEF REVIEW OF COMBUSTION: CLASSIFICATION OF PROCESSES.....	12
1.3. TYPE OF FUELS: PROPANE AND METHANE	15
1.3.1. PROPANE	15
1.3.2. METHANE.....	16
1.4. DIFFUSIVE FLAME IN A QUIET ENVIRONMENT.....	17
1.5. THE THEORETICAL BASIS FOR STUDYING A DIFFUSIVE FLAME	19
1.6. BRIEF DESCRIPTION OF DIFFUSIVE FLAME WITH CROSSWIND	22
1.6.1. FLAME PATTERNS TYPOLOGY	22
1.6.2. MECHANISM OF BLOWOUT	26
1.6.3. FLUID DYNAMICS IN STRAPPING OF A DIFFUSIVE FLAME WITH A CROSSWIND	27
Chapter 2. EXPERIMENTAL SETUP AND CALIBRATION	29
2.1. EXPERIMENTAL SETUP AND DESCRIPTION OF COMPONENTS	29
2.2 DETAILS OF THE USE OF FLOW METERS	36
2.3. TEST PROCEDURE.....	43
2.4. CALIBRATION OF DIGITAL FLOWMETERS	44
2.4.1. Balloon Inflation	45
Chapter 3. EXPERIMENTAL RESULT AND DISCUSSION.....	62
3.1. AIR JET ANALYSIS.....	62
3.1.1. Analysis of Air jet behavior near the fuel nozzle of diameter 10 mm and $z=0$	65
3.1.2. Influence of the nozzle diameter.....	68

3.1.3.	Influence of the nozzle distance.....	71
3.2.	ANALYSIS OF DATA OBTAINED FROM FLAME EXTINGUISHING POINTS	74
3.2.1.	Brief review of the physical model of Blow-out limit based on Damköhler number, Da	78
3.2.1.1.	Analysis of the influence of the z parameter for cases with methane flame.....	81
3.2.1.2.	Description of methane flame extinguishing points with nozzle diameters of 15 mm and 20 mm.....	83
3.2.1.3.	Comparison of blow-out limits as the diameter varies at constant z ($z=0, z=1, z=2$)	84
3.2.1.4.	Flame behavior when the nozzle outlet cross-section varies	85
3.2.2.	Analysis of the influence of the z parameter for cases with a propane flame.....	87
3.2.2.1.	Description of methane flame extinguishing points with fuel nozzle diameters of 15 mm and 20 mm	88
3.2.2.2.	Comparison of blow-out limits with varying diameter at constant z ($z=0, z=1, z=2$)	88
3.2.3.	COMPARISON OF THE TWO FUELS: METHANE VS PROPANE.....	89
Chapter 4.	SCALING OF GRAPHS WITH FLAME EXTINCTION LIMITS AND COMPARISON WITH BLOWOUT CAUSED BY A UNIFORM CROSSWIND	94
4.1.	SCALING OF BLOWOUT LIMITS	94
4.1.1.	Diagramma Re_{air}/R_{fuel} diameter fuel nozzle 10 mm	96
4.1.2.	Diagramma R/J	97
4.2.	COMPARISON OF FLAME EXTINCTION WITH LOCAL AND CROSS JETS.....	100
Chapter 5.	CONCLUSIONS AND FUTURE WORK	104
5.1.	CONCLUSIONS	104
5.2.	FUTURE WORK	105
APPENDIX 1.	Display of the error of each blowout point of methane.....	106
APPENDIX 2.	Display of the error of each blowout point of propane	107
REFERENCES	108

LIST OF FIGURES

Chapter 1

1.1 Structure formula of propane.....	15
1.2 Structure formula of methane.....	16
1.3 Schematic of the reacting flows and patterns [2].....	17
1.4 Height of the flame against fuel speed and transitions observed [2].....	18
1.5 Sketch of the lift-off process [2].....	19
1.6 Balances across a differential element within a diffusion flame (one-dimensional problem) [1]..	19
1.7 Diffusive no lifted propane flame images.....	22
1.8 Cross-flow configuration [3].....	22
1.9 Type of flames under cross-flow conditions: lifted (a) and non-lifted (b) [3].....	23
1.10 No-Lifted flame (a), Lifted flame (b).....	24
1.11 The six different flame .modes, Hatch marks.....	24
1.12 Typical sketches of flames before blowout: (a) liftable flame, (b) never-lift flame [13].....	26
1.13 Zones of a wake-stabilized jet diffusion flame in crossflow [18].....	27
1.14 Potential paths for fuel leakage or stripping [18].....	28

Chapter 2

2.1 Diagram of the experiment.....	29
2.2 Air tank.....	30
2.3 Burner [22].....	32
2.4. Fuel Nozzle.....	34
2.5 MASS-FLOW Select EL F-201CV-5K0-RAD-22-V [20].....	35
2.6 Sensor operation diagram [20].....	36
2.7 Flowmeter dimensioning [20].....	37
2.8 Meter/PC connection [20].....	37
2.9 Communication diagram between operator and instrument [20].....	38
2.10 Configurations of propane/methane Flowmeter.....	39
2.11 Edit configuration flow.....	39
2.12 Screen FlowDDE e FlowView's windows.....	40
2.13 Flowmeters with air and propane.....	41
2.14 Flowmeters with air and methane.....	41
2.15 Oscillation is caused by a momentary malfunction of the instrument.....	42
2.16 Airflow variation.....	42
2.17 Origin of the reference system.....	44
2.18 Fluid path.....	44
2.19 Photo balloon filled with air at different times.....	48
2.20 Picture of an air balloon at t=0s.....	49
2.21 Computed volume versus time and linear approximation for the case of air and nominal flow rate 100 lN/h.....	50
2.22 Computed volume versus time and linear approximation for the case of air and nominal flow rate 200 lN/h.....	50
2.23 Computed volume versus time and linear approximation for the case of air and nominal flow rate 300 lN/h.....	50
2.24 Computed volume versus time and linear approximation for the case of propane and nominal flow rate 1000 mlN/min.....	51
2.25 Computed volume versus time and linear approximation for the case of propane and nominal flow rate 1500 mlN/min.....	52

2.26 Computed volume versus time and linear approximation for the case of propane and nominal flow rate 2000 mlN/min.....	52
2.27 Computed volume versus time and linear approximation for the case of methane and nominal flow rate 1000 mlN/min.....	53
2.28 Computed volume versus time and linear approximation for the case of methane and nominal flow rate 2000 mlN/min.....	53
2.29 Computed volume versus time and linear approximation for the case of methane and nominal flow rate 3000 mlN/min.....	54
2.30 Balloon image processing.....	55
2.31 Computed volume versus time and linear approximation for the case of air and nominal flow rate 100 lN/h.....	56
2.32 Computed volume versus time and linear approximation for the case of air and nominal flow rate 200 lN/h.....	57
2.33 Computed volume versus time and linear approximation for the case of air and nominal flow rate 300 lN/h.....	57
2.34 Computed volume versus time and linear approximation for the case of propane and nominal flow rate 1000 mlN/min.....	58
2.35 Computed volume versus time and linear approximation for the case of propane and nominal flow rate 1500 mlN/min.....	58
2.36 Computed volume versus time and linear approximation for the case of propane and nominal flow rate 2000 mlN/min.....	59
2.37 Computed volume versus time and linear approximation for the case of methane and nominal flow rate 1000 mlN/min.....	59
2.38 Computed volume versus time and linear approximation for the case of methane and nominal flow rate 2000 mlN/min.....	60
2.39 Computed volume versus time and linear approximation for the case of methane and nominal flow rate 3000 mlN/min.....	60

Chapter 3

3.1 Phantom V611.....	62
3.2 Detail of the flame 'pierced' by the laminar air-jet.....	63
3.3 Detail of flame affected by turbulent air jet.....	64
3.4 Airflow whit oil at different flowrates.....	64
3.5 Motion field airflow d=10, z=0 mm.....	65
3.6 Detail of the flame and non-flame regions of the blowout limits of a methane flame with d=10 mm and z=0.....	66
3.7 Blow-out limit with air regions.....	67
3.8 Blow-out limit with air regions.....	68
3.9 Motion field airflow d=15 mm z=0 mm.....	70
3.10 Motion field airflow d=20 mm z=0 mm.....	70
3.11 Motion field airflow d=10 mm z=2.5 mm.....	71
3.12 Motion field airflow d=10 mm z=5 mm.....	71
3.13 Motion field airflow d=15 mm z=2.5 mm.....	73
3.14 Motion field airflow d=15 mm z=5 mm.....	73
3.15 Motion field airflow d=20 mm z=2.5 mm.....	73
3.16 Motion field airflow d=20 mm z=5 mm.....	73
3.17 Blowout propane flame with diameter nozzle 10 mm and z=0 mm.....	75
3.18 Flow rate of methane is constant at 0.212 m/s, and airflow rate variable.....	76
3.19 Sketch cross-wind configuration [4].....	78
3.20 Methane flame blow-off limit with air nozzle outlet section diameter of 10 mm, with speed...81	81

3.21 Methane flame blow-off limit with speed and air nozzle outlet section diameter of 15 mm (a) and 20 mm (b).....	83
3.22 Blow-out limits $z=0$ and variable-diameter.....	84
3.23 Blow-out limits with variable-diameter and $z=1$ (a), $z=2$ (b).....	85
3.24 Nozzle outlet section.....	85
3.25 Methane flame image.....	86
3.26 Propane flame blow-off limit with air nozzle outlet section diameter of 10 mm, with speed....	87
3.27 Propane flame blow-off limit with air nozzle outlet section diameter of 15 mm (a) and 20 mm (b), with speed.....	88
3.28 Propane blow-out limits with $z=0$ (a), $z=1$ (b), $z=2$ (c) and variable-diameter.....	88
3.29 Comparison of propane and methane blow-out limits d outlet fuel 10mm.....	91
3.30 Comparison of propane and methane blow-out limits d outlet fuel 15mm.....	92
3.31 Comparison of propane and methane blow-out limits d outlet fuel 20 mm.....	92

Chapter 4

4.1 Blowout limits for propane and methane flames with Reynolds number.....	96
4.2 Methane flame blowout limit for different values of z and d 10 mm.....	98
4.3 Methane flame blowout limit for different values of z and d 10, 15, 20 mm.....	98
4.4 Methane and propane flame blowout limit for different values of z and d 10 mm.....	99
4.5 Blowout limits under different conditions [5].....	102

Appendix 1

A1 Position error of blowout limits methane: d 10 mm(a); d 15 mm (b), d 20 mm (c).....	106
--	-----

Appendix 2

A2 Position error of blowout limits propane: d 10 mm(a); d 15 mm (b), d 20 mm (c).....	107
--	-----

LIST OF TABLES

Chapter 2

2.1 Parameter of the air tank.....	30
2.2 Parameter of the propane tank.....	31
2.3 Parameter of the methane tank.....	31
2.4 Digital flowmeter general specification.....	35
2.5 Digital flowmeter mechanical specification.....	35
2.6 Digital flowmeter electrical specification.....	36
2.7 Flowmeter dimensioning.....	37
2.8 Information relief images.....	46
2.9 Data evaluated for flowmeter 1 with air.....	51
2.10 Data evaluated for flowmeter 2 with propane.....	52
2.11 Data evaluated for flowmeter 2 with methane.....	54
2.12 Data evaluated for flowmeter 1 with air.....	57
2.13 Data evaluated for flowmeter 2 with propane.....	59
2.14 Data evaluated for flowmeter 2 with methane.....	60

Chapter 3

3.1 Camera parameters.....	62
3.2 Slopes in different zones A, B, and C for the three diameters tested and airflow located at $z=0$ mm.....	69
3.3 Airflow velocities of Figures 3.9 and 3.10.....	71
3.4 Airflow velocities of Figures 3.11 and 3.12.....	72

3.5 Image data.....	86
3.6 Upper and lower limits for the fuel tested.....	90

Chapter 4

4.1 Data fluids at pressure 1 atm and temperature 20 °C.....	96
4.2 Fluid data.....	101
4.3 Data is presented in Figure 5.....	103

RESUMEN

Este trabajo se constituye por un estudio experimental que contempla el ensayo de llamas de difusión que han sido extinguidas con un chorro perpendicular de aire. Se ha analizado la influencia en la extinción de la llama en función de la variación de cuatro tipos de parámetros: (i) combustible propano y metano, (ii) relación de velocidades entre combustible y aire, (iii) diámetro de boquilla del quemador y, finalmente, (iv) distancia axial entre la salida del quemador y la localización del chorro de aire.

El fin de este trabajo ha sido abordar el problema experimentalmente mediante el análisis de técnicas de visualización de imágenes para determinar el tipo de chorro de aire que se ha inyectado y el tipo de extinción que se ha producido al variar los parámetros geométricos y fluidos mencionados. Si nos centramos en el chorro de aire, se ha comprobado mediante visualizaciones de flujo que ante un incremento de velocidad del chorro de aire existen patrones correspondientes a un régimen laminar (L), transitorio o no estacionario (NE) o turbulento (T) en la región cercana a la salida del soplado. En concreto, y a medida que aumenta la velocidad del chorro de aire, se ha comprobado como la región donde el flujo es turbulento se acorta y también como el cono de turbulencia que afecta a la región de la salida del quemador es mayor.

En segundo lugar, si representamos gráficamente la velocidad del combustible frente a la velocidad de soplado de aire se ha observado una tendencia lineal de separación entre las zonas donde está o no presente la llama de difusión. En otras palabras, a mayor velocidad de combustible, mayor es el caudal de aire necesario para conseguir la extinción, siendo lineal este aumento entre ambas velocidades. Se ha observado una clara influencia entre los regímenes L, NE y T porque existe un cambio evidente en la pendiente lineal. Por otro lado, y a medida que aumenta la distancia axial del chorro a la salida del quemador, se ha observado que la pendiente lineal aumenta considerablemente para el menor diámetro del quemador ensayado (10 mm). Sin embargo, y ante un aumento del diámetro del quemador (15 y 20 mm) la pendiente se mantiene prácticamente constante.

ABSTRACT

This work is constituted by an experimental study contemplating the testing of diffusion flames that have been extinguished with a perpendicular jet of air. The influence on flame extinction has been analyzed considering the variation of four types of parameters: (i) propane and methane fuel, (ii) fuel-air velocity ratio, (iii) burner nozzle diameter, and, finally, (iv) axial distance between the burner outlet and the air jet location.

This work has aimed to address the problem experimentally by analyzing image visualization techniques to determine the type of air-jet that has been injected and the type of extinction that has been produced by varying the aforementioned geometrical and fluid parameters. If we focus on the air jet, it has been verified using flow visualizations that with an increase in air-jet velocity there are patterns corresponding to a laminar (L), transient or non-stationary (NE), or turbulent (T) regime in the region close to the outlet of the jet. Specifically, as the air jet velocity increases, it has been shown that the region where the flow is turbulent becomes shorter and also that the turbulence cone affecting the region of the burner outlet is larger.

Secondly, if we plot the fuel velocity versus the air blowing velocity, a linear trend of separation between the areas where the diffusion flame is present or not has been observed. In other words, the higher the fuel velocity, the greater the airflow necessary to achieve extinction, and this increase is linear between the two velocities. A clear influence has been observed between the L, NE, and T regimes because there is a clear change in the linear slope. On the other hand, as the axial distance from the jet to the burner outlet increases, it has been observed that the linear slope increases considerably for the smallest burner diameter tested (10 mm). However, as the burner diameter increases (15 and 20 mm), the slope remains practically constant.

Chapter 1. INTRODUCTION

1.1. BACKGROUND

The phenomenon of extinguishing a diffusive flame in the presence of a transverse air current is of great interest for several reasons concerning safety, combustion stability, and exhaust gas treatment. Being able to predict when the flame will be extinguished by blowing can reduce the risk of fire or explosion and make combustion more stable. A jet flame in a cross-wind configuration has several practical applications, e.g., (i) primary combustion zones in gas turbines, (ii) re-combustion zone in boilers, or (iii) combustion of exhaust or emergency vent gas in flares used in the chemical and oil industries (flaring). In the latter case, a common practice is to burn without energy recovery excess natural gas extracted along with oil when it is too costly to build adequate infrastructure to transport it to places of consumption. The flared gas generates a flame above the oil towers. This practice is frequently used in industrial oil, chemical, and natural gas plants, as well as oil or natural gas production sites that have oil wells [1].

The analysis of this combustion phenomenon should be carried out using reacting flows, thus the basis corresponds to three different fields: fluid mechanics, thermodynamics, and chemical kinetics. The theoretical implications of diffusive flames and their extinction have been attracted the attention of many researchers [2]. Of particular interest is the practical use of crosswind in the flame, due to its great ability to mix fuel and air, thus obtaining higher reaction speeds, more stable combustion, and less pollution in the combustion gases [3]. This type of flame is characterized by a three-dimensional flow field that depends on the momentum of the airflow, the fuel flow, and the thrust due to combustion.

The literature contains numerous studies on the blowout phenomenon and the behavior of the flame under varying conditions both in a stationary environment and in the presence of a crosswind [4] [5] [6]. For the latter case, experimental tests have been carried out in a wind tunnel, where the flow of air transversal to the flame is obtained with fans. This flow is regulated using a flow meter. A honeycomb is used to make the flow completely homogeneous along the whole section of the tunnel. Studies of the diffusive flame with uniform transverse airflow have shown how the characteristic velocities change under different conditions such as tunnel pressure, shape, type of nozzle, presence or absence of a longitudinal wall after the nozzle [7-8]. Each test was carried out for different uniform transverse air-jet velocities. Some researchers have tried to formulate an empirical relationship capable of predicting the blow-out phenomenon for numerous types of fuel and at different levels of mixing with the oxidant.

In this research work, however, the flame extinction is analyzed when the flame interacts with a localized source of air through a nozzle positioned at right angles to the flame. The flame extinguishing time at which the flame is evaluated by varying the air and fuel flow rates, which are regulated by suitable digital flow meters. The test is repeated several times and the appropriate parameters are changed at each step: (a) two different fuels (methane and propane), (b) three fuel nozzles with a circular diameter of 10, 15, and 20 mm, and (c) different heights of the air nozzle. For each type of test performed, the results obtained from this experiment are compared with the results in the bibliography [4-7], which however concern the presence of a uniform crosswind. The similarities and differences in the results for each parameter analyzed between the two types of crossflow are highlighted.

1.2. BRIEF REVIEW OF COMBUSTION: CLASSIFICATION OF PROCESSES

Combustion is a chemical reaction involving the oxidation of fuel by an oxidant (usual oxygen in the air), with the development of heat and electromagnetic radiation, often including light radiation [9]. Combustion is often accompanied by a flame and high-temperature gases produced by combustion, which give rise to smoke. Combustion is an exothermic oxidation-reduction, as one compound is oxidized while another is reduced. Typically, fuel, an oxidizer, and an igniter are required for the reaction to take place. A requirement for an adequate proportion of fuel and oxidizer must also be met for the reaction to take place. There is a flammable range, generated by an upper and a lower flammable limit. Below the lower limit, the gas is not concentrated enough to ignite, although an ignition may produce a fuel-combustion reaction, the reaction does not spread within the mixture. Above the upper limit, on the other hand, the atmosphere is rich in gas but low in oxidizer.

The values of the flammability limits are influenced by the temperature, which increases the upper limit and lowers the lower limit; by the pressure, which widens the limits by making the collisions between the molecules more frequent and thus supports combustion; by the presence of inert gases, which lower the upper limit; or by the presence of other flammable gases.

The combustion reaction is a complex process consisting of several chain reactions:

- Start - strongly endothermic (i.e. heat-absorbing) reactions displace a valence electron to form free radicals, i.e. active species.
- Propagation - active and other molecular species interact to form new active species.
- Branching - the initial active species branch off to create secondary species.

- Termination - the interaction of species creates deactivation or annihilation of active species, forming stable species.

The products of combustion depend on the nature of the fuel and the reaction conditions. Complete combustion is impossible in reality, so there will always be unburnt fuel in the flue gas. The main comburent is air, which is made of nitrogen by 78%. Although nitrogen is inert, under certain conditions (high temperatures, large amounts of air, presence of nitrogen in the fuel) it can react and create NO_x. Depending on the amount of available comburent, CO is also obtained as a reaction product.

At this point it is necessary to distinguish between two different types of combustion: deflagration and detonation:

- **Deflagration** is subsonic combustion, which usually spreads by conduction between hot matter heating adjacent cold matter. It is characterized by a large decrease in gas density downstream of the combustion wave and a slight drop in press. Most combustions in everyday life are technically a deflagration, including the one analyzed in this study, in which an open flame is studied without any change in ambient pressure due to combustion.
- **Detonation** is a type of explosive chemical combustion reaction. It occurs through the propagation of the flame front at supersonic speed, with the formation of a shock wave. It is a chemical-physical phenomenon consisting of an explosion whose flame front propagates at supersonic velocity and forms a shock wave, where the gaseous material is expanding under conditions of high temperature, very high pressure, and almost constant density. During detonation, the density of the combustion gases increases slightly compared with that of the fresh mixture, and these combustion gases slow down compared with the speed of propagation of the flame, which is strongly supersonic. Thus, the combustion gases follow the detonation wave, but see it moving away from them.

Deflagrations fall into 2 main categories: they can be diffusive or premixed. To explain this classification, we refer to the flame, which is defined as the visible part of combustion.

- **Premixed Flame** is formed under certain conditions during the combustion of a premixed charge of fuel and oxidizer. are available throughout a homogeneous stoichiometric premixed charge, the combustion process once initiated sustains itself by way of its heat release. The majority of the chemical transformation in such a combustion process occurs primarily in a thin interfacial region that separates the unburned and the burned gases. The premixed flame interface propagates through the mixture until the entire charge is depleted. The propagation

speed of a premixed flame is known as the flame speed (or burning velocity) which depends on the convection-diffusion-reaction balance within the flame, i.e. on its inner chemical structure. The premixed flame is characterized as laminar or turbulent depending on the velocity distribution in the unburned pre-mixture [11]. The inner structure of a laminar premixed flame is composed of layers over which the decomposition, reaction, and complete oxidation of fuel occur. These chemical processes are much faster than the physical processes such as vortex motion in the flow and, hence, the inner structure of a laminar flame remains intact in most circumstances. The constitutive layers of the inner structure correspond to specified intervals over which the temperature increases from the specified unburned mixture up to as high as the adiabatic flame temperature (AFT). In practical scenarios a laminar premixed flame is never obtained, turbulence is inevitable and, under moderate conditions, turbulence aids the premixed burning process as it enhances the mixing process of fuel and oxidizer. If the premixed charge of gases is not homogeneously mixed, the variations on the equivalence ratio may affect the propagation speed of the flame. In some cases, this is desirable as in the stratified combustion of blended fuels. A turbulent premixed flame can be assumed to propagate as a surface composed of an ensemble of laminar flames so long as the processes that determine the inner structure of the flame are not affected [10]. Under such conditions, the flame surface is wrinkled by turbulent motion in the premixed gases increasing the surface area of the flame. The wrinkling process increases the burning velocity of the turbulent premixed flame in comparison to its laminar counterpart. For example, turbulent premixed combustion is present in spark-ignition engines.

- **Diffusive flame** is also referred to as non-pre flame, in which the oxidizer and fuel are separated before burning. Mixing of the reactants takes place at the interface between them, the fuel diffusing into the oxidant. As the fuel is consumed, more oxidant is drawn into the reaction zone. Combustion is achieved where there is molecular diffusion with local dosing close to the stoichiometric value. The burning rate is however still limited by the rate of diffusion. Diffusion flames tend to burn slower and produce more soot than premixed flames because there may not be sufficient oxidizer for the reaction to go to completion. Depending on the fuel there can be several orders of magnitude of difference between the heat release (or reagent consumption) of a diffusive flame and a premixed flame [10]. This type of flame is present in the combustion of fuel particles in compression-ignition engines when many fuel droplets are surrounded by the flame front while still in a liquid state. This flame can also be

laminar or turbulent. Since the extinction of this type of flame was observed in this work, its characteristics are examined in more detail.

1.3. TYPE OF FUELS: PROPANE AND METHANE

We use two different fuels in this study. The following paragraphs indicate the main characteristics of these fuels, knowledge of which is very useful in understanding the different behavior of the two fuels in the vicinity of flame extinction. Some physical properties of the two fuels will be better highlighted in the section comparing the blowout limits of the two fuels.

1.3.1. PROPANE

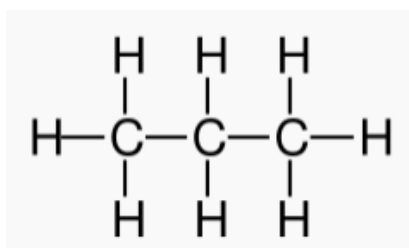


Figure 1.1. Structure formula of propane.

Propane is an aliphatic hydrocarbon with the formula $\text{CH}_3\text{CH}_2\text{CH}_3$ belonging to the series of saturated linear alkanes (see figure 1.1). As an apolar molecule, it is not soluble in water but is well miscible with benzene and chloroform.

Propane occurs naturally as a component of natural gas and crude oil, from which it is extracted by fractional distillation and is also the main constituent of liquefied petroleum gas (LPG), a hydrocarbon mixture commonly obtained from petroleum and widely used as a fuel. As a naturally occurring gas, propane is not normally industrially, mixed synthesized but is preferably obtained by extraction from oil or natural gas. It is a highly flammable substance, i.e. if heated above the auto-ignition temperature, which for this fuel is $490\text{ }^\circ\text{C}$ with pressure at 101325 Pa and temperature $20\text{ }^\circ\text{C}$, it burns with the development of a bright flame. Propane is not toxic, but it is classified as an asphyxiant gas, preventing the process of breathing air.

The most important reaction of propane is undoubtedly combustion, the lower heating value of propane is 46.4 MJ/kg , i.e. the exothermic reaction in which the compound is oxidized by molecular oxygen, the oxidizer par excellence [2]:



In reality, the oxidation of propane can lead to the formation of many undesirable products such as alcohols, aldehydes, and ketones.

1.3.2. METHANE

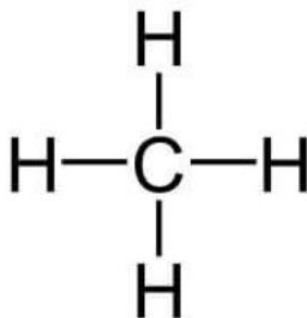


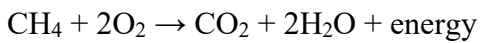
Figure 1.2. Structure formula of methane.

Methane is a simple hydrocarbon (alkane) consisting of one carbon atom and four hydrogen atoms; its chemical formula is CH₄, as shown in figure 1.2, and it is found in nature in the form of a gas. The methane molecule is tetrahedral in shape; the carbon atom is in the center of a regular tetrahedron with the hydrogen atoms at its vertices. At room temperature and pressure, it is a colorless, odorless, and highly flammable gas. Liquid methane, on the other hand, is obtained by cooling the gas to a temperature of -162 °C, again at atmospheric pressure, which is currently the focus of research as it would solve the problems of storage and therefore the autonomy of vehicles using it for propulsion [5]. Methane is the result of the decomposition of certain organic substances in the absence of oxygen. Most methane is obtained by extraction from its underground deposits, where it is often combined with other hydrocarbons, the result of the decomposition of organic substances buried deep in prehistoric times. When oil is extracted, methane also rises to the surface, on average in quantities equal to the oil itself. If the fields are far from where the oil is consumed, or if they are located in the open sea, it is almost impossible to use that methane, so it is either burnt at the exit of the wells without being used in any way, or it is pumped back into the oil fields, using centrifugal or reciprocating compressors, further promoting the exit of the crude oil through pressure.

Methane is a greenhouse gas present in the Earth's atmosphere in much lower concentrations than CO₂. In 1996, approximately 115 billion cubic meters of natural gas were flared or vented by these industries worldwide [11]. Reducing flaring emissions is key to the mitigation of global warming. An increasing number of governments and industries have pledged to eliminate flaring by 2030. In terms of economic loss, the global economy loses billions of dollars annually to gas flaring, and every major oil-producing nation, including Africa's largest oil producer, Nigeria, contributes a significant amount to this loss. The Nigerian National Petroleum Corporation (NNPC) claimed Nigeria flared an estimated 12,602,480 million cubic feet of natural gas in fifteen

years from 1996 to 2010. Since methane has a 21 times greater global warming potential than the carbon dioxide produced from its combustion, it is important to ensure efficient combustion and to avoid blow-off at all costs as weather conditions change, including natural wind.

Methane is the main component of natural gas, its ignition temperature is 632 °C at a pressure of 101325 Pa and temperature of 20 °C. Is an excellent fuel because it has a high lower calorific value of 50 MJ/kg,



The heat of combustion of the reaction is negative (the combustion reaction being an exothermic reaction); considering the same methane combustion reaction as a closed system, the heat of the reaction is -891 kJ/mol.

1.4. DIFFUSIVE FLAME IN A QUIET ENVIRONMENT

Fuel and oxygen mix in the space where combustion takes place in a diffusive flame, and the combustion process starts as soon as the activation energy is chemically appropriate and a suitable (stoichiometric or not) ratio has been reached. The flame appears at the boundary between the fuel zone and the region where the oxygen is present. The products of combustion spread to both sides. For the reaction to be sustained, the reactants must diffuse against these currents. This behavior is achieved by both laminar and turbulent flames; they differ only in the speed at which the reactions take place since in a turbulent flow a stoichiometric ratio is reached first, which initiates combustion, see Figure 1.3.

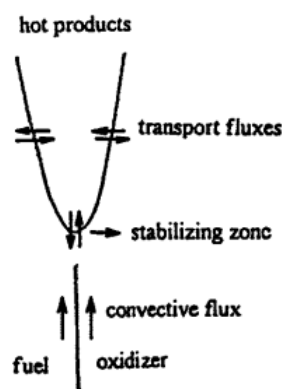


Figure 1.3. Schematic of the reacting flows and patterns [2].

The type of flame pattern, and in particular its height, depends on the fuel flow rate. For a given fuel and burner, starting with a low flow rate, the flame height increases with increasing flow rate

until it reaches a maximum and then shortens. Just before reaching the maximum height, the flame starts to flicker (become turbulent) at the top. This event separates "laminar spreading" from "transient" flames. With a further increase in flow rate, the flickering spreads in a downward direction. This propagation suddenly stops when only the region closest to the nozzle outlet remains free of fluctuations. At this point, the flame height becomes independent of the flow rate, and the transition flame changes to a turbulent flame. A further increase in jet velocity does not reduce the fluctuation-free region and the flame length changes little. The fact that the flame height is independent of the volumetric flow rate means that the higher the jet velocity, the faster the surrounding oxygen mixes with the fuel so that the distance along the jet axis is required for sufficient air mixing to burn the fuel is more or less constant.

The turbulence of the combustion air or fuel is an important parameter influencing the mixing in furnaces and combustion chambers, and consequently improves the efficiency of combustion and reduces the emission of pollution, resulting in shorter flames. The height of the flame versus fuel speed and the transitions observed are depicted in Figure 1.4. There is a first laminar region for low velocities of the fuel jet. As this velocity increases, there is a range where the flame begins to fluctuate to finally, and from a high critical velocity, the structure becomes fully turbulent.

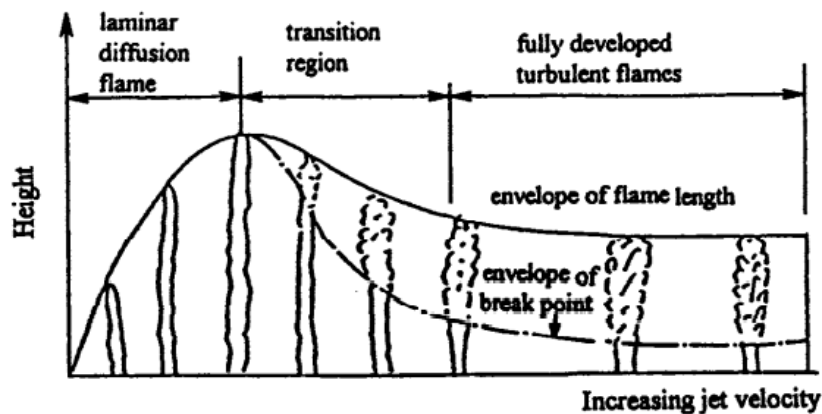


Figure 1.4. Height of the flame against fuel speed and transitions observed [2].

The laminar or turbulent nature of the flame as the fuel escape velocity varies is not sufficient to describe all the characteristics of a diffusive flame.

The other two fundamental quantities are the lift-off velocity (see the sketch in Figure 1.5) and the blow-off velocity. The lift-off velocity of the fuel flow is the one that generates a flame detached from the upper end of the nozzle. As the flow rate increases, the lower part of the flame moves away from the nozzle outlet. The quench rate is the fuel flow velocity at which the flame is extinguished, i.e. without the flame moving further away from the nozzle. Extinguishing occurs

when the jet sweeps the base of the flame in a region where the fuel concentration is too low to allow the oxidation reaction and hence combustion. Optimum combustion has jet velocities that lie between these two quantities just defined. There are extensive studies on this phenomenon [2], especially in an environment where there are no additional air jets. The presence of an airflow orthogonal to the flame has a strong influence on these two characteristic quantities, which retain their definition even in crosswind configuration with some differences in lift-off speed because this is also affected by the speed of the transverse air jet.

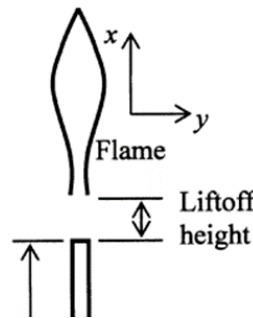


Figure 1.5. Sketch of the lift-off process [2].

A lifted flame is achieved by high fuel discharge velocities or by a combination of fuel momentum and transverse air jet.

1.5. THE THEORETICAL BASIS FOR STUDYING A DIFFUSIVE FLAME

The theoretical study of a diffusive flame can be approached by selecting a differential element along the x-direction of diffusion to which the conservation of heat and mass applies, as shown in Figure 1.6.

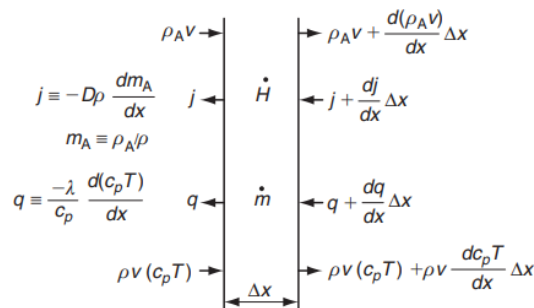


Figure 1.6. Balances across a differential element within a diffusion flame (one-dimensional problem) [1].

In Figure 1.6 q is the heat flux given by Fourier's law of heat conduction; \dot{m}_A is the rate of decrease of mass of species A in the volumetric element ($\Delta x \cdot 1$) ($\text{g}/\text{cm}^3 \text{ s}$), and \dot{H} is the rate of chemical energy released in the volumetric element ($\Delta x \cdot 1$) ($\text{cal}/\text{cm}^3 \text{ s}$).

Using Fick's law, it is written j the mass flux as:

$$j = -D \left(\frac{\partial \rho_A}{\partial x} \right) . \quad (1)$$

The same form can be derived if it is assumed that the total density does not vary with the distance x , and m_A is the mass fraction of species A:

$$j = -D\rho \frac{\partial(\rho_A/\rho)}{\partial x} = -D\rho \frac{\partial m_A}{\partial x} . \quad (2)$$

The expression for conservation of a species A, for the one-dimensional problem is:

$$\frac{\partial \rho_A}{\partial t} = \frac{\partial}{\partial x} \left[(D\rho) \frac{\partial m_A}{\partial x} \right] - \frac{\partial(\rho_A v)}{\partial x} - \dot{m}_A , \quad (3)$$

where ρ is the total mass density, ρ_A the partial density of species A, and v the bulk velocity in direction x . For a steady fuel mass input (as most practical combustion problems) there is a steady mass consumption and the equation (3) becomes:

$$\frac{d(\rho_A v)}{dx} = \frac{d[(\rho v)(\rho_A/\rho)]}{dx} = (\rho v) \frac{d m_A}{dx} . \quad (4)$$

The term (ρv) is a constant in the problem since there are no sources or sinks. With the further assumption from simple kinetic theory that $D\rho$ is independent of temperature, and hence of x , equation (3) becomes:

$$D\rho \frac{d^2 m_A}{dx^2} - (\rho v) \frac{d m_A}{dx} = \dot{m}_A . \quad (5)$$

The same equation must also apply to the other species B, but its gradient is opposite to that of A:

$$D\rho \frac{d^2 m_B}{dx^2} - (\rho v) \frac{d m_B}{dx} = \dot{m}_B = i \dot{m}_A , \quad (6)$$

where \dot{m}_B is the rate of decrease of species B in the volumetric element ($\Delta x \cdot 1$) and i the mass stoichiometric coefficient:

$$i = \frac{\dot{m}_A}{\dot{m}_B} . \quad (7)$$

The energy equation evolves:

$$\frac{\lambda}{c_p} \frac{d^2(c_p T)}{dx^2} - (\rho v) \frac{d(c_p T)}{dx} = +\dot{H} = -i \dot{m}_A H , \quad (8)$$

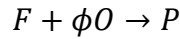
where \dot{H} is the rate of chemical energy release per unit volume and H the heat release per unit mass of fuel consumed (in joules per gram):

$$-\dot{m}_B H = \dot{H}, \quad -i\dot{m}_A H = \dot{H}. \quad (9)$$

Multiplying Eq. (5) by iH , then combining it with Eq. (8) for the condition $Le=1$ or $D\rho=\lambda/(c_p)$, one obtain (the Schvab–Zeldovich transformation):

$$D\rho \frac{d^2}{dx^2} (c_p T + m_A H) - (\rho v) \frac{d}{dx} (c_p T + m_A H) = 0 \quad (10)$$

Mathematically, what has been accomplished is that the nonhomogeneous terms (\dot{m} and \dot{H}) have been eliminated and a homogeneous differential equation [Eq. (10)] has been obtained. The equations could have been developed for a generalized coordinate system. However, for notation simplicity— and because energy release is of most importance for most combustion and propulsion systems—an overall rate expression for a reaction of the type which follows will suffice, where F is the fuel, O the oxidizer, P the product, and ϕ the molar stoichiometric index:



Then, Equation (8) may be written as:

$$\nabla \cdot \left[(\rho v) \frac{m_j}{MW_j v_j} - (\rho D) \nabla \frac{m_j}{MW_j v_j} \right] = \dot{M}, \quad (11)$$

$$\nabla \cdot \left[(\rho v) \frac{c_p T}{HMW_j v_j} - (\rho D) \nabla \frac{c_p T}{HMW_j v_j} \right] = \dot{M}, \quad (12)$$

where MW is the molecular weight, $\dot{M}=\dot{m}_j/MW_j v_j$; $v_j=\phi$; for the oxidizer, and $v_j=1$ for the fuel. Both equations have the form:

$$\nabla \cdot [(\rho v)\alpha - (\rho D)\nabla\alpha] = \dot{M}. \quad (13)$$

And the definitions are $\alpha_T = \frac{c_p T}{HMW_j v_j}$; $\alpha_j = \frac{m_j}{MW_j v_j}$.

They may be expressed as:

$$L(\alpha) = \dot{M}, \quad (14)$$

where the linear operator $L(\alpha)$ is defined as:

$$L(\alpha) = \nabla \cdot [(\rho v)\alpha - (\rho D)\nabla\alpha]. \quad (15)$$

The nonlinear term may be eliminated from all but one of the relationships (14), for example:

$$L(\alpha_1) = \dot{M}, \quad (16)$$

can be solved for α_1 , then the other flow variables can be determined from the linear equations for a simple coupling function Ω so that:

$$L(\Omega) = 0. \quad (17)$$

From this analytical basis, it is possible to determine the shape, the length, and the extinction of a diffusive flame, obviously making careful assumptions, and to relate these quantities to the rate of escape of the fuel. Fig.1.7 shows photos of a methane diffusive flame without a transverse air jet. It can be seen immediately that as the speed of the propane increases, the length of the flame increases.

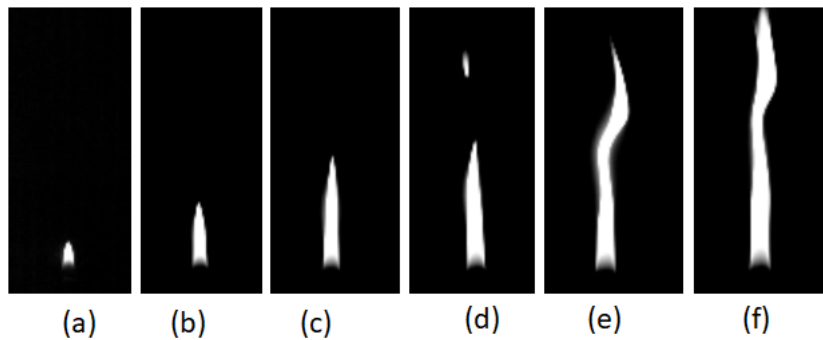


Figure 1.7. Diffusive no lifted propane flame images, speed propane: 0.1 m/s (a); 0.15 m/s (b), 0.20 m/s (c); 0.25 m/s (d); 0.3 m/s (e).

It can be seen from photo (d) that a turbulent flame begins to appear, but the length of the flame still tends to increase. The maximum flame length is reached in (f).

1.6. BRIEF DESCRIPTION OF DIFFUSIVE FLAME WITH CROSSWIND

1.6.1. FLAME PATTERNS TYPOLOGY

Combustion with a crosswind, see Figure 1.8, is the subject of many studies for various reasons. As mentioned above, this type of combustion is present in flaring. Today, this solution has been greatly reduced, thanks to the incentives of various governments against carbon dioxide production.

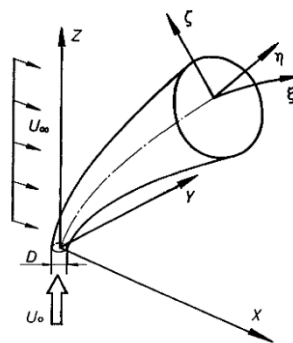


Figure 1.8. Cross-flow configuration [3].

On the other hand, a crosswind hitting a diffusive flame ensures better mixing of fuel and oxidizer within a certain range, which is why this type of solution or even more complex ones (e.g. mixed crossflows) are used in industrial combustors or gas turbines.

To describe the behaviour of this type of flame, it is necessary to define the momentum flux ratios J :

$$J = \frac{\rho_j V_j^2}{\rho_\infty U_\infty^2}, \quad (18)$$

where ρ is the density, V and U are velocity, and subscripts j and ∞ denote the fuel jet and crossflow respectively.

The jet-to-crossflow velocity ratio R :

$$R = \frac{V_j}{U_\infty}. \quad (19)$$

The jet Reynolds number:

$$Re_\infty = \frac{\rho_\infty U_\infty D}{\mu_\infty}, \quad (20)$$

where D is the jet nozzle diameter or for a non-circular cross-section, the hydraulic diameter, μ is dynamic viscosity.

These parameters are fundamental for the analysis of the results obtained from flame extinguishing tests.

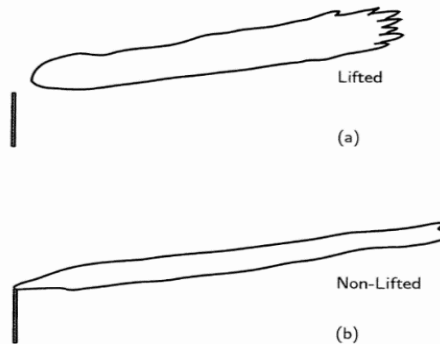


Figure 1.9. Type of flames under cross flow conditions: lifted (a) and non-lifted (b) [3].

The first classification of diffusive crosswind flames can be made according to the speed of the fuel jet and its momentum flow concerning the airflow, diffusive flames can be of different types. In Figure 1.9 we represent lifted flames (a) that have a flame base that is away from the fuel source outlet, and non-lifted flames (b), that have a flame base attached to the outlet of the source. It will be seen later that a transverse jet of air can cause a diffusive flame to switch from non-lifted to lifted, and the extinction of the flame is greatly influenced by whether it is lifted or not.



Figure 1.10. No-Lifted flame (a), Lifted flame (b).

Figure 1.10 shows (a) a no-lifted propane flame and (b) a lifted propane flame. The photos were taken with a high-speed camera. The fuel nozzle can be seen at the bottom left. During the evaluation of blowout limits carried out in this work, both configurations were presented. For this reason, additional information is provided.

Paying our attention to Figure 1.11, non-lifted flames of Figure 1.8 (b) are classified into six sub-classes and denoted as down-washed (a), flashing (b), developing (c), dual (d), flickering (e), pre-blow-off (f).

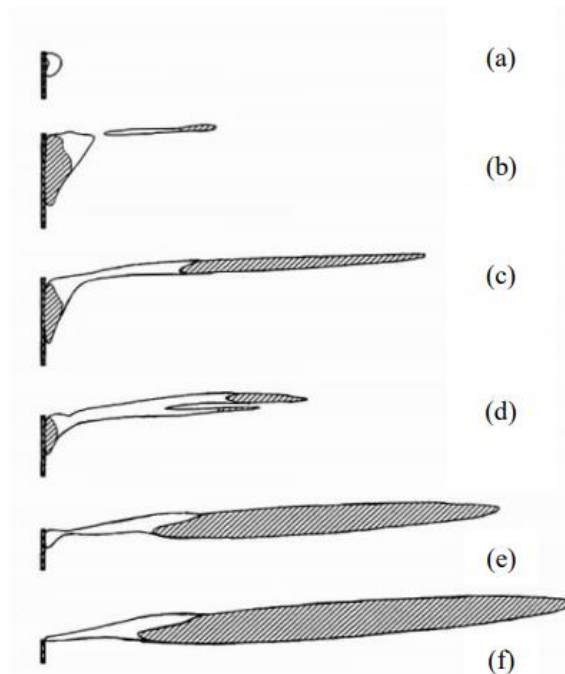


Figure 1.11. The six different flame modes, Hatch marks.

For low values of jet-to-crossflow velocity ratio R , equation (19), the region in which the flame is present is near the nozzle outlet. The jet of fuel, whether methane or propane, is bent downwards by the crossflow and forms a recirculation area near the nozzle outlet, due to the down-washed effect. As R increases, an intermittent blue flame is obtained, which stabilizes in a region following the current. This region narrows as R becomes greater. As R continues to increase, the flames begin to shorten and the double-flame pattern appears, but it tends to close as R gets larger. Subsequently, flickering flames occur, the downstream part of the flame begins to flicker, and its transverse size increases [12]. Finally, the small blue flame in the recirculation zone disappears and the length of the flame does not increase appreciably with the speed of the jet. Just before extinguishing, the blue zone is still above the tip of the burner instead of remaining in the wake of the fuel jet, on the opposite side from which the cross-wind arrives.

This type of classification was obtained by processing the images of a rich propane air mixture [13]. But from other tests carried out with a very similar setup, the creators of this classification, Huang and Wang [13], noted that the six flame types are not easily observable and repeatable. For this reason, an attempt at clarifying these modes was made by Huang and Wang, redefining them in terms of the relative jet and cross-flow momentums. Their five modes and range of applicability are: down-wash ($R < 0.1$) crossflow dominated ($0.1 < R < 1.6$), transitional ($1.6 < R < 3.0$), jet dominated ($3.0 < R < 10$), and strong jet ($R > 10$).

Other types of classification exist in the literature but are beyond the scope of this work, in which the focus is on the extinguishing of the flame and thus on the last subclassification pre-blow-off (f). In particular, there is a classification of typical sketches of flames before blowout shown in Figure 1.12 between liftable flame (a) and never-lift flame (b). These flow patterns will be described in the results chapter of this study. The difference between these two structures lies in the curvature that the diffusion flame undergoes under the action of the air jet that is intended to extinguish the flame. As can be seen, the curvature is very abrupt (almost normal to the flame) in the case of a never-lift flame (b).

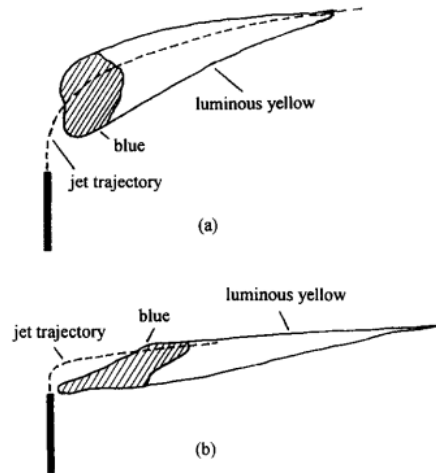


Figure 1.12. Typical sketches of flames before blowout: (a) liftable flame, (b) never-lift flame [13].

1.6.2. MECHANISM OF BLOWOUT

This work focuses, particularly on a flame blowout. This aspect being very important for combustion quality and safety, it has been studied at length by many researchers, who have tried to understand the mechanism by which blowout occurs, through analytical, numerical, and experimental studies, creating models.

The jet blowout literature can be loosely categorized as dividing along with two general proposed phenomenological mechanisms with some variation among authors for each mechanism. **One proposed mechanism** is that blowout occurs when the local flow velocity exceeds the maximum turbulent burning velocity. This mechanism was proposed by Vanquickenborne and van Tigglen [14]. They proposed that the shape of a flame at the stabilization point consists of an annular premixed flame with flame fronts in the lean and rich mixtures anchored at the stoichiometric contour and a trailing ordinary diffusion flame where the unburned fuel and air come together. A close inspection of their results indicates that the majority of the stabilization points are somewhat closer to the jet axis, that is, in richer fuel mixtures.

A second proposed blowout mechanism is that blowout occurs when "the hot combustion products are mixed so rapidly with the unburned jet fluid that there is insufficient time for ignition before the temperature and radical species concentrations drop below some critical value." This mechanism was proposed by Broadwell [15]. The competition between the physical mixing time and the chemical time was used to create an equation for diffusion flame blowout.

As far as blowout models are concerned, the most important are certainly those developed by Broadwell [16] and Kalghatgi [17]. Kalghatgi developed an empirical expression to relate the

blowout velocity to the nozzle diameter by fitting a functional form to his data. Broadwell developed an equation to relate the blowout velocity to the nozzle diameter using the stability mechanism assuming a competition between physical and chemical time scales in large-scale flow structures.

1.6.3. FLUID DYNAMICS IN STRIPPING OF A DIFFUSIVE FLAME WITH A CROSSWIND

This section describes one of the main phenomena that cause a diffusive flame to extinguish. At low-momentum flux ratios, the flame is "wake-stabilized" by a standing vortex that exists on the leeward side of the burner tube as shown in Figure 1.13. A planar stationary vortex attached to the burner tube defines the first zone; the long axisymmetric tail of the flame forms the third zone, and the junction that connects these two main parts of the flame defines the second zone. Initially, the effect of the crosswind is to increase the overall length of the flame. However, after reaching its peak length, the flame shortens with further increases in wind speed. This maximum length corresponds with the appearance of detached pockets of combustion. The width of the flame decreases monotonically with increased wind speed. Ultimately, at very low R , the main tail of the flame is extinguished and only the recirculating vortex of zone 1 remains of the original three-zone flame. Previously, it was demonstrated through gas chromatographic analyses of the unburned hydrocarbons collected in the tunnel show that they have a very similar volume fraction distribution as the hydrocarbon fuel stream (i.e., hydrocarbon emissions from natural gas flares are primarily methane whereas emissions from propane flares are primarily propane) [18]. These results suggest that inefficiencies of the flare are mainly due to a portion of the fuel being stripped from the flare stream before the flow reaches any flame zone to burn these gases.

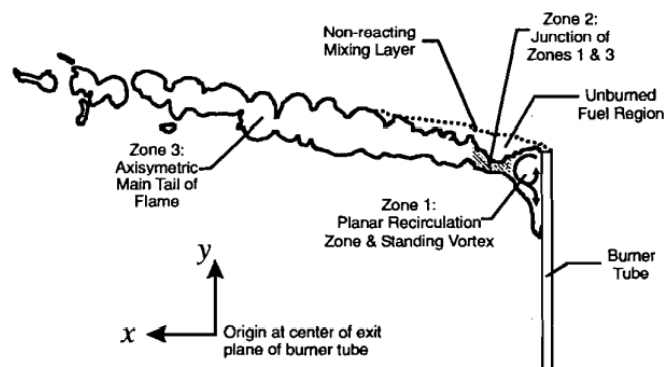


Figure 1.13. Zones of a wake-stabilized jet diffusion flame in crossflow [18].

This stripping mechanism is supported by the local extinctions as a result of intense mixing with air that dilutes the fuel beyond its lean limit.

Experimentally, it was observed that there are five possible paths along which fuel could be exiting a control volume surrounding system, as shown in Figure 1.14: (i) upward dispersion of unburned fuel from the non-reacting mixing layer that exists on the upper surface of the flame, (ii) the wake-stabilized flame is known to burn as a series of discrete flame pockets, it is possible that some unburned fuel exists between these flame pockets and is subsequently ejected from the tip of the flame, (iii) counter-rotating vortex pair that exists when a jet is injected into a transverse stream and is bent over, (iv) the recirculation region in zone 1 of the flame and leak down the leeward side of the burner tube, (v) the fuel stream could be drawn down through gaps between the flame pockets to the underside of the flame where it is then transported away from the flame by the mean flow [18].

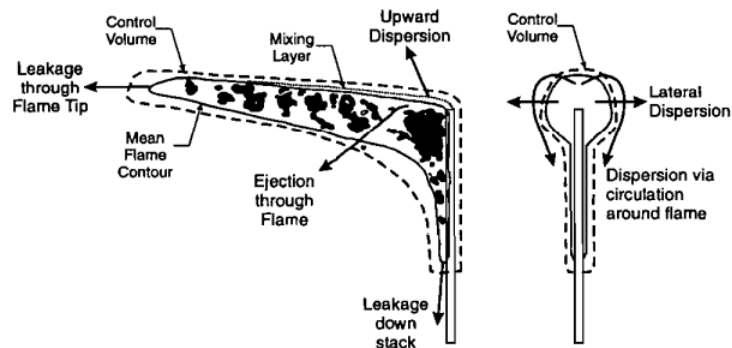


Figure 1.14. Potential paths for fuel leakage or stripping [18].

The diffusive flame has many applications thanks to its simplicity, as there is no need for a chamber in which the fuel mixes with the combustion agent beforehand. This also means that there is less risk of accidents than with a premixed flame, which has many other advantages, first and foremost a higher heat release.

It may seem easy to analytically study a diffusive flame, but when a crosswind is present, the model becomes very complex [19]. It was pointed out the high computational cost of solving the problem, despite the assumption of steady-state conditions. Furthermore, in practice, it has been shown that when hit by a transverse current, the flame can behave in very different ways, depending of course on the configuration: the flame can be extinguished, tilted, shortened, or even stabilized, thanks to the increased supply of air which promotes mixing with the fuel.

Chapter 2. EXPERIMENTAL SETUP AND CALIBRATION

The first step to execute this Thesis was to design and fine-tune the experimental setup to perform the experiments. Since the idea of the experiment is to visualize the extinction of a flame while it is affected by an air jet, the main components of the experimental setup are the burner, the air jet, and a high-speed camera. However, there are many additional components required for the proper functioning of the experiments that have to be installed and, in some cases, calibrated.

The tests were carried out in the department's fluid mechanics laboratory at *Escuela de Ingenierías Industriales de la Universidad de Málaga*.

2.1. EXPERIMENTAL SETUP AND DESCRIPTION OF COMPONENTS

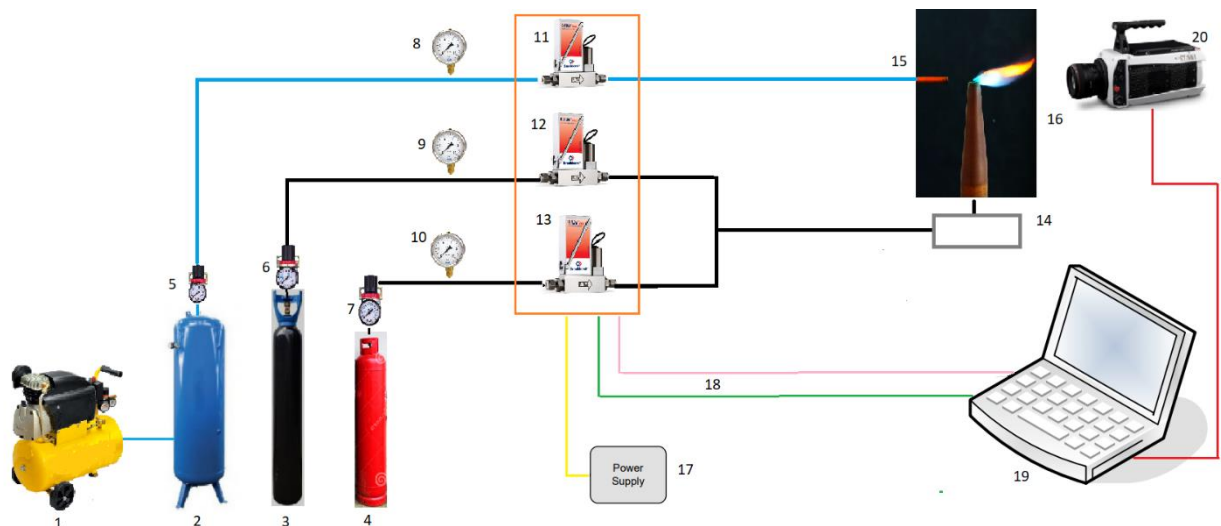


Figure 2.1. Diagram of the experiment: compressor (1); air tank (2); propane tank (3); methane tank (4); pressure reducer (5) (6) (7); pressure gauges (8) (9) (10); digital flowmeter (11) (12) (13); burner (14); nozzle air (15); nozzle fuel (16); power supply (17); cable (18); PC (19); Phantom v611 (20).

Figure 2.1 shows a diagram of the experimental setup with its different components. First of all, an external compressor is required to pump the air at the required conditions. This compressor is connected to the air tank that produces the air jet using a flowmeter to control the flow rate. The combustion gases, propane or methane, are connected to the burner using another flowmeter. Both flowmeters are controlled by a computer if they are digital. Lastly, to visualize the experiment, a high-speed camera is used and the images post-processed. A detailed description of the components of the workstation follows.

External compressor supplying air to all laboratory stations, up to a pressure of 10 bar.

Air tank, which has the following characteristics:

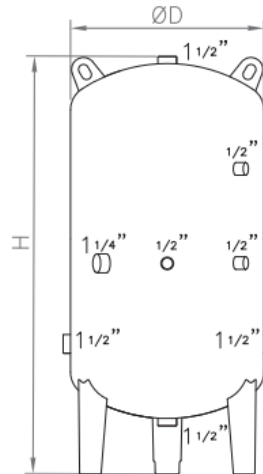


Figure 2.2. Air tank.

Table 2.1. Parameter of the air tank.

Model	100 DG
Diameter D [mm]	400
Weight [kg]	22
Height [mm]	1040
Capacity [l]	100
Temperature range [°C]	-10°C / 60°C
Pressure nominal [bar]	10
Pressure test [bar]	15
Material	Steel

Propane tank:*Table 2.2. Parameter of the propane tank.*

Pressure [bar]	6.5
Gas bottle size	B10
Capacity [kg]	4.2
Molecular weight [g/mol]	44
Relative density, gas	1,50 (air = 1)
Relative density, liquid	1,58 (water=1)
Tank connection	ITC EP-6 Tipo E - IS M 21,7 x 1,814
Smell	None
Color	Colorless
Components	C ₃ H ₈ > 99,95 %
Impurities (ppm v/v)	H ₂ O<5 O ₂ <10 H ₂ <40 CO ₂ <5 N ₂ <40 C ₃ H ₆ <200 C _n H _m < 200

Methane tank:*Table 2.3. Parameter of the methane tank.*

Pressure [bar]	200
Gas bottle size	L50
Capacity [m ³]	12,60
Molecular weight [g/mol]	16
Relative density, gas	0,60 (air =1)
Relative density, liquid	0,42 (water =1)
Tank connection	ITC EP-6 Tipo E - IS M 21,7 x 1,814
Smell	None

Color	Colorless
Components	CH ₄ > 99,95 %
Impurities (ppm v/v)	H ₂ O < 5 O ₂ < 10 C ₂ H ₆ < 200 C _n H _m other than C ₂ H ₆ < 50 CO ₂ < 10 N ₂ < 200 H ₂ < 20

Pressure reducer at the outlet of each tank. The tests were carried out with the following pressures:

- Methane pressure: the methane tank requires 2 pressure reducers, the first reduces the pressure from 200 bar to 8 bar, the second from 10 bar to 3 bar.
- Propane pressure 2 bar
- Air pressure 4 bar

Pressure gauges, which display the pressure value before the flow meters. These gauges are important because they allow us to understand whether pressure losses are important. The tanks and their flow meters are connected by pipes approximately 2 meters long.

Burner

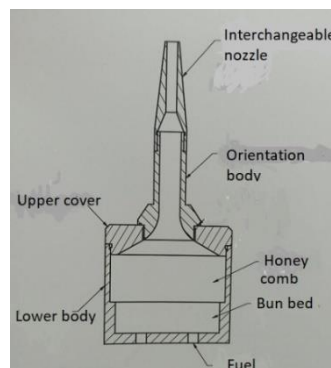


Figure 2.3. Burner [22].

All components of the burner are made of aluminum, due to its excellent oxidation resistance. The design was developed in a final project work [3]. A schematic of the burner is shown in figure 2.3. For the realization, the following requirements have been met:

- the minimum volume of the orientation chamber
- maximum concentricity of the fuel injector
- easy and economical construction
- maximum tightness

There is an O-ring in the lower body which guarantees a good gas seal. The orientation body is interchangeable and has been knurled to facilitate assembly/disassembly.

The burner has been designed to operate with both a diffusive flame and a premixed flame. There is an air injector in the lower part and the shape of the object as a whole, also thanks to the honeycomb, the burner can guarantee the creation of a premixed flame, i.e. the correct mixing of air and fuel before the oxidation reaction takes place.

The fuel is introduced through an M6x10 mm screw with a through-hole. The orifice must meet the critical orifice condition to avoid flashback, in this case, a critical hole of 1.5 mm was chosen. This value has been calculated based on the type of fuel and flow rates typically used with this burner, the quenching distance depended on the fuel type, the mixture concentration, and the direction of flame propagation. This type of safety is redundant throughout, as the digital flow meters and pressure reducers at the tank connections also prevent flashbacks.

The fuel injector guarantees a centered injection, reduction of the lower chamber volume, and can be interchangeable.

It is important to highlight how the diameter of the fuel inlet hole was calculated, as it is extremely important for the safety of the experiment. The calculation was based on the work of Professors Gutkowski and Parra-Santos [23], they have performed numerous tests about flames in propane/air mixtures propagating in square d_s and circular d_c ducts of small sizes. The flames propagated upwards and downwards from the open end of the duct to the closed one. They found how the shape of the duct, the direction of flame propagation, its length and width affect the speed of flame propagation S_L and on flame quenching, the cause of which is the removal of heat from the duct walls.

The quenching diameter is associated with parameters of the flammable mixture by the critical Peclet number:

$$Pe = \frac{S_L^0 d_q}{\alpha}, \quad (1)$$

where α is the thermal diffusivity of the cold mixture and d_q is the quenching characteristic diameter of the duct. It is widely accepted that the Peclet number is determined for downward propagating flames. Peclet number in the operating ranges of the burner blow-off evaluation tests is approximately 42-45.

Nozzle air

The air nozzle is a cylinder with an internal diameter of 3 mm and a length of 40 mm, made of brass.

Nozzle fuel

Tests were carried out using three nozzles which differ only in the diameter of the outlet. The nozzles are made of brass and have a thread at the lower end to allow assembly with the burner. It is necessary to remove combustion residues frequently because they change the effective nozzle diameter.



Figure 2.4. Fuel Nozzle.

Power supply type E-7500-05. It serves to supply the digital flowmeters with a voltage of 15Vdc-2A. Its power is 40 VA and its maximum operating temperature is 50 °C.

RS-232/USB cable to linked PC with flowmeters

Description Mass flow meters MASS-FLOWSelect

The mass flow meters are manufactured by Bronkhorst High-Tech. They have a great deal of flexibility in terms of their operating range, pressure, and mass flow, as well as the possibility of working with different fluids. They are very precise instruments with excellent repeatability and accuracy. Their operation is based on the thermal effect, which is explained later.

In this experiment we used the model **EL F-201CV-5K0-RAD-22-V**, the EL series is designed by the manufacturer to work in clean environments and fluids, such as those in a laboratory.



Figure 2.5 MASS-FLOW Select EL F-201CV-5K0-RAD-22-V [20].

Technical specifications

Measurement / control system

Table 2.4. Digital flowmeter general specification.

Accuracy	$\pm 0,5\%$
Turndown	1: 50 (in digital mode up to 1:187,5)
Repeatability	$< 0,2\%$ Rd
Settling time (controller)	1...2 seconds
Control stability	$< \pm 0,1\%$ FS (typical for 1 l/min N ₂)
Operating temperature	-10 / +70°C
Temperature sensitivity	zero: $< 0,05\%$ FS/°C; span: $< 0,05\%$ Rd/°C
Pressure sensitivity	0,1% Rd/bar typical N ₂ ; 0,01% Rd/bar typical H ₂
Leak integrity, outboard	tested $< 2 \times 10^{-9}$ mbar l/s He
Warm-up time	30 min. for optimum accuracy

Mechanical parts

Table 2.5. Digital flowmeter mechanical specification.

Material (wetted parts)	stainless steel 316L or comparable
Process connections	compression type or face seal couplings

Ingress protection (housing)	IP40
------------------------------	------

Electrical properties

Table 2.6. Digital flowmeter electrical specification.

Power supply	+15 / 24 Vdc
Analog output/command	0...5 (10) Vdc or 0 (4)...20 mA
Digital communication	RS232

2.2 DETAILS OF THE USE OF FLOW METERS

Thermal mass flow measuring principle [20]

The heart of the thermal mass flow meter/controller is the sensor, which consists of a stainless steel capillary tube with resistance thermometer elements. A part of the gas flows through this bypass sensor and is warmed up by heating elements. The measured temperatures T_1 and T_2 drift apart. The temperature difference is directly proportional to mass flow through the sensor. In the main channel, Bronkhorst High-Tech applies a patented laminar flow element consisting of a stack of stainless-steel discs with precision-etched flow channels. Thanks to the perfect flow split the sensor output is proportional to the total mass flow rate. The following figure illustrates this.

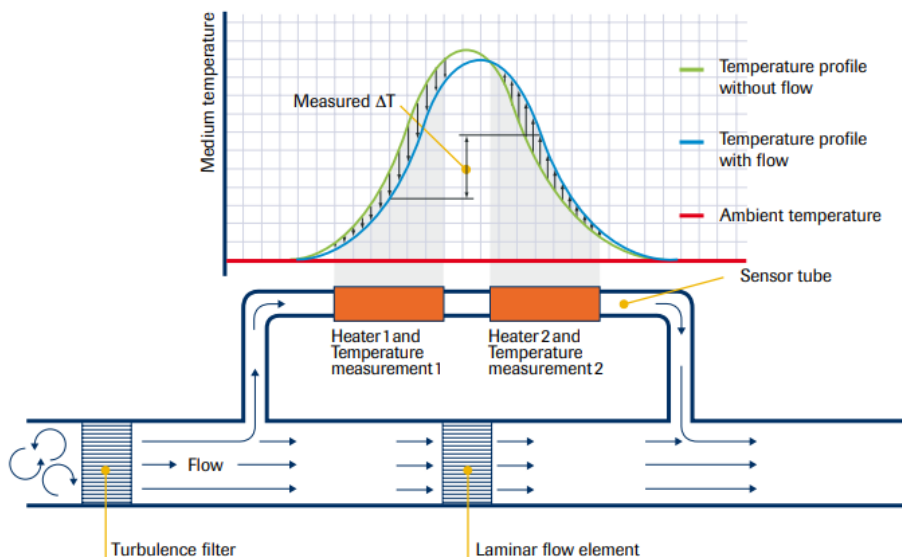


Figure 2.6. Sensor operation diagram [20].

$$\Delta T = k \cdot C_p \cdot \dot{M} = T_2 - T_1 [K] \quad (2)$$

where C_p is the specific heat and \dot{M} is the mass flow. Therefore, the flow mass rate is obtained directly.

Dimension EL F-201CV-5K0-RAD-22-V:

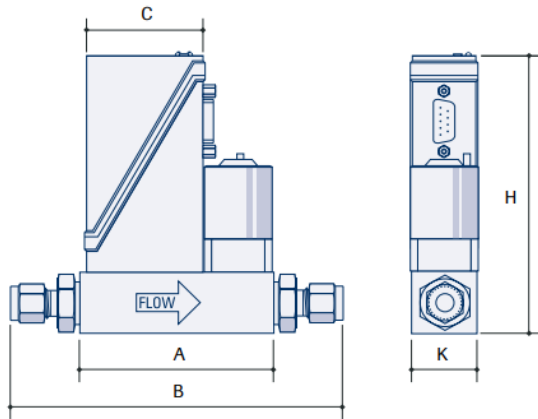


Figure 2.7 Flowmeter dimensioning [20]

Table 2.7. Flowmeter dimensioning.

A [mm]	78
B [mm]	135
C [mm]	47
H [mm]	123
K [mm]	26
Weight [kg]	0.7

Meter/PC connection

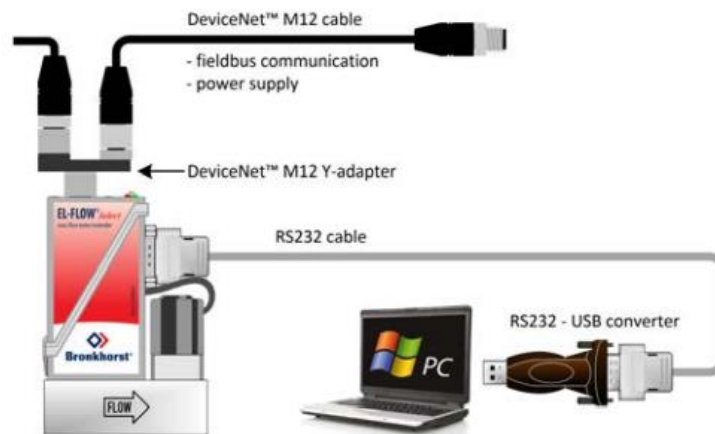


Figure 2.8. Meter/PC connection [20].

The flow meters were connected in parallel with each other and connected to the power supply. The necessary energy is supplied via a power supply device. The sensors are also connected to transmit and receive information, in particular, this is done via the RS232 port that connects the instruments to the PC. To exchange data, it was necessary to install the FlowDDE software, supplied by the flow meter manufacturer. The FlowDDE software is not sufficient to perform all the actions necessary for the experiment. The additional tools FlowTune, FlowView, and

FlowPlot were also used. The first has the function of entering the data relating to the fluid to be used so that the instrument can work at its best, the second has the function of displaying the instantaneous quantities of pressure and mass flow and indicating the flow values to be obtained, the third provides the trend in time of the values of the measured quantities.

To allow the experiment to be repeated and to facilitate the use of the instruments, it is necessary to download the drivers for reading the RS232/USB adapter needed to connect the PC to the flowmeters [21].

FlowDDE™

A DDE operator communicates to FlowDDE using DDE messages. FlowDDE uses the parameter database for parameter information and the Flowb32.dll to perform the low-level communication to the FLOW-BUS. The Flowb32.dll has methods to easily send or request a parameter value to a certain node, process, parameter, and to get the answers. From the calls to these methods, it constructs the required FLOW-BUS messages in the binary ProPar protocol, sends these messages, and receives and interprets the answers from the instruments.

The logical scheme of operations of the instrument/operator interface software is shown in Fig. 2.9:

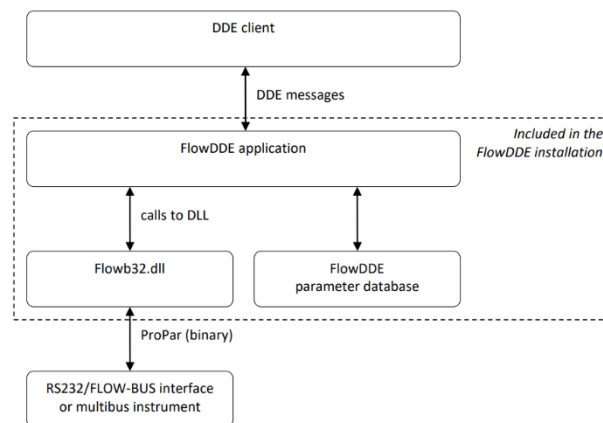


Figure 2.9. Communication diagram between operator and instrument [20].

FlowTune™

The instrument is calibrated by the company with a specific gas, this is indicated on the instrument and FlowTune also highlights this as it reads the instrument. Each instrument has a precise operating range in terms of pressure, temperature and flow. FlowTune gives the possibility to change the characteristics of inlet pressure, outlet pressure, fluid temperature, type of fluid, unit of measurement with which you want to display the flow, speed of change of flow at the time the

command is given, obviously all these quantities must be within the operating range. Once the values of all these parameters have been established, the software recalculates the optimal flow rate range in which it can operate. Conversion is based on fluid properties, sensor and restriction properties, valve properties, and the original calibration curve. Up to eight different configurations can be stored from the possible setting combinations.

Fig. 2.10 shows the configurations of the flowmeter that was used for the fuels (methane and propane) in this work. The manufacturer has programmed the instrument to work with 4 gases, which can be seen from the company logo next to the fluid name. Calibration was performed at inlet and outlet pressures of 3.013 bar and 1.013 bar respectively, at a temperature of 20 °C.

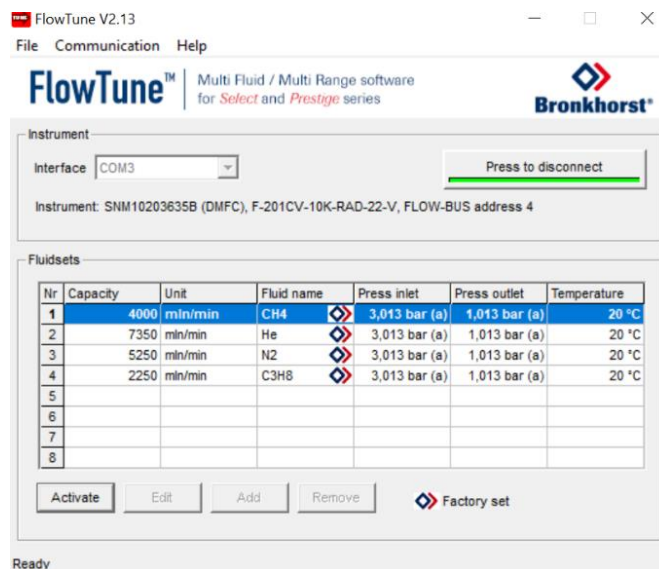


Figure 2.10. Configurations of propane/methane Flowmeter.

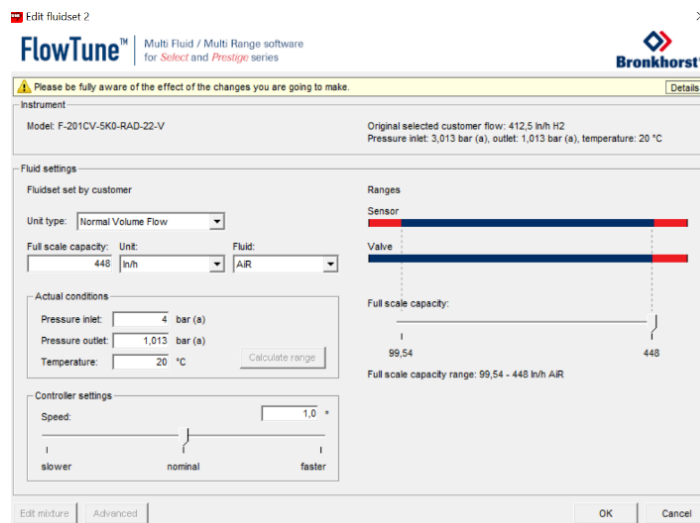


Figure 2.11. Edit configuration flow.

Pressing the edit button will take you through all possible configuration settings and allow you to change parameters such as inlet/outlet pressure, temperature, and the unit of measure used to indicate the flow rate. FlowTune can correct the measured value with the newly chosen parameters.

Fig. 2.11 shows the capabilities of the FlowTune software. It illustrates the screen for changing the air-fluid boundary parameters. It is also possible to change the data exchange rate between the physical instrument and the operator.

FlowView™

This software is the concrete interface on which the operator acts, which communicates with FlowDDE which in turn translates the commands to the instruments. For each flowmeter it is necessary to open a FlowView window, at the top is indicated the name of the corresponding instrument. The operator can set the desired flow rate in different ways:

- Acting on a graduated cylinder that schematizes the flow meter
- Manually entering the flow rate value with the unit of measurement previously selected with
- Entering the percentage value (referring to the full scale) in the corresponding box.

Depending on the requirements, one of the solutions, or even combinations, can be chosen; to assess the blow-off, the flame is gradually approached, using a different command depending on the moment.

From each window, it is also possible to choose a configuration previously created with FlowTune or to execute basic commands to the valves such as total opening/closing, reset, or emergency stop,

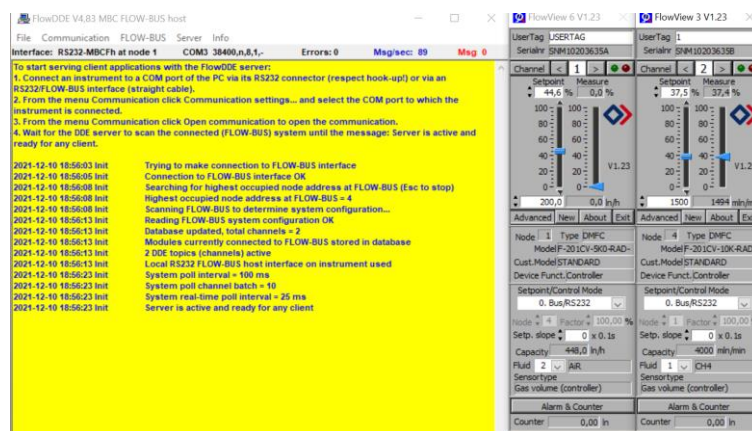


Figure 2.12. Screen FlowDDE e FlowView's windows.

Fig. 2.12 shows on the left in yellow the FlowDDE interface screen and on the right the FlowView windows to control the flowmeters. As you can see from the picture, the FlowDDE screen gives

information about the PC/Flowmeter connection. The software also gives the possibility to display possible malfunctions and errors through tabulated codes, as well as to report in real-time the flow values indicated by the flowmeters and the data exchange rate.

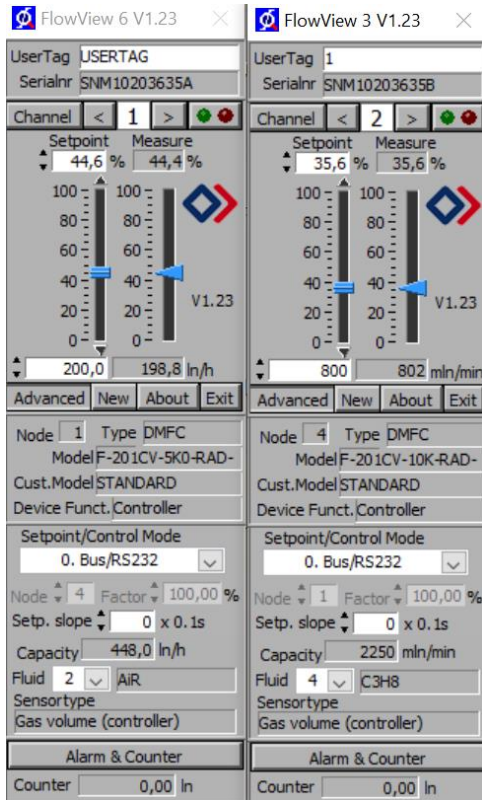


Figure 2.13. Flowmeters with air and propane.

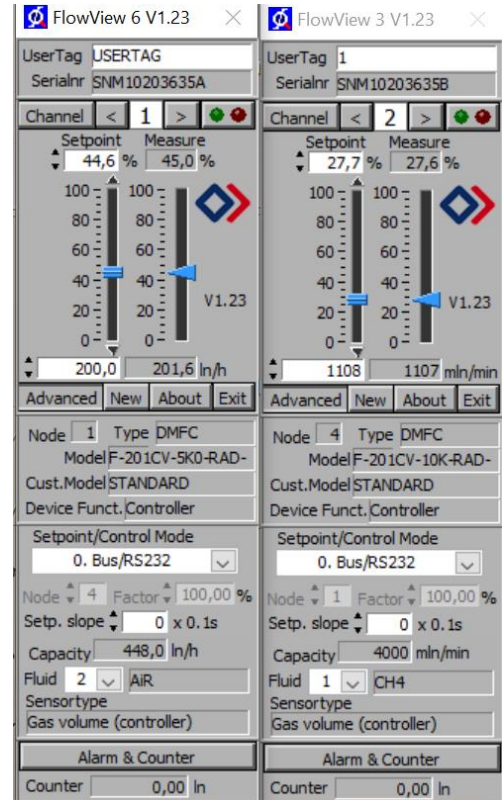


Figure 2.14. Flowmeters with air and methane.

As can be seen from Figs. 2.13 and 2.14, the flowmeter regulating the airflow has been connected to channel 1, while the flowmeter regulating the fuel flow is on channel 2. Whenever the working fluid is changed, i.e. when the respective tank is connected, it is necessary to indicate the new working fluid with FlowView, as shown in Fig. 2.13 and 2.14, so that an optimal measurement can be obtained.

FlowPlot™

The software needs to be manually aligned with FlowDDE to enable effective communication with the instruments. Once this is done, it is possible to get a real-time reading of the values. When using real-time measurement, up to four special processes in the interface will be programmed by FlowPlot. All data for the selected parameters connected to a plotline will be collected using this interface. The interface collects the data and adds time stamp information to it. While the PC may be temporarily busy, the interface will continue collecting data and it will be less likely to miss important data. The graph may lag a little but will contain more accurate

information. The scan time can be changed in FlowPlot to set the sample time for data acquiring by the real-time processes in the interface. This scan time is determined automatically based on the real-time poll time in FlowDDE and in most cases, it is not required to change it.

FlowPlot then creates real-time graphs of the selected quantities as a function of time. This is very useful because it allows understanding if during a test there are flow oscillations, caused by an instantaneous incorrect operation of the instrumentation. In addition, as can be seen from the image, there is a slight fluctuation in the gas flow rate when the flame is extinguished. This is possible thanks to the high sensitivity of the instrument and allows a more accurate assessment of the instant in which blow-off occurs.

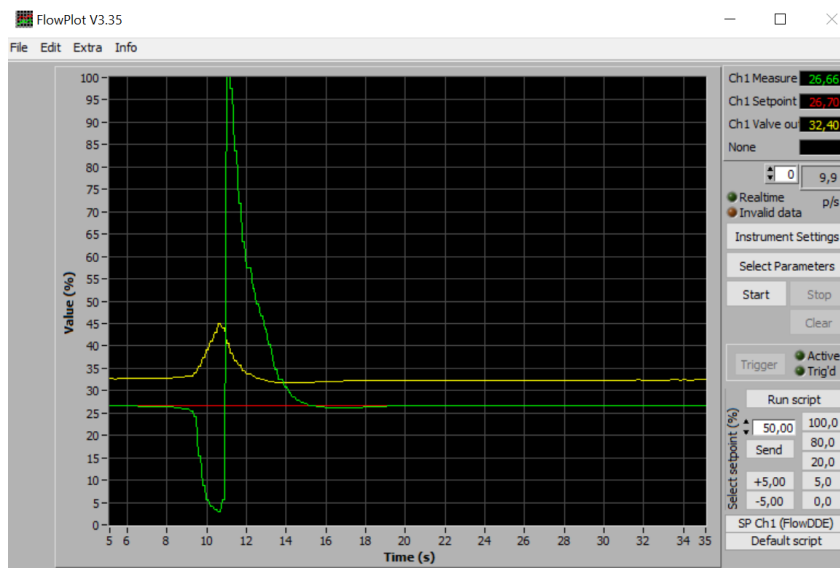


Figure 2.15. Oscillation is caused by a momentary malfunction of the instrument.

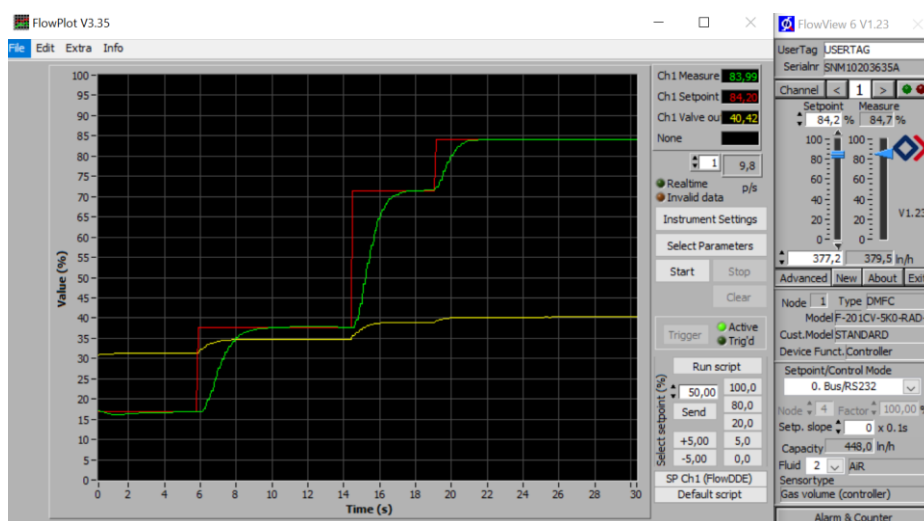


Figure 2.16. Airflow variation.

Fig. 2.15 and 2.16 show respectively the trend of the methane and airflow in % compared to the maximum flow rate value that the instrument can evaluate with the chosen set of values, as a function of time. The graph has 3 curves: red shows the flow value set by the user through one of the FlowView commands, green shows the actual flow rate value measured by the instrument, while yellow shows the actuator signal, i.e. the device that converts the electrical signal into the mechanical opening of the valve.

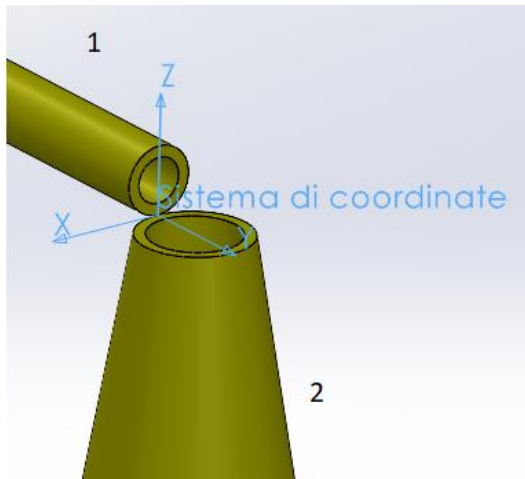
In Fig. 2.15 it can be seen that the control is fixed at 26.7% of the maximum value of the methane flow rate, a constant red line, while the value measured by the instrument (green curve) has an abrupt oscillation, first decreasing below the set value and then increasing very quickly, even exceeding the maximum value of the optimal operating range. This problem has occurred several times, especially in the first few minutes of flow meter operation. If combustion is present, when this sudden increase in flow occurs it is necessary to intervene on the safety valve to avoid an excessively large flame. It happened to obtain a flame length of around 35/40 cm in these cases, while in regular tests a length of 15 cm was never exceeded.

Fig. 2.16 shows the flow rate when the command to increase the airflow is given. The command is stepped (red curve) while the actual increase is not instantaneous but there is a transient (green curve). The duration of the variation can be adjusted by acting on the configuration parameters via the FlowDDE interface. The screen shows 3 jumps, starting from 16% to get to 38%, then 72%, and finally 84.2% of the maximum flow rate value in the usable range of the instrument in this configuration, which coincides with 377.2 l/h on a maximum of 448.0 l/h.

2.3. TEST PROCEDURE

The analysis of diffusive flame extinction of fuel was carried out by evaluating the blow-off at a constant height L1 of the air nozzle, varying the volumetric flow rate of air and fuel. The tests were then carried out for different air nozzle heights.

The origin of the reference system is taken by ideally intersecting the outlet section of the two nozzles, air, and fuel, as can be seen from the picture.



- 1 Air nozzle internal diameter 3 mm constant
- 2 Fuel nozzle (CH_4 or C_3H_8)

Figure 2.17. Origin of the reference system.

In the course of the tests, the z coordinates of the air nozzle will be varied L_2 . The blue arrow indicates the air path and the red arrow the methane or propane path.

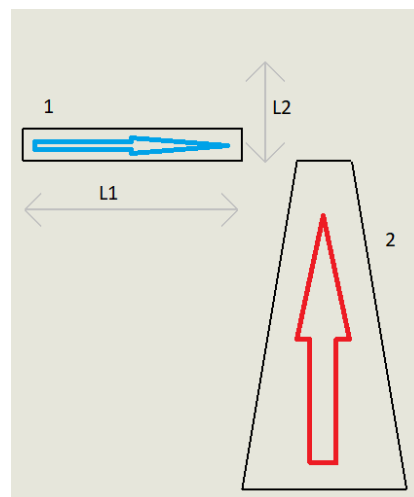


Figure 2.18. Fluid path..

Each test, for each point and condition, was carried out 3 times, to have flow rate values as close to blow-off as possible, the error obtained from the three evaluations will be indicated, giving an idea of the margin of the positioning of the evaluated blowout limits.

2.4. CALIBRATION OF DIGITAL FLOWMETERS

As digital flowmeters have not been used recently, to be sure that the measurements made with them are correct, tests were carried out to measure the air and fuel flow rates.

2.4.1. Balloon Inflation

The main idea of this method is to measure the gas flow rate indirectly by measuring the change in volume of a balloon while it is filled with gas. An empty inflatable balloon is attached to the end of the nozzle. By giving the command to open the digital flowmeter, the balloon fills with fluid. Using a video camera positioned orthogonally to the balloon, the inflation of the balloon is evaluated. The images obtained are analyzed with MATLAB to obtain the volume of the balloon at different times. Deriving the curve obtained, volume as a function of time, we obtain the flow rate which theoretically should be constant. In reality, it was found that at the beginning of the inflation, when the balloon has a very different shape from a sphere and also when its volume is very large, it is not possible to assess the volume trend as a function of time, so only the central part of the inflation was taken.

The volume versus time graph was obtained using two different methods.

The first is based on a very strong assumption, namely, to consider the balloon as a sphere. This makes it very easy to calculate the volume of the balloon from a two-dimensional image. Using the Matlab image processing toolbox the next steps are followed: first cutting the unnecessary part of the image, next transforming the remaining part of the image to make it black and white, and then evaluating the area of the section of the balloon. Using the value of the area the radius was calculated and from it the volume.

The second method is more refined, so that, as can be seen from the graphs, it succeeds in more realistically describing the volume trend as a function of time. It consists of finding an equation that describes the profile of the balloon. Once this equation has been found, by appropriately converting the pixels into mm and choosing a reference system that highlights the axisymmetric of the balloon, a solid of revolution is obtained through the revolution of the curve around the axis of the balloon. Being fully parameterized in MATLAB this region can be studied using the software functions. In this way, the volume can be calculated to the solid of the revolution.

2.4.1.1. Evaluation of volume versus time by approximating the balloon to a sphere

Inflation tests were carried out on a balloon connected to the air nozzle and fuel nozzle with three airflow, methane flow, and propane flow values indicated by the digital flowmeter:

Each inflation was filmed with a video camera. From the video obtained, 11 images were taken, and from each of them, the volume was calculated. The time instants, in seconds, in which the images were taken are indicated next in tables to the corresponding flow rates:

Tabel 2.8 information relief images

		Flow Rate	Sample time (s)	Total time (s)
Air	Case 1	100 ln/h	5	50
	Case 2	200 ln/h	3	30
	Case 3	300 ln/h	2	20
Propane	Case 4	1000 mln/min	30	300
	Case 5	1500 mln/min	20	200
	Case 6	2000 mln/min	10	100
Methane	Case 7	1000 mln/min	30	300
	Case 8	2000 mln/min	10	100
	Case 9	3000 mln/min	5	50

Each graph on the following pages shows the nominal flow rate value displayed by the flowmeter, the flow rate value obtained from the linear regression of the points obtained from the processing of the images, and therefore real, the relative and absolute errors between the nominal and real flow rates, and finally a variance index, i.e. the reliability of the linear regression made on the points of the volume/time graph obtained from the processing of the images. The flowmeter verification procedure was also carried out for the other two fluids used in the work, methane, and propane.

In this way, it was possible to draw a volume curve as a function of time.

We now show the algorithm used to calculate the volume of balloons, using air inflation as an example. For the other fluids, the algorithm is the same, only the units of measurement and the time interval in which the balloons are studied change. All results are then reported.

2.4.1.2. Image processing with Matlab

The Matlab software offers the possibility to process digital images through a toolbox called 'Image Processing Toolbox™'. It provides a complete set of standard reference algorithms and apps for working with image processing, analysis, visualization, and algorithm development. Image segmentation, correction and registration, noise reduction, geometric transformations, and 3D image processing can be performed. The main steps for processing are:

1. Data capture and import: import images and video generated by a wide range of devices, including webcams, digital cameras, satellite, and ground-based sensors, medical imaging devices, microscopes, telescopes, and other scientific instruments.
2. Image pre-processing: Increase the signal-to-noise ratio and accentuate image features using custom or predefined filters.
3. Image analysis: extracting meaningful information from images, for example by identifying shapes, counting objects, identifying colors, or measuring properties of objects.
4. Image registration: align images to perform quantitative analysis or qualitative comparisons.

The import of an image in Matlab environment is done through the command 'imread', in this way the software saves the image in a variable that has dimensions $A \times B \times 3$ where the values of A and B depend on the dimensions of the image read (in pixels), the x3 means that each point is saved according to the intensity of three basic colors, each color of each point has its value. In this way it is possible to reproduce each color through the intensities of the 3 main ones, each value is between 0 and 255 (8 bytes). Once the image has been read, it is possible to:

- Fractionate the image
- Change the intensity of the colors
- Take only the parts that have a certain type of the main color
- Transform it into black and white
- Rotate it

For a more detailed analysis, it is necessary to use the 'imbinarize' function, which creates a binary image from the 2-D greyscale image, replacing all values above a globally determined threshold with 1 and setting all other values to 0. In this work, the default algorithm that binarizes the matrix (imbinarize uses a 256-bin image histogram to compute Otsu's threshold) was used. To obtain

good binary images it was necessary to pre-process them, changing intensity or contrast, and above all to choose appropriate balloon colors. In the resulting binary matrices, we have 0/black and 1/white.

In this way, it is possible to use the Matlab function 'regionprops', which returns a lot of information, including:

- 'Area': Actual number of pixels in the region, returned as a scalar.
- 'BoundingBox': Position and size of the smallest box containing the region.
- 'Centroid': Center of mass of the region.
- 'Perimeter': Distance around the boundary of the region returned as a scalar.

2.4.1.3. Example for evaluating the volume of the image of a balloon inflated with air with a nominal flow rate of 100lN/h, approximating the volume to a sphere

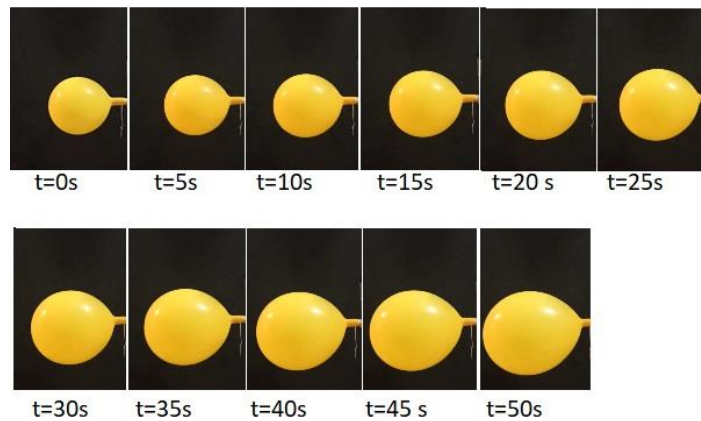


Figure 2.19. Photo balloon filled with air at different times.

Figure 2.19 shows in sequence the images of the inflation of an air balloon with a nominal flow rate of 100 lN/h. The instant $t=0$ s already coincides with a non-zero volume of the balloon. This was done to avoid an incorrect evaluation of the volume from the code written in Matlab. Especially for larger volumes, it is immediately noticeable that the shape of the balloon becomes more and more distant from a sphere.

Each image shown in Fig.2.19 was processed as indicated below.

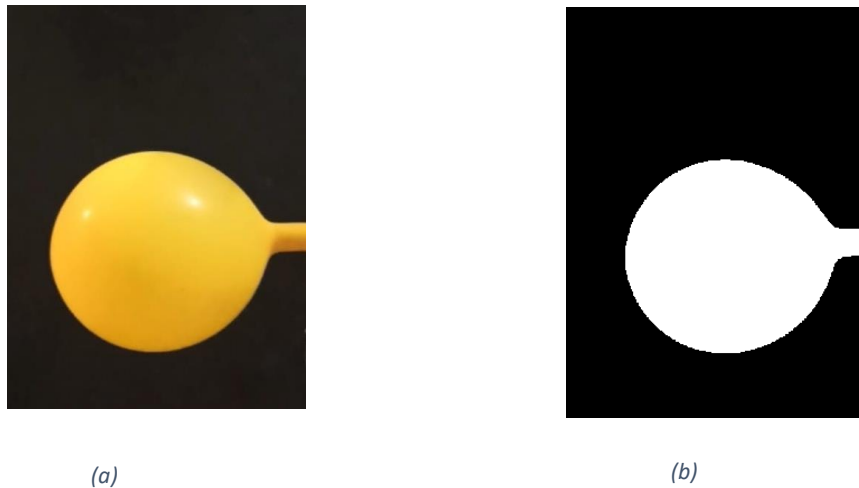


Figure 2.20: Picture of an air balloon at $t=0s$: (a) original, (b) binarized.

Figure 2.20 shows an example of the original picture and its binarize version obtained with MATLAB. The main steps to obtain the volume of the sphere are:

- 1) Reading the image with Matlab
- 2) Assessing, from known image size, the proportion between mm and pixels
- 3) Cut off the part of the image that is not needed and could hinder the evaluation of the area
- 4) Transforming the image with the 'imbinarize' command
- 5) Use the functions 'RegionProps' to measure the desired area
- 6) Obtain the area of the maximum section of the balloon in pixels. To go from pixels to mm it needs a reference, which in our case will be the diameter of the nozzle (6mm). This area corresponds to the area of the maximum section of the balloon: $A = \pi \cdot r^2$
- 7) From this it is possible derive the radius and calculate the volume of the balloon: $V = \frac{4}{3} \pi \cdot r^3$

2.4.1.4. Results were obtained with the different gases at different flow rates

In each of the following graphs is the R^2 value, the coefficient of determination. This is a measure of how well a model can predict the data and is between 0 and 1, the higher the value, the better the approximation of the data.

The definition of R^2 is:

$$R^2 = 1 - \frac{SS_{resid}}{SS_{tot}}$$

Where SS_{resid} is the sum of the squared residuals from the regression and SS_{total} is the sum of the squared differences from the mean of the dependent variable (total sum of squares). Residuals are

the difference between the observed values of the response (dependent) variable and the values that a model predicts.

- Flowmeter 1 with air

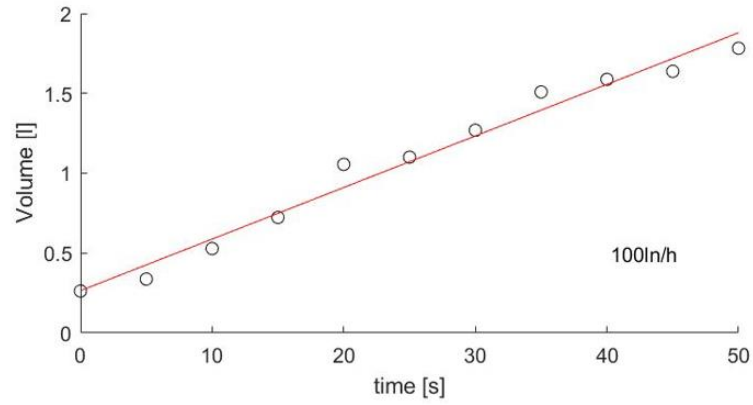


Figure 2.21. Computed volume versus time and linear approximation for the case of air and nominal flow rate 100 lN/h.

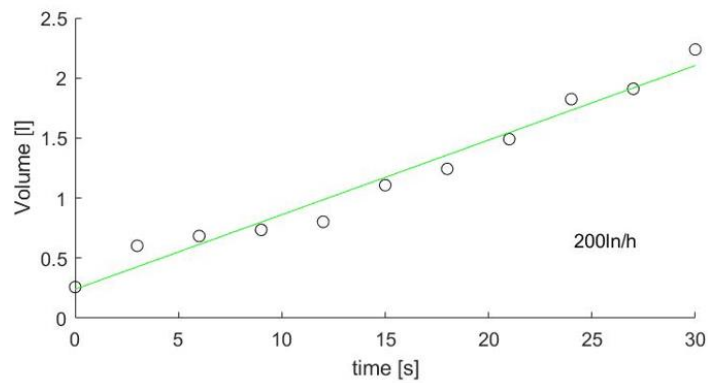


Figure 2.22. Computed volume versus time and linear approximation for the case of air and nominal flow rate 200 lN/h.

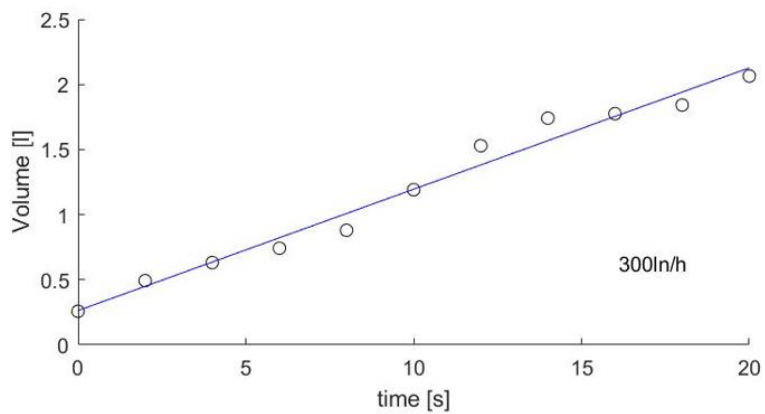


Figure 2.23. Computed volume versus time and linear approximation for the case of air and nominal flow rate 300 lN/h.

Table 2.9. Data evaluated for flowmeter 1 with air.

	Case 1	Case 2	Case 3
Nominal flow rate Q	100 ln/h	200 ln/h	300 ln/h
Real flow rate Q_r	116.27 ln/h	223.50 ln/h	335.60 ln/h
Absolute error E_A	16.27 ln/h	23.50 ln/h	35.60 ln/h
Relative error E_R	16.27%	11.9%	11.88%
R^2	97.7%	96.8%	97.67%

Case 1 shows the results for the case of air at a nominal flow rate of 100 l/h. It can be observed that the trend is increasing but the obtained data does not exactly fit a linear approximation. The real flow rate obtained with the linear approximation is 116.27 l/h leading to a relative error of 16.27%. The coefficient of determination is high, which means that the error in range assessment is due either to the image processing algorithm or to the images themselves.

Case 2 shows the results for the case of air at a nominal flow rate of 200 l/h. The real flow rate obtained with the linear approximation is 223.50 l/h leading to a relative error of 11.9%. The time interval in which blowing was observed is shorter. In this way, very similar volumes were obtained between tests, and very large volumes were avoided (for air this is not a problem but for methane or propane it is not very pleasant).

Case 3 shows the results for the case of air at a nominal flow rate of 300 l/h. The real flow rate obtained with the linear approximation is 335.60 l/h leading to a relative error of 11.88%. Again, R^2 has a rather high value, and the large relative error is caused by the volume assessment method.

- Flowmeter 2 whit propane

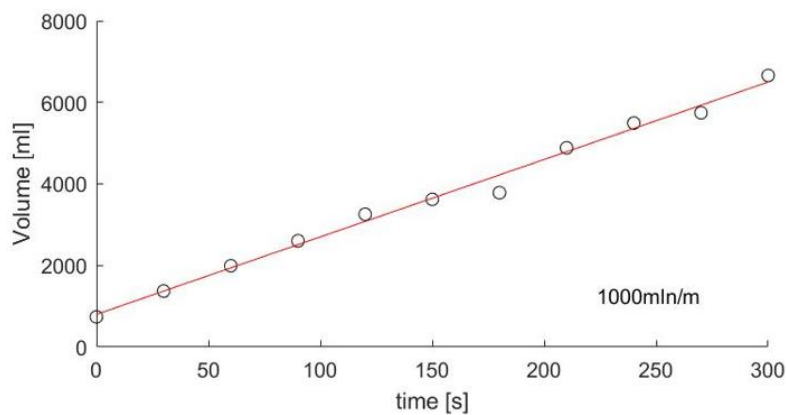


Figure 2.24. Computed volume versus time and linear approximation for the case of propane and nominal flow rate 1000 mlN/min.

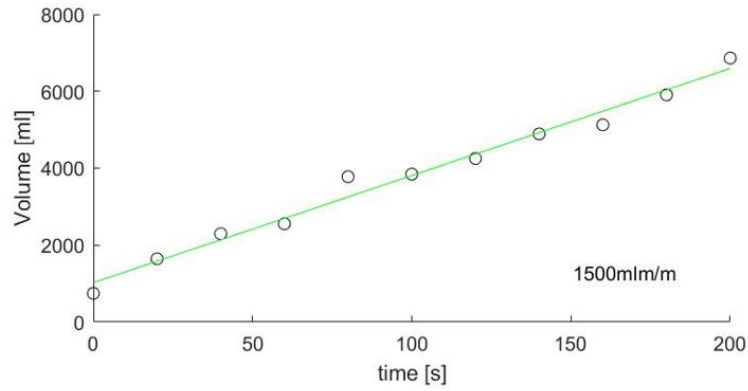


Figure 2.25. Computed volume versus time and linear approximation for the case of propane and nominal flow rate 1500 mlN/min.

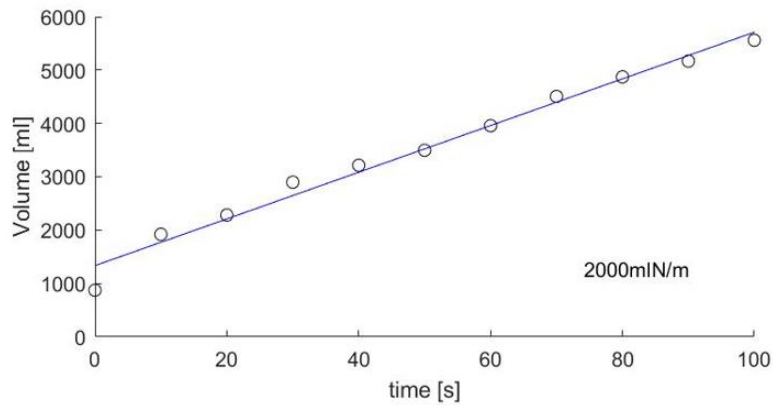


Figure 2.26. Computed volume versus time and linear approximation for the case of propane and nominal flow rate 2000 mlN/min.

Table 2.10. Data evaluated for flowmeter 2 with propane.

	Case 4	Case 5	Case 6
Nominal flow rate Q	1000 mln/min	1500 mln/min	2000 mln/min
Real flow rate Q_r	1139.60 mln/min	1670.80 mln/min	2625.80 mln/min
Absolute error E_A	139.60 mln/min	170.80 mln/min	625.80 mln/min
Relative error E_R	13.97%	11.37%	31.3%
R^2	99.1%	98.1%	98.3%

Case 4 shows the results for the case of air at a nominal flow rate of 1000 mln/min. The real flow rate obtained with the linear approximation is 1139.60 l/h leading to a relative error of 13.97%. Compared to the graphs of inflation with air, it is immediately apparent that the volume growth is more linear and that a much larger time interval has been observed, as the propane flow rate of flowmeter 2 is lower. The coefficient of determination is very high at 0.991.

Case 5 shows the results for the case of air at a nominal flow rate of 1500 mln/min. The real flow rate obtained with the linear approximation is 1670.80 mln/min leading to a relative error of 11.37%.

Case 6 shows the results for the case of air at a nominal flow rate of 2000 mln/min. The real flow rate obtained with the linear approximation is 2625.80 mln/min leading to a relative error of 31.3%, which is very consistent suggests that something is not working well.

- Flowmeter 2 with methane

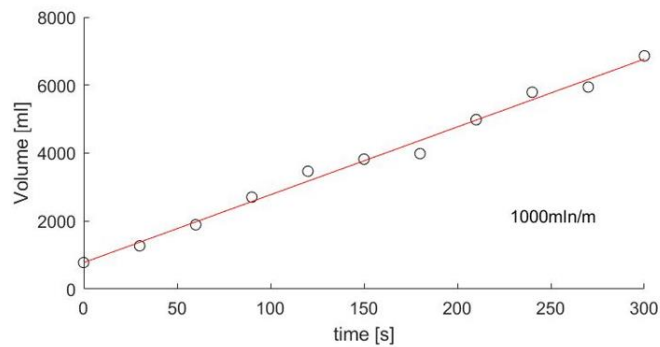


Figure 2.27. Computed volume versus time and linear approximation for the case of methane and nominal flow rate 1000 mlN/min.

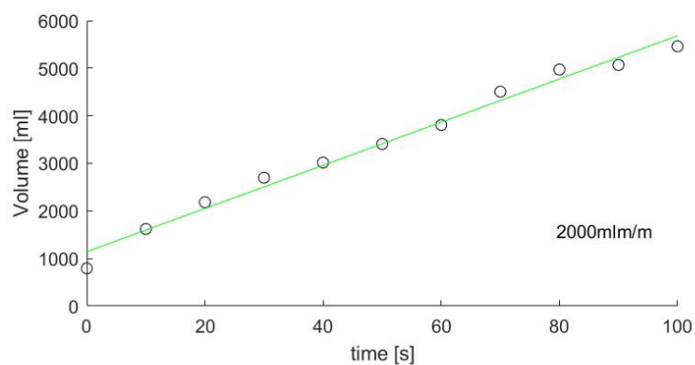


Figure 2.28. Computed volume versus time and linear approximation for the case of methane and nominal flow rate 2000 mlN/min.

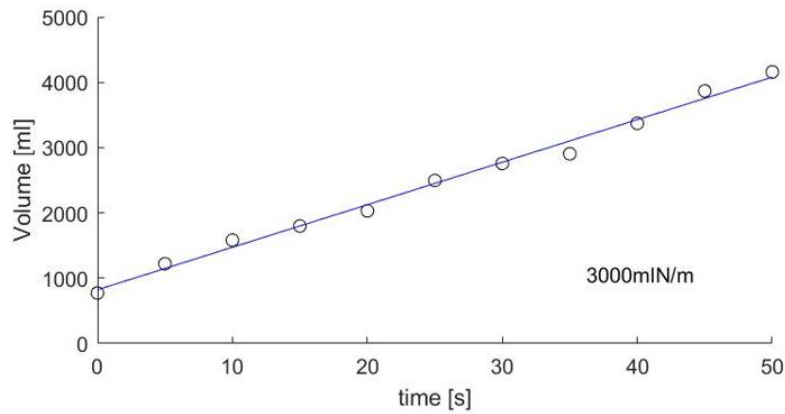


Figure 2.29. Computed volume versus time and linear approximation for the case of methane and nominal flow rate 3000 mlN/min.

Table 2.11. Data evaluated for flowmeter 2 with methane.

	Case 7	Case 8	Case 9
Nominal flow rate Q	1000 mln/min	2000 mln/min	3000 mln/min
Real flow rate Q_r	1197.5 mln/min	2721.20 mln/min	3908.20mln/min
Absolute error E_A	197.5 mln/min	721.20 mln/min	908.20 mln/min
Relative error E_R	19.75%	36.06%	30.27%
R^2	99.0%	98.5%	99.1%

The presence of a large relative error in the evaluation of the volume of the methane balloon as a function of time, for a flow rate of 2000 mlN/min there is a relative error of 36%, at the same time as an R^2 which is however high, has shown that there can be an error in the operation of the digital flowmeter 2 with methane. Even with a more sophisticated volume assessment, there will be a non-negligible relative error.

2.4.1.5. Calculation of balloon volume through the revolution of the profile parameterization

The presence of a very large relative error indicates that approximating the balloon to a sphere is either not a good idea or that the flowmeters are damaged and cannot measure correctly. For this reason, the images have been reprocessed more finely, resulting in much more accurate results.

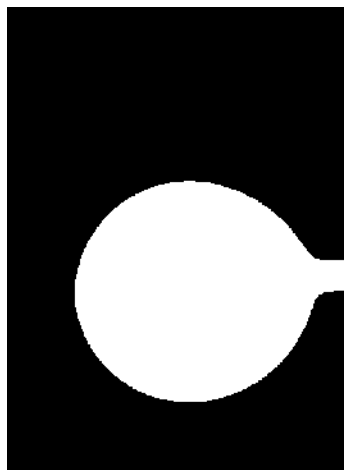
Example of image volume evaluation of a balloon inflated with air with a nominal flow rate of 100 lN/h at time instant $t = 0$ s, profile parameterization method

The images analyzed with this method are the same as before. The first part of the code is also the same. The procedure to obtain the volume, in this case, follows the next steps:

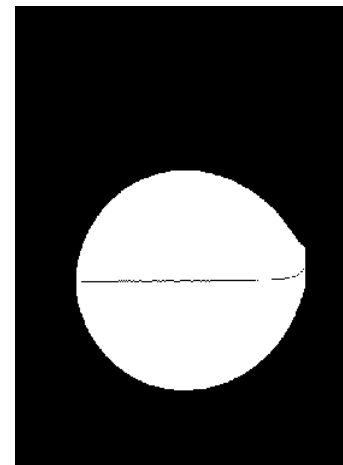
1. Reading the image with Matlab
2. Assessing, from known image size, the proportion between mm and pixels
3. Cut off the part of the image that is not needed and could hinder the evaluation of the area
Fig. 2.30a
4. Transforming the image with the 'imbinarize' command Fig.2.30b
5. Find the axis of the balloon around which to rotate Fig.2.30c
6. Parameterising the balloon profile Fig.2.30d
7. Create a solid obtained by rotating the parameterized profile around the axis of symmetry previously found Fig.2.30e
8. Finding the volume of the rotational solid



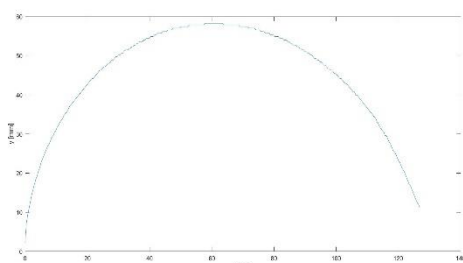
(a)



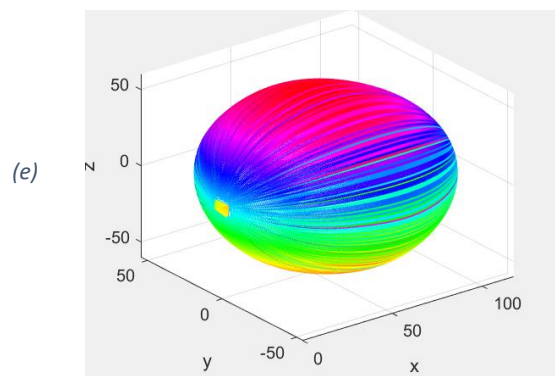
(b)



(c)



(d)



(e)

Figure 2.30. Balloon image processing: balloon photo(a); imbinarized image (b); balloon axis (c); parameterising the balloon profile (d); balloon volume in MATLAB environment (e).

The parameterization of the upper profile of the balloon was done in the following way:

- a. we take the portion of the image in which the balloon is contained, it is a matrix $M \times N$ composed of 0 (black pixel) and 1 (white pixel)
- b. fix a value of M (abscissa) and scroll through the whole column (ordinate), until the pixel value goes from 0 to 1, and when this occurs save the values of M and N in two vectors, x and y respectively
- c. repeat step b for all values of M
- d. once obtained the vectors x and y , it is now necessary to scale them concerning a new reference system that has as origin the intersection between the symmetry axis of the image of the balloon and the first value of M for which the passage from 0 to 1 occurred, and the new x -axis coincides with the symmetry axis found previously
- e. convert the x and y vectors from pixels to mm
- f. plot x and y gives the profile of the balloon in Matlab, and it is then possible to parameterize an equation
- g. the equation is rotated around the x -axis, which is also the symmetry axis of the balloon, thus obtaining a solid of revolution in Matlab, with which all the tools and functions in the software can be used.

- Flowmeter 1 with air

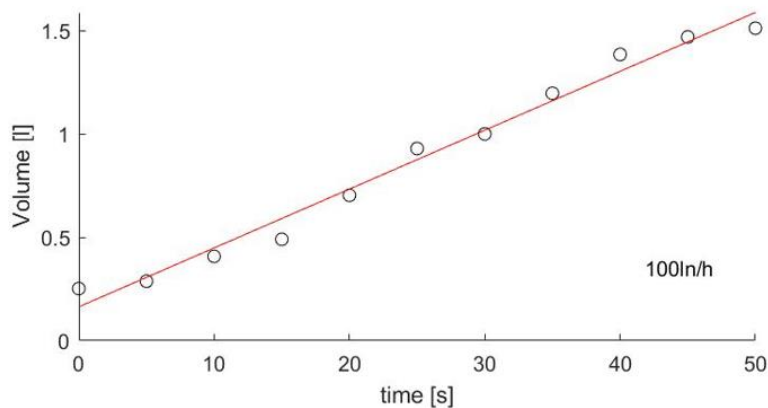


Figure 2.31. Computed volume versus time and linear approximation for the case of air and nominal flow rate 100 lN/h.

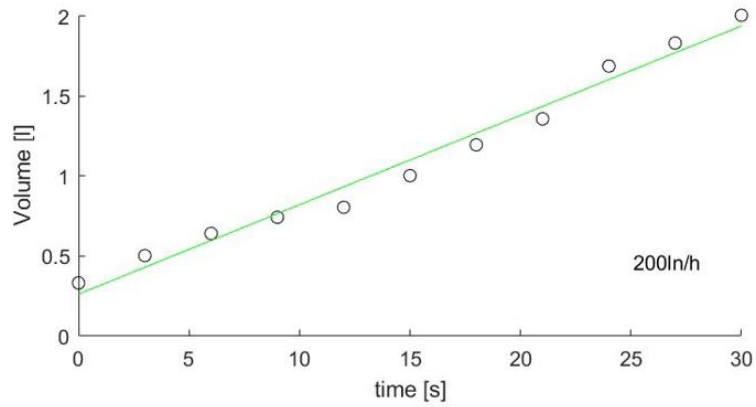


Figure 2.32. Computed volume versus time and linear approximation for the case of air and nominal flow rate 200 l/h.

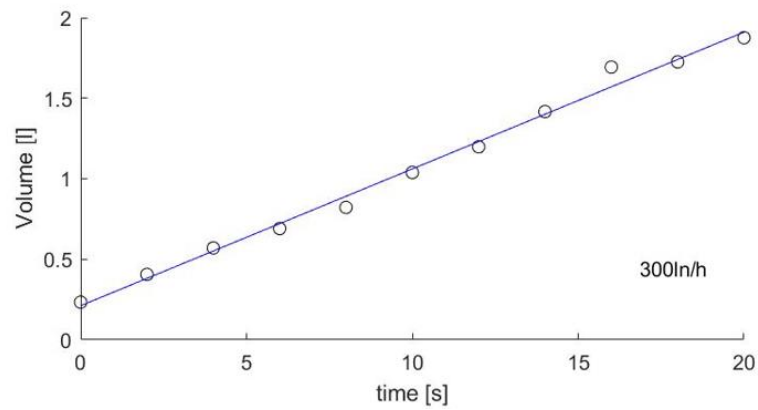


Figure 2.33. Computed volume versus time and linear approximation for the case of air and nominal flow rate 300 l/h.

Table 2.12. Data evaluated for flowmeter 1 with air.

	Case 1	Case 2	Case 3
Nominal flow rate Q	100 l/h	200 l/h	300 l/h
Real flow rate Q_r	102.62 l/h	204.91 l/h	305.77 l/h
Absolute error E_A	2.62 l/h	4.91 l/h	5.77 l/h
Relative error E_R	2.62%	2.45%	1.92%
R^2	98.31%	97.94%	99.2%

Case 1 shows the development of the volume as a function of the time of a balloon inflated with air with a nominal flow rate of 100 l/h. Analyzing the trend using a linear approximation, it is estimated that the flow is 102.62 l/h. This is a very acceptable result. The relative error of 2.62%

indicates that the volume approximation method is very valid and that the quality of the processed images is also good. The R2 value, which is also high, indicates that the linear approximation interpolates the real data well and that indeed the flow rate indicated by flowmeter 1 can be considered constant.

Even with a nominal flow rate of 200 l/h and 300 l/h, the evaluation of the volume as a function of time yielded good results, with relative errors of 2.45% and 1.92% respectively. The linear approximation appears to be very good, meaning that the digital flowmeter guarantees a constant flow rate without fluctuations.

- Flowmeter 2 with propane

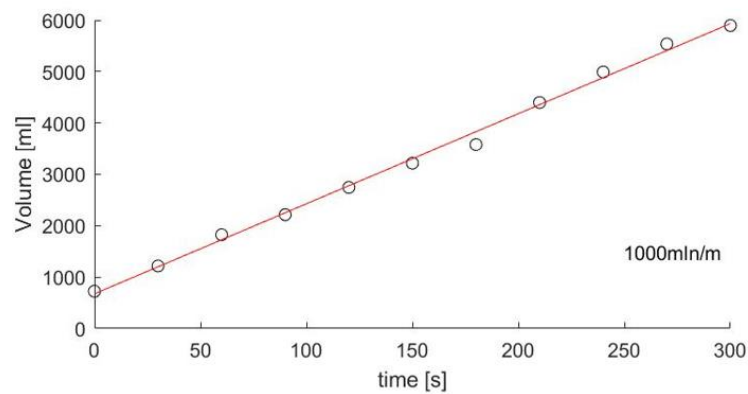


Figure 2.34. Computed volume versus time and linear approximation for the case of propane and nominal flow rate 1000 mlN/min..

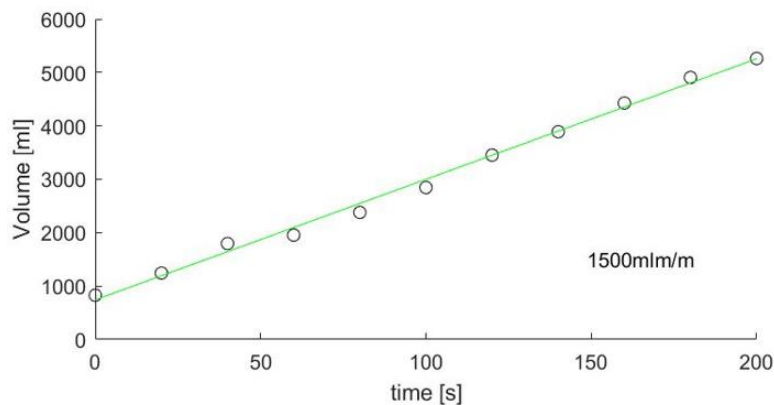


Figure 2.35. Computed volume versus time and linear approximation for the case of propane and nominal flow rate 1500 mlN/min.

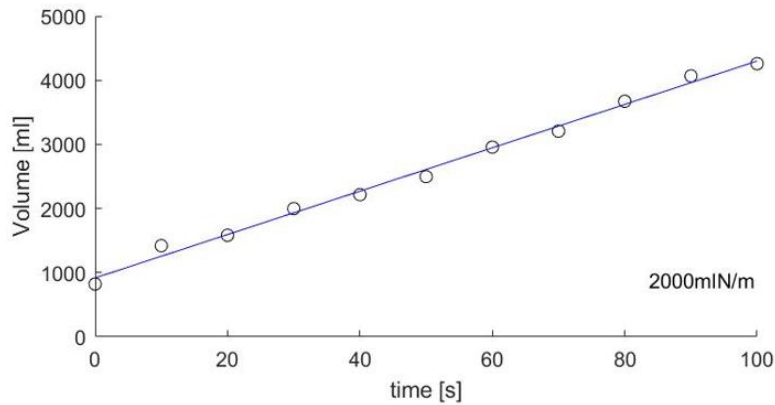


Figure 2.36. Computed volume versus time and linear approximation for the case of propane and nominal flow rate 2000 mlN/min.

Table 2.13. Data evaluated for flowmeter 2 with propane.

	Case 4	Case 5	Case 6
Nominal flow rate Q	1000 mlN/min	1500 mlN/min	2000 mlN/min
Real flow rate Q_r	993.45 mlN/min	1335.4 mlN/min	2027.4 mlN/min
Absolute error E_A	6.55 mlN/min	164.6 mlN/min	27.4 mlN/min
Relative error E_R	0.66%	2.94%	1.37%
R^2	98.81%	99.47%	99.39%

The nominal flow rates of propane, indicated by the digital flow meters, are 1000 mlN/min, 1500 mlN/min and 2000 mlN/min to which correspond, respectively, the values found by the linear approximation of volume versus time, 993.45 mlN/min 1335.4 mlN/min and 2027.4 mlN/min. For the first two cases, the flow rate was found to be lower than the nominal flow rate and for the last case higher. The relative errors are, however, acceptable.

- Flowmeter 2 with methane

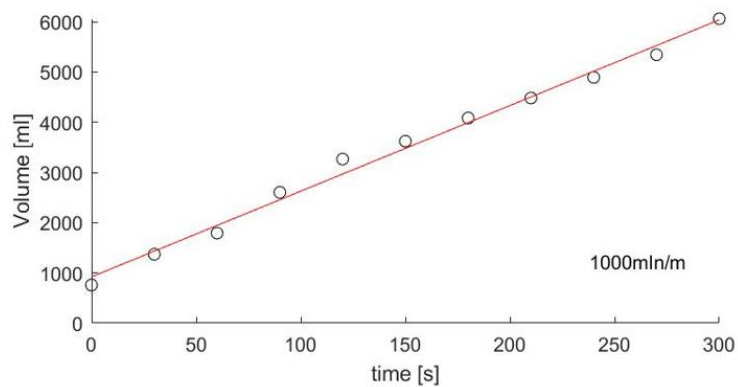


Figure 2.37. Computed volume versus time and linear approximation for the case of methane and nominal flow rate 1000 mlN/min.

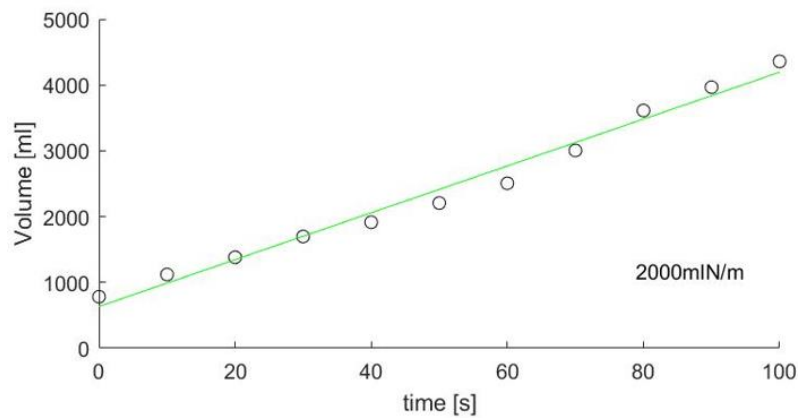


Figure 2.38. Computed volume versus time and linear approximation for the case of methane and nominal flow rate 2000 mlN/min.

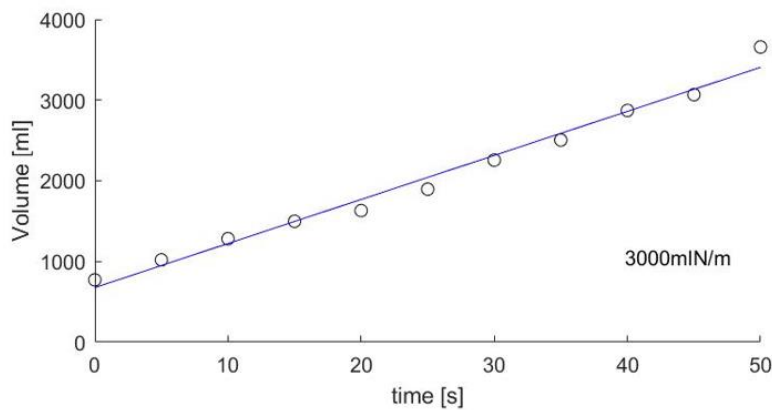


Figure 2.39. Computed volume versus time and linear approximation for the case of methane and nominal flow rate 3000 mlN/min.

Table 2.14. Data evaluated for flowmeter 2 with methane.

	Case 7	Case 8	Case 9
Nominal flow rate Q	1000 mln/min	2000 mln/min	3000 mln/min
Real flow rate Q_r	1023.0 mln/min	2135.9 mln/min	3275.4 mln/min
Absolute error E_A	23.0 mln/min	135.9 mln/min	275.4 mln/min
Relative error E_R	2.3%	6.7%	9.18%
R^2	99.17%	98.25%	98.37%

As can be seen from the new values obtained, the nominal flow rate is very similar to that assessed by the image processing. However, a small error is present, but this can be caused by a variety of factors involving both the instruments and the method of image processing.

For the methane flow, on the other hand, the relative errors are consistent even with the second volume estimation method. Comparing the various graphs for each flow rate of each fluid with the two methods shows that approximating the balloon to a sphere results in an overestimation of the volume and this becomes more pronounced as the volume increases.

Chapter 3. EXPERIMENTAL RESULT AND DISCUSSION

3.1. AIR JET ANALYSIS

This work investigates the effect generated by a local flow of air hitting a diffusive flame near the extinction of combustion. To give a better understanding of this process we shall study the nature of the regime, i.e. whether the airflow presents laminar (L), transient (TR), or turbulent (TU) patterns.

To obtain flow visualizations from the airflow it was necessary to pollute it with oil droplets by connecting an oil tank to the outlet of flowmeter 1. As the airflow enters the reservoir, it carries oil molecules (of approximately 1-micrometer diameter) and these can be reflected by laser sheet without affecting its fundamental properties including the density.

The images of the airflow mixed with oil droplets were recorded with the Phantom camera model v611, see a picture in Figure 3.1. In each image, it can be observed the nozzle, which has an external diameter of 6 mm. The images are then processed with the PCC and PVP software provided by Phantom. It is important to remark that each image includes the nozzle, which has an external diameter of 6 mm and can be used to get the appropriate scaling of the images.



Figure 3.1. Phantom V611.

Table 3.1 shows the set of camera parameters that led to these images.

Table 3.1. Camera parameters.

Resolution	800x600
Bits per pixel	12
Sample rate [fps]	600
Exposure [μ s]	1600

EDR [μs]	700
Frame Delay [μs]	0
Auto Exposure	Off

The flow appears as an emulsion between air and oil droplets. From the images depicted in Figure 3.4, however, one can observe the transition from laminar to a turbulent regime that takes place when the flow rate increases using the digital flowmeter 1 from 50 (a) to 400 (f) l/h (normal liters per hour). The performance of the diffusion flame extinction shall vary depending on the regime of the airflow, as it will be shown below.

To give a brief description, it will be shown that for a laminar airflow, the flame appears to be pierced by the jet without being extinguished. A hole of similar diameter to that of the nozzle is created in the flame, with the circular outline changing from an orange to a blue color, so that the flame becomes premixed instead of diffusive.



Figure 3.2. Detail of the flame 'pierced' by the laminar air jet.

Fig. 3.2 shows the flame with the central hole caused by the transverse air jet, which is completely in the laminar regime. The flame does not change its main characteristics such as inclination, characteristic length, or color, its volume remains unchanged except for the area directly hit by the jet.



Figure 3.3. Detail of flame affected by turbulent air jet.

For the same fuel flow rate and increasing airflow rates, in addition to having a greater 'sweep of fuel particles' leading to a local mixture that is too poor for combustion to take place, there is also a greater increase in the region affected by the transverse air jet. The latter belongs to a turbulent regime. In this work, it has been observed that a laminar air regime is unable to extinguish the flame as the diameter of the fuel outlet section is much larger than that of the air. As can be seen from Fig. 3.3, as well as involving a larger flame volume, the flame itself has a turbulent behavior which it would not have in the absence of the air jet, as can be seen from the flame tongues, and the brightness of the flame decreases.

The transition between laminar (L) and turbulent (TU) airflow regimes is not clear-cut. There is a transient that affects the instability of the flame. Extinguishing it through a non-laminar jet is more difficult to detect and forces the flame to have numerous tongues of fire before blowoff.

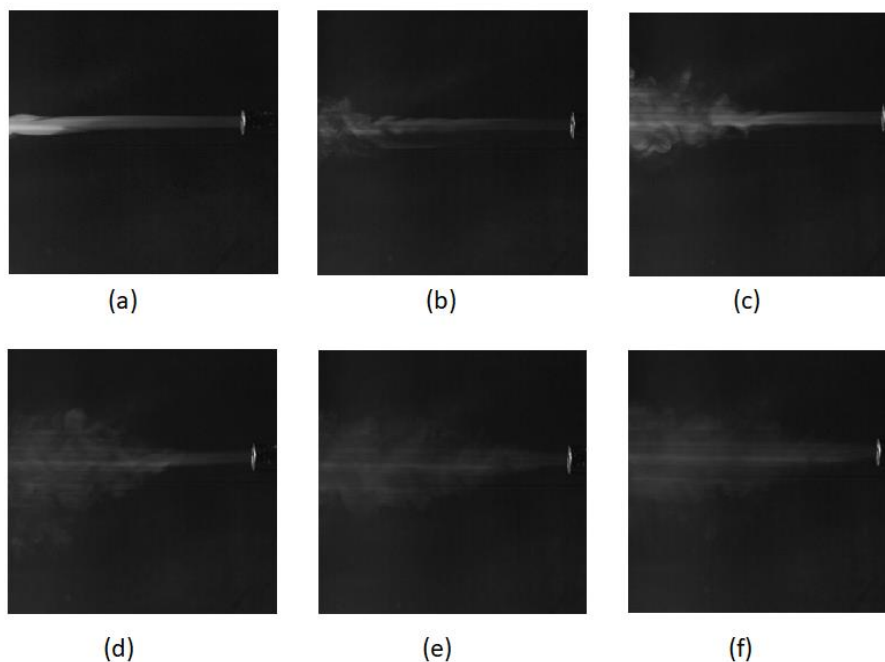


Figure 3.4. Airflow whit oil at different flowrates: 50 (a), 100 (b), 150 (c), 200 (d), 300 (e), and 400 (f) l/h.

From the images presented in Figure 3.4, it can be seen that the airflow changes in nature over the analysis range of this work. This affected the assessment of flame extinction, in fact in some ranges of transverse airflow an anomalous blow-off behavior was sharply observed, which is also very far from certain results in the bibliography. It is therefore impossible to analyze flame extinction without taking into account the nature of the airflow when this phenomenon occurs. Therefore, we focus first on the analysis of the air jet near the region where the propane or methane flame occurs.

3.1.1. Analysis of Air jet behavior near the fuel nozzle of diameter 10 mm and $z=0$

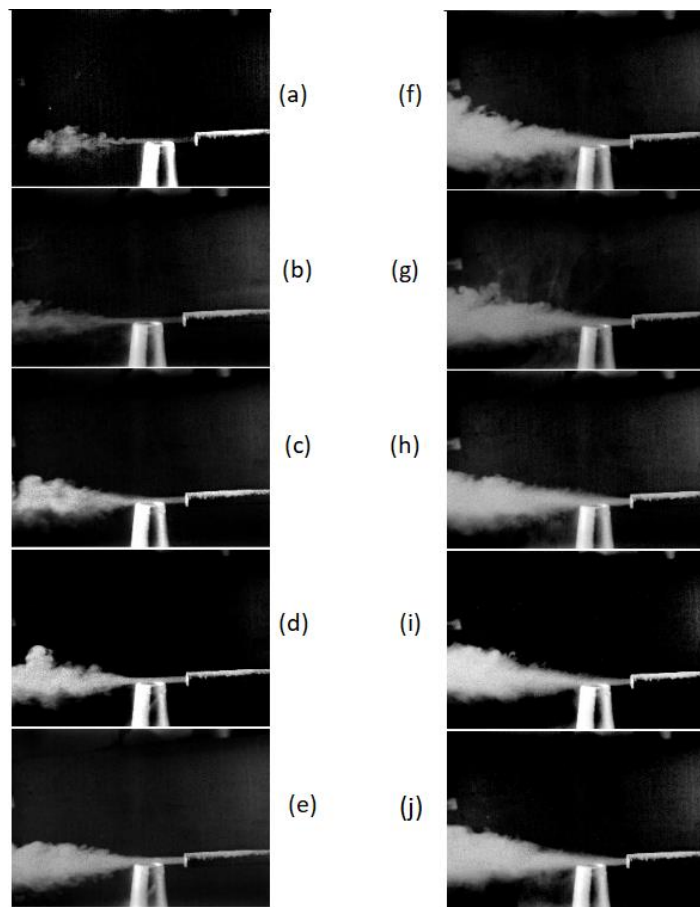


Figure 3.5. Motion field airflow $d=10$, $z=0$ mm for 4.7 (a), 6 (b), 7.5 (c), 9 (d), 10.5 (e), 11 (f), 12.5 (g), 14.8 (h), 15.5 (i) and 17 m/s (j).

In Figure 3.5 the snapshots illustrate the regime of the air jet near the region where the propane or methane flame occurs increasing the flow rate. The relative height is $z=0$ mm while the diameter of the fuel nozzle is 10mm. As the velocity of the air jet increases, it can be observed that, first of all, the distance at which the flow begins to have turbulent behavior shortens, and, secondly, there is a greater volume of influence. By tracing the field of motion of the air jet it is possible to observe especially in cases of Figures 3.5 (f), (g), (h), (i), (j) (velocities greater than 11 m/s) that

for high values of the air jet there are air motions also in the area where the fuel nozzle creates a real shield. This region is very important and greatly influences the ability of the flame to resist and not to extinguish (down-wash phenomenon).

From the images of Fig. 3.5, a clear difference in the field of motion in the area of interest can be seen, especially for speeds between 3 and 10.5 m/s. Above this value, a further increase (up to 10.5 m/s) in the field of motion is observed. Above this value, a further increase (up to 17 m/s) does not influence the observed volume too much. In Figures 3.5 (a) and (b) the low spill velocities mean that not all of the spill section of the fuel nozzle is directly affected, which caused the flame to be more stable, adapt to the conditions, and not extinguish.

Therefore, the flame characteristics are influencing the blow-out limits. The blow-out limit is defined as the minimum flow air velocity necessary to extinguish the flame. By changing the flow rate of the gases is possible to represent a graph to analyze this limit.

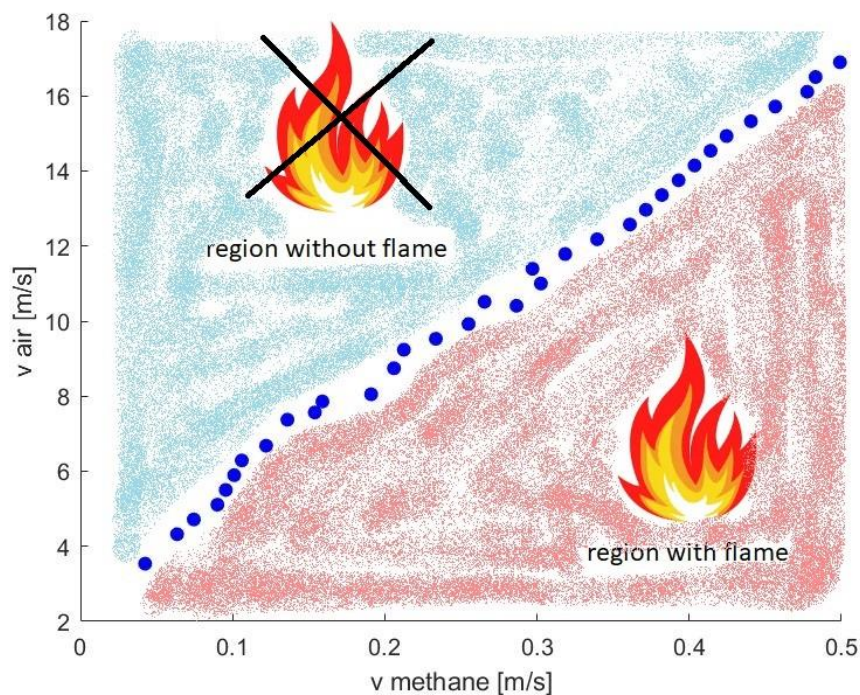


Figure 3.6. Detail of the flame and non-flame regions of the blowout limits of a methane flame with $d=10$ mm and $z=0$.

Figure 3.6 shows graphically an example of this representation (flame/no flame). The details about how to obtain this representation will be described in detention in section 1.4.

In addition to the blow-out limits obtained experimentally, it is interesting to divide the diagram in which the flame extinction limit is indicated into three main regions. Each of them represents

a different kind of flame behavior. Figure 3.7 represents the minimum air velocity that extinguishes the flame at the respective fuel velocity together with the zone divisions.

Appendix 1 shows the error of the three tests to compute Figure 3.6, 3.7, or 3.8.

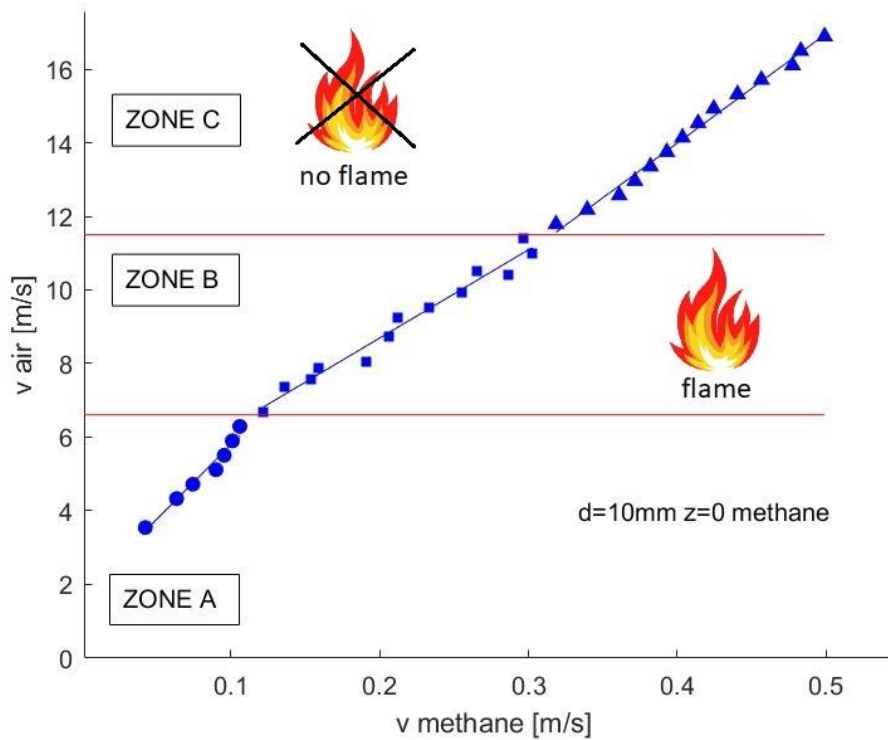


Figure 3.7. Blow-out limit with air regions.

The different zones are defined as follow:

- Zone A: range airflow velocity (from 0 m/s to 6.6 m/s). For an air velocity of less than 3 m/s the airflow is laminar throughout the region affected by the flame. It was therefore not possible to investigate the blowoff. In the range 3-6.6 m/s there is a turbulent air jet from the end of the outlet section of the fuel nozzle, while the airflow along it is laminar, see Figure 3 (a) and (b). The slope of the linear interpolation of the blowout limits of this zone is $k_{A,10}=40$.
- Zone B: range air velocity (from 6.6 m/s to 11.5 m/s). In this range of air velocity, there is a flow of air that gradually becomes turbulent also along the entire outlet section of the fuel nozzle, as depicted in Figures 3 (c), (d), (e), and (f). The slope of the linear interpolation of the blowout limits of this zone is $k_{B,10}=27$.
- Zone C: from 11.5 m/s. Above this escape velocity, the airflow belongs to a turbulent regime and it behaves similarly to a further increase in velocity, as shown in Figures (g), (h), (i), and (j). The slope of the linear interpolation of the blowout limits of this zone is $k_{C,10}=25$.

The Observation on extinguishing limits can be summed up as follows.

- 1) From the evaluated points that are part of zone A, it can be seen from the slope of the linear approximation, that a large increase in air velocity is required to extinguish an increasing flow of fuel. In this zone, the still laminar regime allows the flame to 'dodge' the air and survive more easily.
- 2) The points in Zone B have high variability, since the volume in which the turbulent regime occurs (the latter is not fully developed) increases as the air velocity increases. Despite this, macroscopically it is observed that as the methane escape velocity increases, an increase in the air escape velocity is necessary to obtain flame extinction.
- 3) The points evaluated in zone C are the ones to be considered the most reliable, precisely because there is a turbulent air regime in the entire zone that affects the flame. The slope of the linear approximation of the points is smaller than in zone A, while it is very similar to that of zone B. This allows us to evaluate the trend of blowout limits between zones B and C together. In all subsequent graphs, the points of these two zones only will be shown and the A-zone limits of each tested configuration will be cut off due to their unstable and not very repetitive measurement.

3.1.2. Influence of the nozzle diameter

Now we pay attention to the influence of the diameter of the nozzle. To do so three different diameters were used: 10, 15, and 20 mm, and $z=0$.

The following images show the flame extinction limits for the 15 mm and 20 mm diameters at $z=0$. While the comments made for the 10 mm case apply, it is important to note that the zone limits have changed. This is because the outlet section of the fuel nozzle is larger and therefore the region in which the flame develops changes.

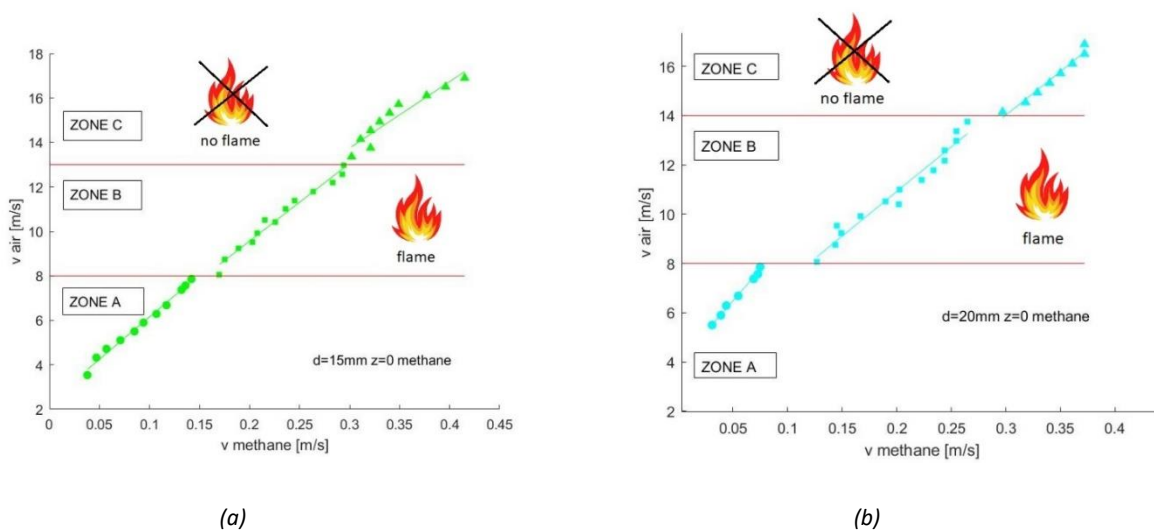


Figure 3.8. Blow-out limit with air regions $d=15$ (a) and $d=20$ mm (b).

From the results depicted in Fig. 3.8, it can be seen that in ZONE A, as the diameter increases, the flame can be stable at lower speeds. This result is the most important difference between the blow-out limits in a crosswind flame configuration in which the limit speeds remain unaffected to diameter changes. The reason for this lies in the fact that a laminar jet of air or in any case one that is not turbulent is not able to involve the entire outlet section of the fuel nozzle and the flame can therefore move to the areas with the lowest airflow field. For this reason, from now on when comparing graphs with different fuel nozzle diameters, ZONE A will not be considered as also expressed above for the case with d 10 mm.

Comparing in Figure 3.7 ($d=10$ mm) and Figures 3.8 (a) and (b) for $d=15$ and 20 mm respectively, in the different zones A, B, and C have a different trend of the limit points:

- ZONE A: there is an increasing growth rate as the diameter increases. This is because more air is required to extinguish the flame, as it has a larger base and is, therefore, more stable. The slopes of the linear interpolations of the blowout limits of this zone are $k_{A,15}=44$, and $k_{A,20}=50$.
- ZONE B: this transition zone increases as the diameter increases, and also in these cases, there is a high dispersion of the points. The slopes of the linear interpolations of the blowout limits of this zone are $k_{B,15}=33$, and $k_{B,20}=36$.
- ZONE C: the points have a linear trend, as the airflow is now a little variable and completely turbulent. The slopes of the linear interpolations of the blowout limits of this zone are $k_{C,15}=30$, and $k_{C,20}=35$.

Table 3.2. Slopes in different zones A, B, and C for the three diameters tested and airflow located at $z=0$ mm.

Diameter	Zone A	Zone B	Zone C
10 mm	$k_{A,10}=40$	$k_{B,10}=27$	$k_{C,10}=25$
15 mm	$k_{A,15}=44$	$k_{B,15}=33$	$k_{C,15}=30$
20 mm	$k_{A,20}=50$	$k_{B,20}=36$	$k_{C,20}=35$

It is necessary to discuss a novel phenomenon that takes place in the transition from ZONE A to ZONE B for the three cases with different diameters. It can be observed that as the diameter increases, the distance between the blowout limits between the two zones increases. If for the case with d 10 mm the transition from zone A to zone B is not very marked and the points are close together, in the cases with diameters 15 and 20 the limits move apart creating a discontinuity between the flame limit points. For the diameter $d=15$ mm the gap is worth a range in terms of fuel spillage velocity of 0.3 m/s while for the case with d 20 mm this range is 0.6 m/s. The reason for this may be explained in terms of how the laminar air-jet disappears and starts being transient

and turbulent, thus exponentially increasing its region of influence on the fuel exit section. This turbulent regime increases in the absolute value of the fuel exit velocity required to sustain the flame, and since for the 20 mm case there are lower absolute values of fuel, the phenomenon is more pronounced.

The formation of the three zones A, B, and C are now being investigated.

The reason for these new zones is immediately clear when describing the airflow in Figures 3.9 and 3.10. Since the position of the combustor is fixed, by applying the nozzle with the largest outlet section diameter, it is closer to the air nozzle but also further away from the opposite end. This aspect is very marked in the case of the 20 mm diameter, which has a very large ZONE B (Figure 3.8 (b)).

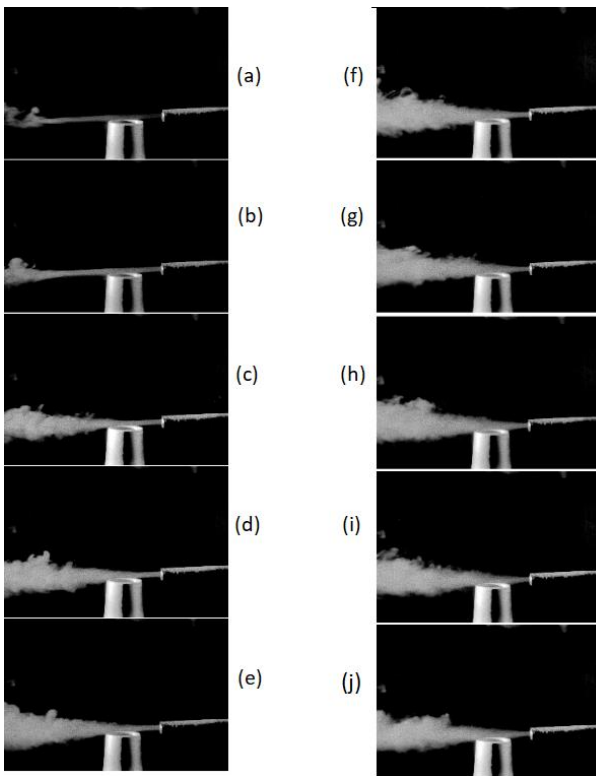


Figure 3.9. Motion field airflow $d=15\text{ mm}$ $z=0\text{ mm}$.

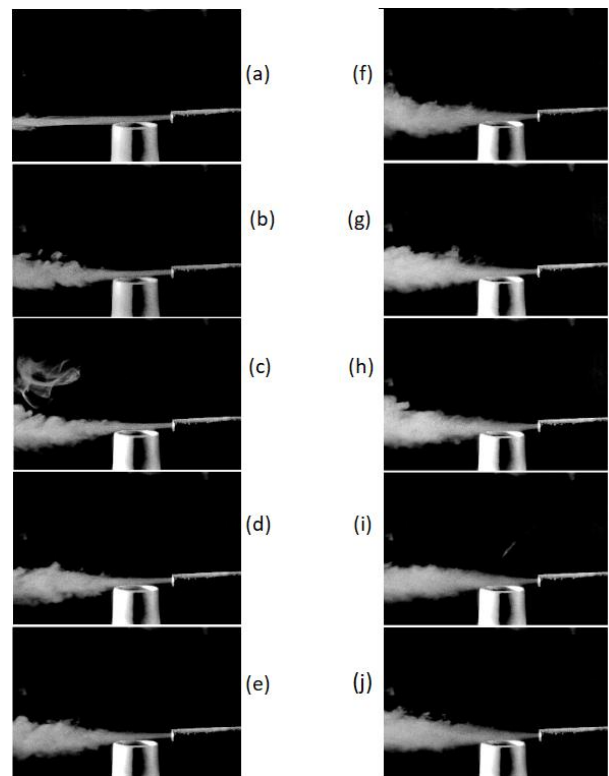


Figure 3.10. Motion field airflow $d=20\text{ mm}$ $z=0\text{ mm}$.

Each snapshot in Figures 3.9 and 3.10 was obtained with the air velocities given in Table 3.3, which are the same as the 10 mm case to make a targeted comparison.

Table 3.3. Airflow velocities of Figures 3.9 and 3.10.

(a) 4.7 m/s	(b) 6 m/s	(c) 7.5 m/s	(d) 9 m/s	(e) 10.5 m/s
(f) 11 m/s	(g) 12.5 m/s	(h) 14 m/s	(i) 15.5 m/s	(j) 17 m/s

From Figures 3.9 and 3.10 it can be observed that even in these cases, once an air velocity of 11 m/s has been exceeded, the air behavior remains unchanged, which results in the blow-out diagram in the linearity of the extinction points. On the whole, it can be observed that, however, by analyzing the extinction limits more macroscopically, a good linear approximation is obtained for all the cases and it is, therefore, possible to compare these data with others present in the bibliography, obviously paying attention to some precautions due to the different nature of the airflow.

3.1.3. Influence of the nozzle distance

Apart from the influence of the fuel diameter, the distance of the nozzle will be also analyzed. To that end, we studied a nozzle fuel of $d=10$ mm while the airflow is located at $z=2.5$ and $z=5$ mm.

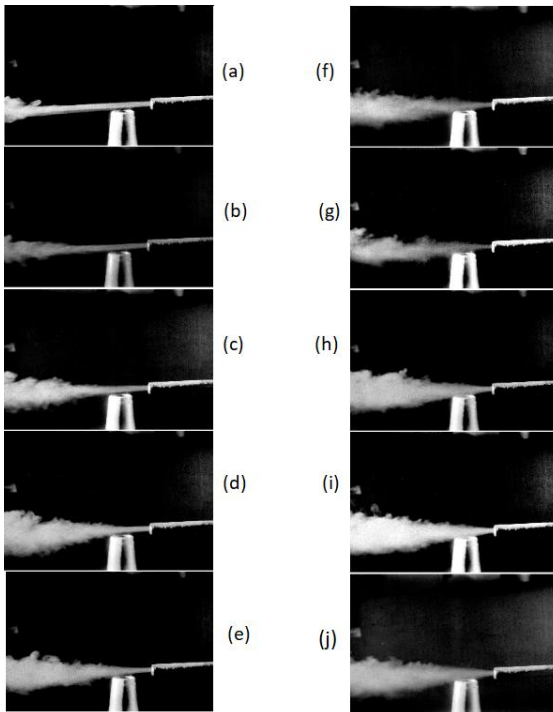


Figure 3.11. Motion field airflow $d=10$ mm $z=2.5$ mm.

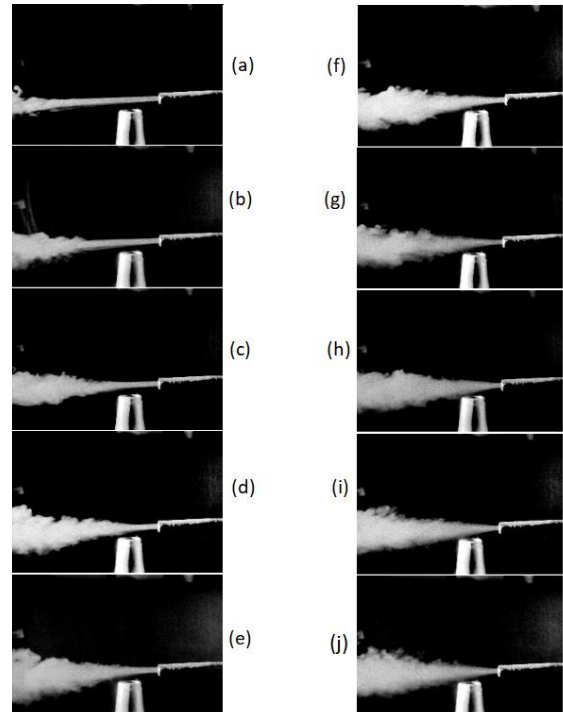


Figure 3.12. Motion field airflow $d=10$ mm $z=5$ mm.

Each snapshot in Figures 3.11 and 3.12 was obtained with the air velocities given in Table 3.4.

Table 3.4. Airflow velocities of Figures 3.11 and 3.12.

(a) 4.7 m/s	(b) 6 m/s	(c) 7.5 m/s	(d) 9 m/s	(e) 10.5 m/s
(f) 11 m/s	(g) 12.5 m/s	(h) 14 m/s	(i) 15.5 m/s	(l) 17 m/s

In Figures 3.11 and 3.12, the relative height is $z=2.5$ and 5 mm, respectively while the diameter of the fuel nozzle is constant at $d=10$ mm.

The effect of increasing the axial distance from $z=0$ mm to 2.5 and 5 mm is explained as follows. The air nozzle away from the fuel nozzle increases the velocity range so that the air jet travels through the entire section of the fuel nozzle in a laminar regime. When a velocity of 11 m/s is reached, see Figures 3.11 and 3.12 (f), it is observed that the flow is turbulent throughout the region of flame activity, it will be seen later how this will affect the blow-off.

Comparing Figures 3.11 and 3.12 it can be observed that in the latter, for each value of blow-off velocity there is a region near the fuel nozzle exit section which is not affected by air and does not interfere directly in this area.

In contrast to the case with $z=0$, in the two cases of $z=2.5$ mm and $z=5.0$ mm, it can be seen that there is no air motion field present in the downwind region of the fuel nozzle, this greatly influences the down-wash behavior of the flame, as can be seen from the next figure as z increases the region of the v/v graph in which methane combustion can survive increases greatly.

When comparing the extinction limits of the methane flame as z changes, it was decided not to consider the extinction limits at airflow velocities below 6 m/s. This choice resulted from two observations. Firstly, a laminar airflow regime creates too much variability in the points of the graph and homogeneous results are not obtained in this area. Secondly, as z increases, as does the diameter, the flame is not extinguished because the air jet is localized in too small a volume and therefore its field of motion is also too small.

For the reasons given above, it does not make sense to investigate the flame extinction beyond a distance z of 5 mm. As will be seen in the blowout diagrams, within the range of the air velocities given by the digital flowmeters, a flame extinction is never obtained. For completeness, the air velocity ranges near the fuel nozzle at $z=2.5$ mm and $z=5$ mm are shown for fuel nozzle blow-out section diameters of 15 and 20 mm.

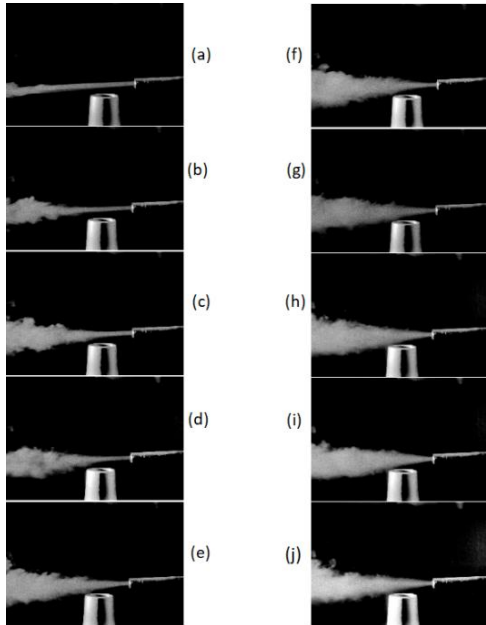


Figure 3.13. Motion field airflow $d=15\text{ mm}$ $z=2.5\text{ mm}$.

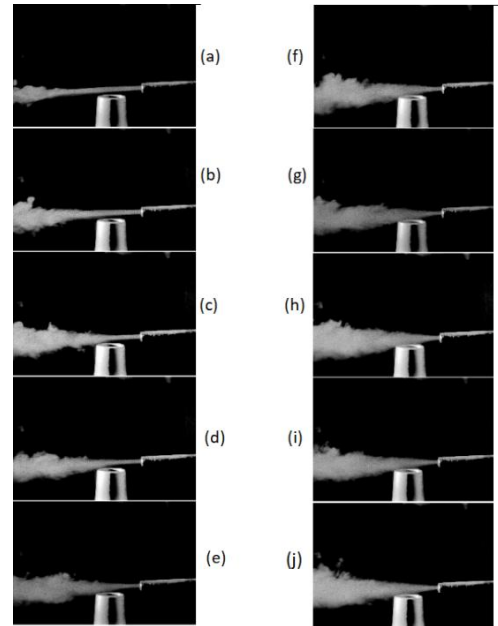


Figure 3.14. Motion field airflow $d=15\text{ mm}$ $z=5\text{ mm}$.

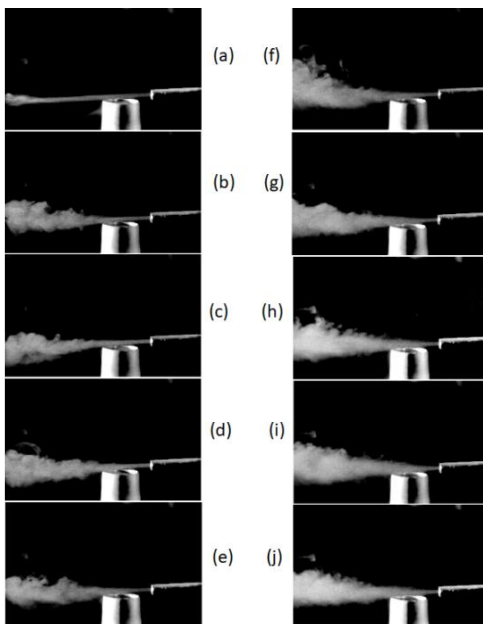


Figure 3.15. Motion field airflow $d=20\text{ mm}$ $z=2.5\text{ mm}$.

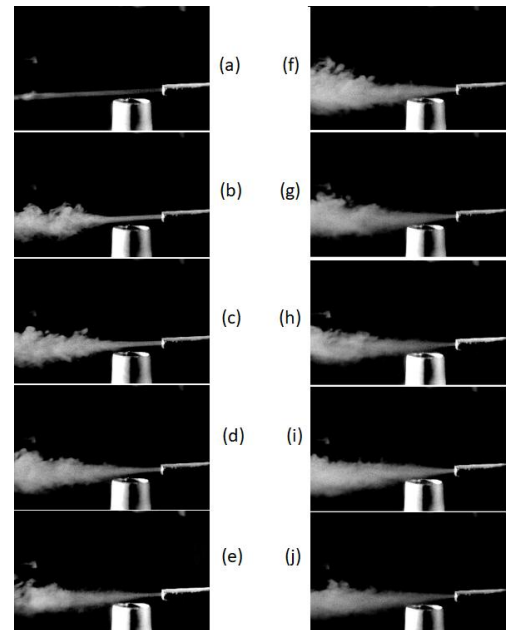


Figure 3.16. Motion field airflow $d=20\text{ mm}$ $z=5\text{ mm}$.

The observations made for the airflow fields in the vicinity of the 10 mm diameter fuel nozzle also apply to these cases. Comparison of the images shows that the fuel nozzle has no direct influence on the airflow field, i.e. there is no change in the flow lines of the air jet, whether turbulent or laminar, as the diameter increases. A flame with a larger base, however, will have more room to survive and to adapt to the airflow field, which remains more or less unchanged.

This effect, together with the lesser influence of the air on the flame as z increases, leads to a very large region of the case with d 20 mm in which the flame survives.

A completely different matter is in the presence of a uniform crosswind which also involves part of the fuel nozzle or burner. When the latter become larger, they can give more shelter to the flame in the area opposite where the wind is coming from.

3.2. ANALYSIS OF DATA OBTAINED FROM FLAME EXTINGUISHING POINTS

This section reports the evidence obtained from the points at which flame extinction with the transverse air jet was evaluated. It was necessary to obtain from the volumetric flow rates displayed by the digital flowmeters, the velocities of escape of the fuel (methane or propane) and the airflow. By using the bulk velocity, it is easy to highlight the characteristics of the phenomenon which will be described below, and it is also easier to compare the results of this work with those given in other research papers in the bibliography.

The units of measurement of the flow rates evaluated by the digital flowmeters are lN/h (normal liters per hour) for airflow and mln/min (normal milliliters per hour) for methane and propane. The conversion to m/s was performed knowing the diameter of the outlet section of the respective nozzles, from which it was possible to calculate the area of the outlet section. The normal conditions refer to a temperature of 20 °C and pressure of 101325 Pa, i.e. 1 atm.

The points of extinction of the flame are shown on different graphs along the section which have on the x-axis the speed of the fuel in m/s, on the y-axis the speed of the air also in m/s, e.g. see Figure 3.17. Each point was obtained from the average of three different tests. The blowout limit is indicated with a circle in the graphs; it represents the last point at which there is stable combustion for at least three minutes. Three different nozzles with diameters of 10 mm, 15 mm, and 20 mm were used for the fuels. To prevent the nozzle diameter from changing due to combustion (soot) residues, frequent nozzle cleaning was used. The design of the combustor/nozzle system gives the possibility of varying the height of the air nozzle about the fuel nozzle while keeping them at right angles to each other. In this work, shutdown points were analyzed at 6 different relative heights indicated by z , the z -axis passing through the axis of the fuel nozzle. The heights tested are $z=0, 1, 2, 3, 4,$ and 5 mm. This variation was illustrated and explained in more detail in chapter 2, Experimental setup and methodology.

The example shown in Figure 3.17 refers to the evaluation of the extinguishing of a methane flame with a fuel nozzle of 10 mm and the distance between the axes of the two nozzles equal to

0 mm ($z=0$ mm). This plot is the same as Figure 3.7 when we described the three zones A, B, C. However, we will focus now on the extinction process to compare the linear dependence as a function of three parameters, that is to say, fuel nozzle diameter, a distance of the airflow jet from the nozzle, and type of fuel (methane and propane). To perform a precise methodology, the key points to obtain Figure 3.17 are as follows:

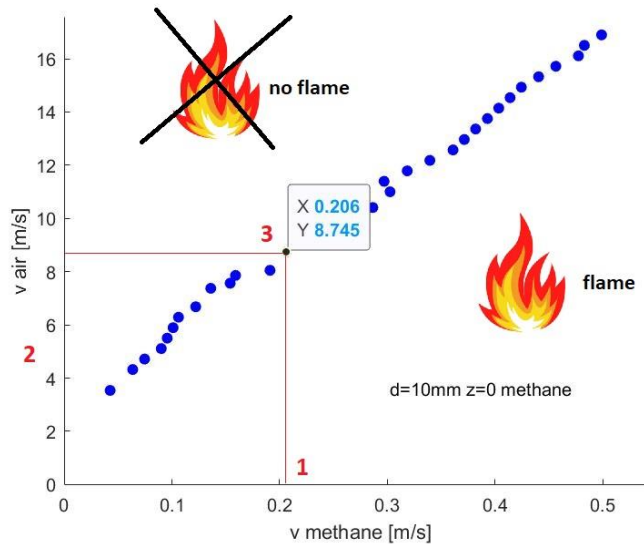


Figure 3.17. Blowout propane flame with diameter nozzle 10 mm and $z=0$ mm.

1. Fix the methane velocity. In this example, it is 0.206 m/s (1).
2. Gradually increase the airflow velocity (2). It is very important to increase the speed very slowly, especially near the shutdown, because the inertia of the fluid can lead to an incorrect assessment.
3. As soon as the flame is close to extinction, which is also indicated by a typical jagged noise, wait three minutes to see if combustion is stable. In this case, this occurs at a transverse air jet velocity of 8.745 m/s (3).
4. Flame extinction is obtained for relatively low fuel jet velocities, which means that the blow-off did not occur in the 'fuel jet dominant' regime, where the cause of the phenomenon may be the jet velocity itself, the latter being much greater than the laminar combustion velocity of propane, but the extinction occurs in the 'CROSS FLOW DOMINANT' regime, i.e. the cause of the flame extinction is the air jet that sweeps away the propane and creates a mixture that is too poor to maintain combustion.

To give a better understanding of how the flow visualizations behave, we shall show an example of flame extinction with a methane flow velocity of 0.212 m/s, the diameter of the fuel nozzle outlet section of 10 mm, and being airflow located at $z=0$ mm. This is done in Figure 3.18.

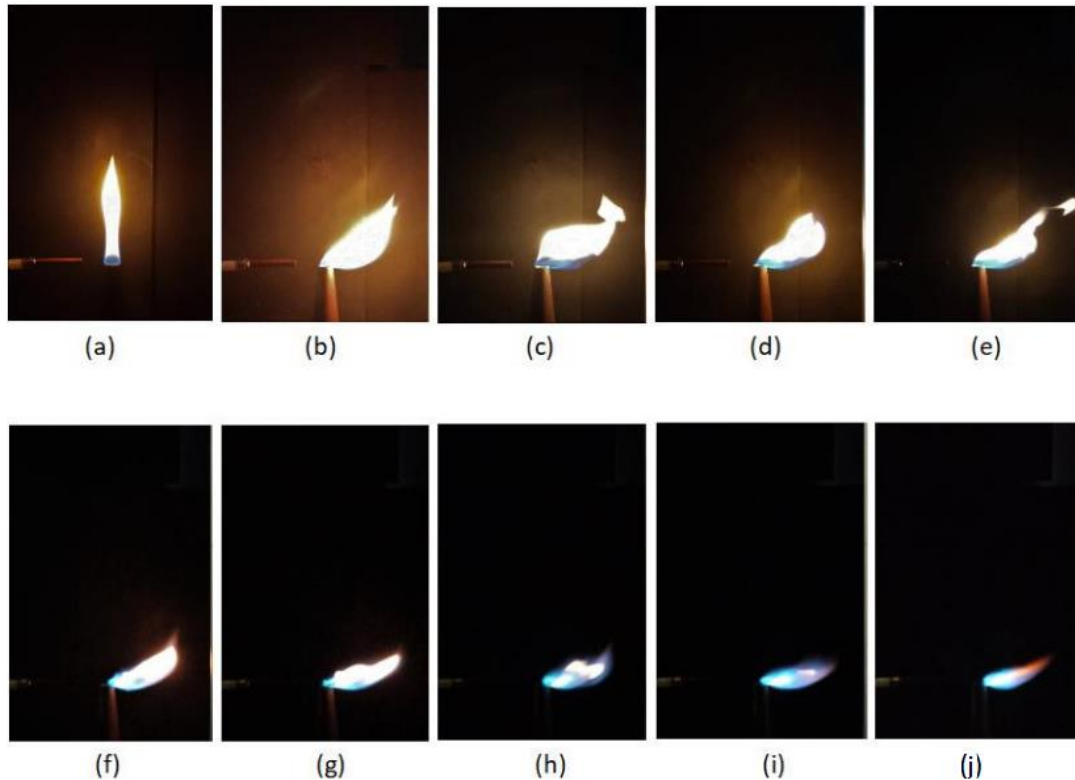


Figure 3.18. Flow rate of methane is constant at 0.212 m/s, and airflow rate variable: 4.7 (a), 6 (b), 7.5 (c), 9 (d), 10.5 (e), 11 (f), 12.5 (g), 14.8 (h), 15.5 (i) and 17 m/s (j).

The snapshots of Figure 3.18 show the flame with a constant methane flow rate of 1000 ml/min, which corresponds to an exit velocity of 0.212 m/s. The diameter of the exit section of the propane nozzle is 10 mm, while the relative height between the exit sections is zero ($z=0$ mm). With each successive image, the flow of air hitting the flame orthogonally was increased. In the first three images, the air and fuel nozzles can be seen. Figure 3.18 (a) shows some very important characteristics of the methane flame: it is in the laminar regime and is non-lifted, i.e. it is attached to the nozzle. As the flow increases, the flame tilts rapidly, but from one angle onwards a larger airflow is required to achieve further tilt. In Figure 3.18 (c) the flame begins to appear jagged at its tip, and as the airflow increases the tongues of fire begin to detach, as can be seen in image (d). Up to this point, the flame has been lengthening as the airflow increases, from now on there is a shortening. The predominant color of the flame in the first images is yellow/orange, but once the airflow has increased to 8 m/s, the main color of the flame becomes blue, typical of a premixed methane flame. Remember that the typical yellow/orange color of a diffusive flame is caused by the incandescence of the soot particles which are created because oxidation takes place in a lack of oxygen. The supply of transverse air improves combustion and allows more complete oxidation, which is why the flame changes color with this jet of air.

At this point, the inclination of the flame reaches a maximum value close to 90° , and from this moment on the down-wash phenomenon occurs. This is known to occur because the fuel easily enters the downwind region for stable combustion in crosswind conditions and forms a stable ignition source, i.e. the flame takes shelter behind the nozzle due to the vortices created. For these air velocities, it can be seen that the flame starts to detach from the fuel nozzle, first from the direction in which the collision occurs, and finally towards extinction it is completely detached. As the airflow rate increases, the angle of inclination remains more or less the same, while the length of the flame decreases until it reaches a critical length beyond which extinction occurs. This last phenomenon will be analyzed more closely in the last part of this chapter.

Considering the difficulty of evaluating flame extinction and the reliability of the measurement obtained by digital flowmeters in some particular measurement intervals, it was preferred to cut the area of the graphs with very small and very large velocities. As far as the measurement of the airflow is concerned, a minimum value of 90 lN/h and a maximum value of 430 lN/h was taken as the minimum for the tests, which correspond to speeds of 3.54 m/s and 16.90 m/s respectively. These values were chosen based on the measurement range that the digital flowmeter 1 calculated, depending on the chosen boundary conditions. Similar reasoning was carried out for digital flowmeter 2 when both methane and propane were used.

Although working in a smaller range than the full scale of the digital flowmeters, some complications occurred during the tests concerning the instability of the flame and consequently of the respective extinguishing evaluation. In practice, if the three tests performed for each flame quench point gave very different results, or, visual/auditory difficulties were encountered for the quench evaluation, this point was not considered. Furthermore, for high z-values ($z=4\text{mm}$, $z=5\text{mm}$) it often happened that the air jet could not extinguish the flame even for very small fuel flow values. Another phenomenon observed is that with very large nozzle sizes (20 mm diameter), with a small fuel flow rate, the flame flattens out and is distributed within the nozzle itself, which acts as a shield against the transverse air jet.

3.2.1. Brief review of the physical model of Blow-out limit based on Damköhler number, Da

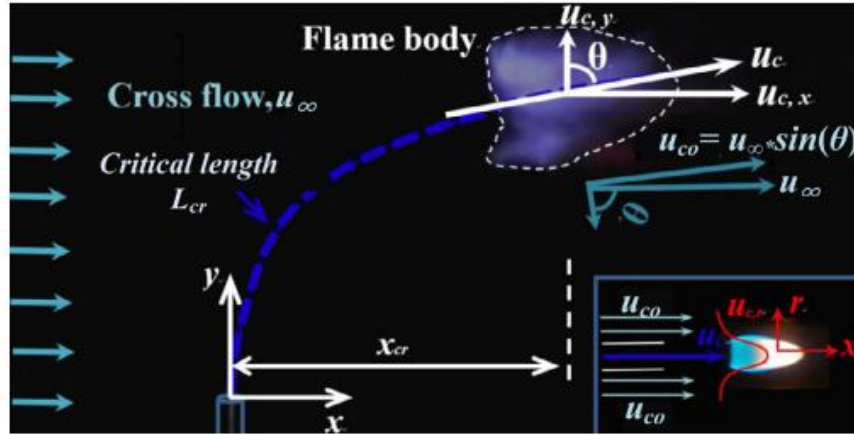


Figure 3.19. Sketch cross-wind configuration [4].

To better understand the phenomenon of the extinction of a flame with a transverse flow, a physical model based on the Damköhler number, Da , was used to try to correlate the blow-out limit with some of the typical quantities of this configuration (mainly its critical length). This model, therefore, can predict whether a flame with this configuration can be stable by directly observing the flame and measuring its length [4] as shown in Figure 3.19.

The Damköhler number (Da) is a dimensionless number used in chemical engineering to relate the chemical reaction timescale (reaction rate) to the transport phenomena rate occurring in a system.

It is defined as the ratio of the mixing time, τ_m , to the characteristic reaction time, τ_c

$$Da \equiv \frac{\tau_m}{\tau_c} \quad , \quad (1)$$

in turn, the mixing time can be defined as:

$$\tau_m = \frac{L}{u} \quad , \quad (2)$$

where L is the characteristic mixing length and u is the characteristic velocity, and the characteristic reaction time can be defined as:

$$\tau_c = \frac{\alpha}{S_L^2} \quad , \quad (3)$$

where α is the thermal diffusivity ($\alpha = \lambda/\rho c_p$, where λ is the thermal conductivity, ρ is the density, and c_p is the specific heat at constant pressure) and S_L is the laminar flame speed. Therefore, the Damköhler number becomes:

$$Da = \frac{L/u}{\alpha/S_L^2} \quad . \quad (4)$$

From which we obtain:

$$u L \frac{S_L^2}{\alpha Da} = 1. \quad (5)$$

In the vicinity of the blow-out at the characteristic velocity, the flame edge is nearly parallel to the cross-flow direction with the angle of inclination, θ , from the jet axis close to 90° . In such a case, the flow configuration of a nearly horizontal flame with cross-flow can be considered as a co-flow flame. Since this configuration has been extensively studied, one can study the cross-flow blowout from the expressions found in the works of [6-8] where the effects of the fuel jet and an air co-flow were analyzed:

$$u_{eff} = u_e + C \sqrt{\frac{\rho_e}{\rho_\infty}} \cdot u_\infty. \quad (6)$$

Where:

C is a constant of 40 [26], u_e the velocity of fuel ejected from nozzle (m/s), u_∞ velocity of cross flow (m/s), ρ_e fuel density (kg/m^3), ρ_∞ ambient air density (kg/m^3).

Similarly, with transverse flow, the effective velocity can be defined as:

$$u_c = u_e + C \sqrt{\frac{\rho_e}{\rho_\infty}} \cdot u_\infty \cdot \sin\theta, \quad (7)$$

where u_c is the local centreline velocity (fuel partially mixed with entrained air) and the value of $\sin\theta$, is close to 1.

The local central velocity, u_c , can be determined based on the velocity profile of the central line in crossflow jet flames [27].

The scaling law of the velocity profile was represented with the momentum ratio R , between the jet stream and the crossflow as:

$$R = \sqrt{\frac{\rho_e u_e^2}{\rho_\infty u_\infty^2}}. \quad (8)$$

In the far-field region ($(y/D)/R \gg 1$) where the horizontal and vertical velocity components, u_{cx} and u_{cy} , approach u_∞ and 0, respectively. The velocity components of the centreline in the x and y directions are expressed as:

$$\frac{u_\infty - u_{c,x}}{u_\infty} = \frac{c_{vf}}{(9c_{ew})^{\frac{1}{3}}} \frac{1}{R} \left(\frac{\rho_e}{\rho_\infty}\right)^{1/2} \left(\frac{x}{RD}\right)^{-2/3} (x - direction), \quad (9)$$

$$\frac{u_{c,y}}{u_e} = \frac{c_{uf}}{(9c_{ew})^{\frac{1}{3}}} \frac{1}{R} \left(\frac{\rho_e}{\rho_\infty}\right)^{1/2} \left(\frac{x}{RD}\right)^{-2/3} (y - direction). \quad (10)$$

Here, the drag coefficients are $c_{vf} \approx 2.0$, $c_{ujf}/(9c_{ew})^{1/3} = 1.1$ and $c_{ew} = 0.32-0.73$ with $c_{ew} \approx 0.73$ in the far field [36].

Thus, the local fuel velocity on the centre line can be calculated from:

$$u_c = \sqrt{u_{c,x}^2 + u_{c,y}^2} . \quad (11)$$

According to Eq. (3) and (5), a blow-out may occur when the air velocity of the crossflow becomes excessive. The length scale, L , in the definition of the Damköhler number, can be the critical length, L_{cr} , of the flame trajectory line in the last stable condition.

The length of the arc is calculated from its coordinates (x, y) along the trajectory line, which are based on the momentum ratio (R) between the fuel jet and the transverse air flow. The trajectory line has coordinates (x, y) given by [24,25]:

$$\frac{y}{RD} = A \left(\frac{x}{RD} \right)^B , \quad (12)$$

where R is the momentum ratio of the fuel jet to the transverse flow, D is the diameter of the nozzle; A and B are constant and their values are given in the literature [26] ($B = 1/3$ and A in the range of $1.2 < A < 2.6$ having its exact value determined for each case from the coordinates of the bursting point (x, y) measured in the present experiments).

The length of the trajectory line (s) from its origin to any horizontal distance x can be calculated with the following integration [25]:

$$s = \int_0^s ds = \int_0^x \left[\left(\frac{dy}{dx} \right)^2 + 1 \right]^{1/2} dx . \quad (13)$$

Its value corresponding to the critical blow-out condition (the critical horizontal distance x_{cr} can be measured by experiments) is found as the length scale, L_{cr} :

$$L_{cr} = s_{x=x_{cr}} = \int_0^{x_{cr}} \left[\left(\frac{dy}{dx} \right)^2 + 1 \right]^{1/2} dx . \quad (14)$$

Note that L_{cr} without crossflow (quiescent air) is the lift-off height, which is proportional to $u_e \tau_c$ [5].

3.2.1.1. Analysis of the influence of the z parameter for cases with methane flame

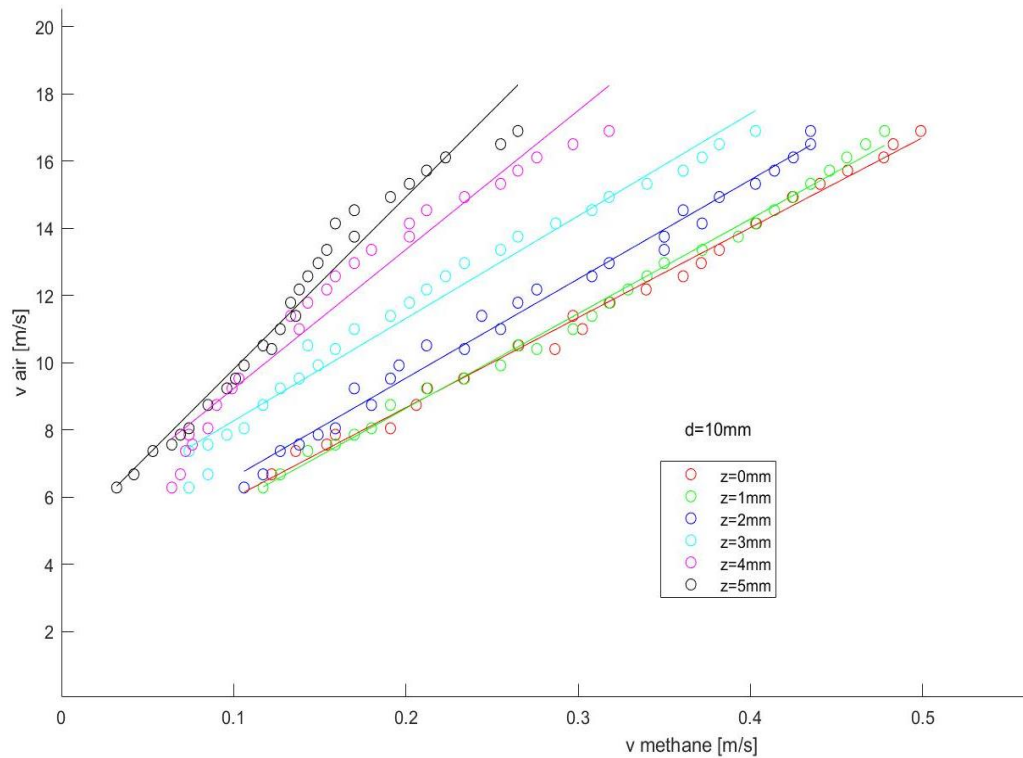


Figure 3.20. Methane flame blow-off limit with air nozzle outlet section diameter of 10 mm, with speed.

The figure shows the values of the methane blow-out velocities with varying z values but a constant fuel nozzle outlet section diameter of 10 mm. The graphs have been obtained without considering the zones or points which, as mentioned above, hinder the understanding of the mechanisms investigated in this work.

Focusing attention on the points in red ($z=0$) it can be seen that as the methane blow-out velocity increases, a greater transverse air jet velocity is required to extinguish the flame because the fuel flow has greater inertia.

The boundary conditions of this experiment place the points in the 'CROSS-FLOW DOMINATION' region, which means that the extinction of the flame is caused by the achievement of the critical extinction length (seen above with the physical model of Da), which is mainly obtained from the air velocity, the fuel escape velocities being small compared to it.

However, it is very clear how important the relative height of the two nozzles (air and fuel) is on the extinction limits. As z increases, the points move to the upper left, and the linear approximation increases in slope. This means that for the same fuel velocity, a greater airflow is required to extinguish the flame. The reason for this is quickly understood if you look closely at the airflow field as a function of z and escape velocity.

For very high values of z ($z=4$ and $z=5$), as mentioned above, there is no significant airflow field in the region closest to the fuel nozzle outlet, nor the downwind region of the nozzle. Everything leads to higher air velocities at the flame extinction limit.

The angular coefficients of the straight lines that linearly approximate the flame extinction points for constant z values are given:

$$k_{z0}=26.7 \quad k_{z1}=28.2 \quad k_{z2}=29.5 \quad k_{z3}=30.46 \quad k_{z4}=41.35 \quad k_{z5}=51.24$$

It can be seen immediately that the growth of the slope has an exponential trend. This is because as you move further and further away from the outlet section of the fuel nozzle, the influence of the air jet is less and less. For $z=0$ and $z=1$, the points on the graph are in such close positions that they are confused, precisely because the airflow has practically the same influence on the volume, directly and indirectly, affecting the flame.

Taking a methane flow rate value of 1000 ml/min, the following air flow rates are required to extinguish the flame for different z values:

- $z=0$ mm $Q_{\text{air}}=3743$ ml/min
- $z=1$ mm $Q_{\text{air}}=3833$ ml/min
- $z=2$ mm $Q_{\text{air}}=4184$ ml/min
- $z=3$ mm $Q_{\text{air}}=4898$ ml/min
- $z=4$ mm $Q_{\text{air}}=5887$ ml/min
- $z=5$ mm $Q_{\text{air}}=6667$ ml/min

Another important aspect is that the linear approximations of the flame extinction points for constant z values have a greater variance as z increases. The points for higher z are more dispersed and the reason for this is the behavior of the air jet in the volume in which the flame develops.

$$R_{z1}^2= 0.9972 \quad R_{z2}^2= 0.9937 \quad R_{z3}^2=0.9731 \quad R_{z4}^2= 0.9564 \quad R_{z5}^2= 0.9672$$

3.2.1.2. Description of methane flame extinguishing points with nozzle diameters of 15 mm and 20 mm

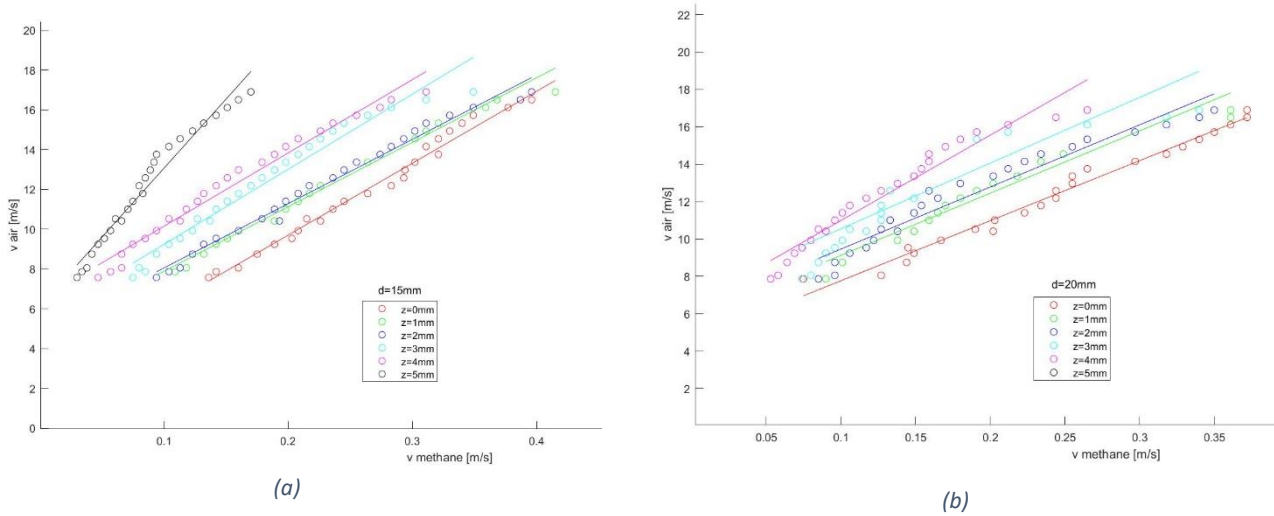


Figure 3.21. Methane flame blow-off limit with speed and air nozzle outlet section diameter of 15 mm (a) and 20 mm (b).

Figures 3.21(a) and 3.21(b) show the blow-out limits for different values of z and diameter of the fuel nozzle outlet section of 15 mm and 20 mm respectively.

With these diameters it has been observed that a laminar air jet is not able to extinguish the flame, this phenomenon is accentuated as z increases. For this reason, the graphs show the extinguishing limits starting from a transverse air jet velocity of 7 m/s.

In figure 3.21(b) it can be seen that there are no blow-out points assessed with $z=5\text{ mm}$, because in this configuration the flame is never extinguished, thanks to the fact that the air motion field in the region of the fuel nozzle outlet section is too weak and cannot sweep away the methane in areas where the stoichiometric ratio is too high, and the air cannot even carry away enough heat to prevent the combustion reaction from taking place.

3.2.1.3. Comparison of blow-out limits as the diameter varies at constant z ($z=0$, $z=1$, $z=2$)

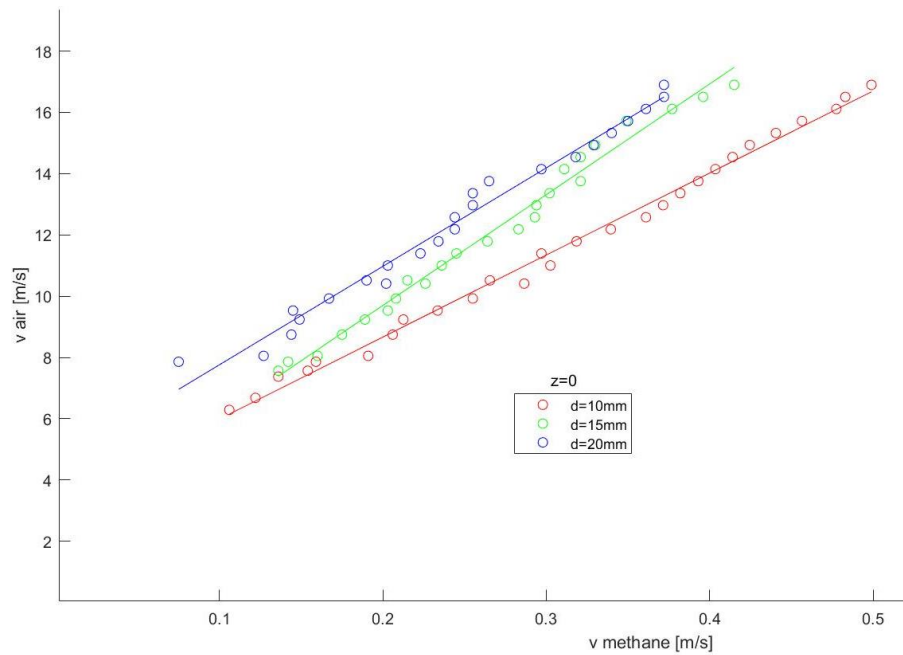


Figure 3.22. Blow-out limits $z=0$ and variable-diameter

In Figure 3.22 the blow-out limit points at constant $z=0$ mm are observed for the three different types of fuel nozzles used, and as mentioned previously here it can be seen that the points do not coincide between all the diameters, a phenomenon which occurs instead when analyzing a uniform transverse flow obtained with a fan and a honeycomb filter. There is a change in the trend of the linear slope as the diameter increases. It can be explained because the flame resists the airflow better as it has a greater volume at its disposal which is not affected by it.

Figures 3.23(a) and 3.23(b) show similar graphs, but with different z values. As z increases for $z=1$ mm and 2 mm the trend of the linear slope seems to be the same, so the airflow location does not affect strongly the extinction process.

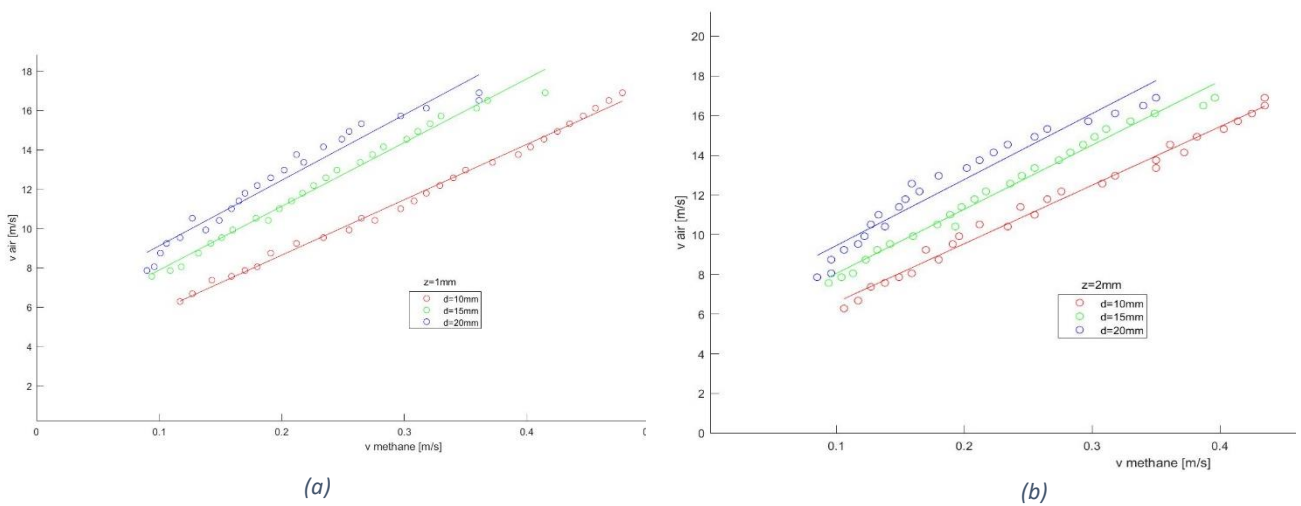


Figure 3.23. Blow-out limits with variable-diameter and $z=1$ (a), $z=2$ (b).

3.2.1.4. Flame behavior when the nozzle outlet cross-section varies

In this section, an attempt is made to explain a phenomenon that was noticed during flame extinguishing tests and which is directly related to the diameter of the nozzle outlet section.

With the same velocity of the transverse air jet and the same fuel outflow, a flame obtained with a larger diameter of the nozzle outlet section tends to have a greater resistance to bending and this means that it lifts sooner from the propane nozzle outlet. To explain this, the moment of inertia of the methane column is calculated:

$$W = \frac{\pi d^4}{64},$$

where d is the diameter of the nozzle, see Figure 3.26.

From which we obtain:

- $d=10$ mm: $W=491 \text{ mm}^4$
- $d=15$ mm: $W=2485 \text{ mm}^4$
- $d=20$ mm: $W=7854 \text{ mm}^4$

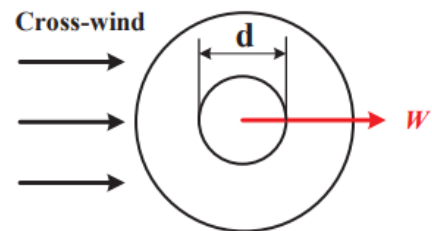


Figure 3.24. Nozzle outlet section.

The bending resistance is therefore directly related to the moment of inertia and for this reason, the flame can be more or less inclined by the air jet depending on the outlet cross-section.

This has been well clarified in the research of Changchun Liu and Linyuan Huang [7], who by testing different nozzle shapes, cross, rectangular, circular, and triangular, demonstrated how the

shape of the fuel nozzle outlet section affects all flame parameters such as critical length, shape, behavior, extinction, and angle of inclination.

Fig. 3.25 shows pictures of three cases, case 1 with a fuel nozzle outlet section diameter of 10 mm, case 2 of 15 mm, and case 3 of 20 mm.

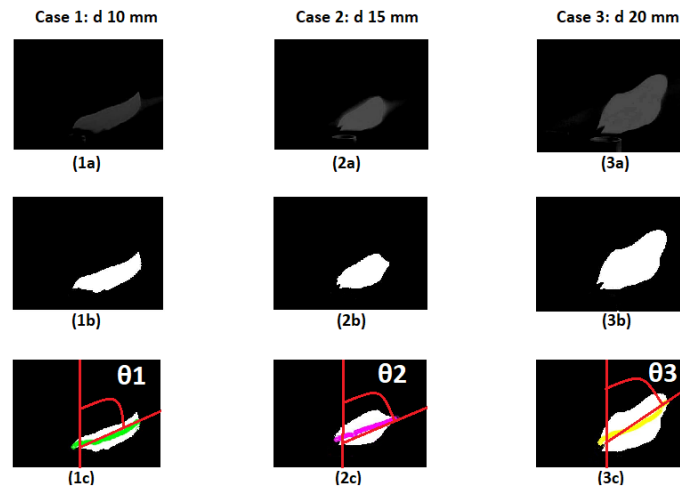


Figure 3.25. Methane flame image.

The flames are hit with a transverse air jet of 150 l/h, which corresponds to a velocity of 5.9 m/s and z equal to 0. About the fuel flows between the 3 different cases, there is the same methane escape velocity which is 0.07 m/s. Such low speeds were chosen to have stable and laminar flames, i.e. without fluctuations, but still effective in highlighting their inclination.

Table 3.5 summarises the characteristic quantities for Figure 3.25.

Tabel 3.5. Image data.

	Case 1	Case 2	Case 3
nozzle diameter [mm]	10	15	20
methane velocity [m/s]	0.07	0.07	0.07
methane flow [ln/min]	0.330	0.73	1.3
flame angle [deg]	61	55	50

The images from Figure 3.25 (a) were obtained by photographing the flames. In all cases, we are in the laminar diffusive flame regime. To obtain the angle of inclination, the images were processed with Matlab. The mean profile of the flame and the set of points equidistant from the

upper and lower contour were found. By linearly approximating these points with a straight line, the angle was obtained using the coefficient k .

As indicated in the work of Changchun Liu and Linyuan Huang [7], increasing the diameter of the outlet section of the fuel nozzle creates a flame with greater inertia and which therefore resists the transverse air-jet better, tilting less, at the same fluid exit velocity and therefore equal R .

3.2.2. Analysis of the influence of the z parameter for cases with a propane flame

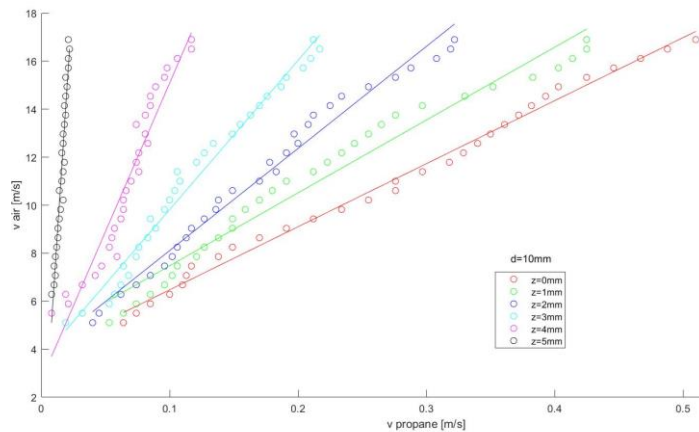


Figure 3.26. Propane flame blow-off limit with air nozzle outlet section diameter of 10 mm, with speed.

The previous figures show the propane flame blow-out points for different values of z with the diameter of the fuel nozzle outlet section of 10 mm.

Fig. 3.26 shows the extinguishing limits with the fluid velocities using propane.

As with methane, propane requires a transverse air jet to hit the flame with greater velocity as the fuel velocity increases. As z increases, the region in which the flame survives always increases for the reasons already explained when discussing methane. Appendix 2 shows the errors for Figures 3.26 and 3.27.

3.2.2.1. Description of methane flame extinguishing points with fuel nozzle diameters of 15 mm and 20 mm

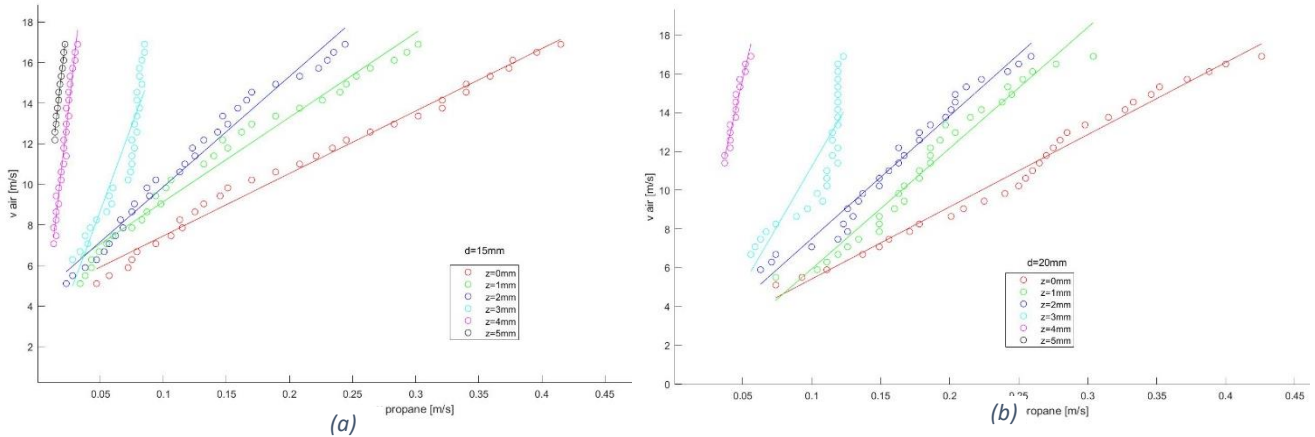


Figure 3.27. Propane flame blow-off limit with air nozzle outlet section diameter of 15 mm (a) and 20 mm (b), with speed..

Fig. 3.27(a) and Fig. 3.27(b) show the flame extinction limits for diameters of 15 and 20 mm using propane.

The size of the fuel outlet section has a great influence on the values since the air jet is punctual and not constant over the whole section. For the 20 mm diameter a very different behavior is observed between the values at $z=0$ mm and $z=1$ mm, while the latter height leads to a similar flame behavior at $z=2$ mm. At $z=5$ mm there is never any flame extinction, the air jet is not extended enough. As z increases, the blow-off points decrease, as can be seen from the circles in blue and magenta ($z=3$ mm and $z=4$ mm).

3.2.2.2. Comparison of blow-out limits with varying diameter at constant z ($z=0$, $z=1$, $z=2$)

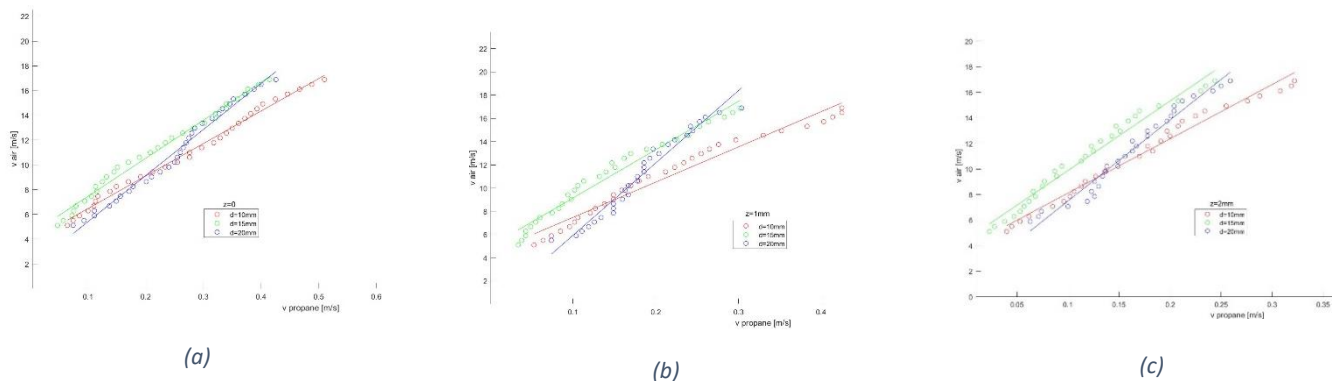


Figure 3.28. Propane blow-out limits with $z=0$ (a), $z=1$ (b), $z=2$ (c) and variable-diameter.

In the case of propane, it can be observed that, as the diameter varies, flame extinction points with different characteristic velocities are obtained. Using velocity magnitude does not disengage from

the nozzle, unlike a configuration with a uniform transverse venter. From the figures, it can be seen that while for methane there is a clear difference in velocity between the diameters, for propane it is very close and a larger diameter does not result in a lower fuel exit velocity to resist the airflow.

3.2.3. COMPARISON OF THE TWO FUELS: METHANE VS PROPANE

In this work, the flame extinction of methane and propane has been analyzed. Before highlighting the similarities and differences with graphs, important characteristics of these fuels are mentioned, which influence the observed phenomenon and allow a better understanding of the experimental results. The flammability range and the laminar burning rate are now indicated. At first glance, it may seem inconsistent and incorrect to bring these quantities into play when dealing with diffusive flames, as they are very important in characterizing premixed combustion. However, transverse air-jet extinguishing mechanisms affect precisely these aspects.

- Density

The two fuels have very different densities at a temperature of 20 °C and atmospheric pressure. This quantity is very important because the inertia of the fuel column depends on it. The densities of methane and propane are respectively 0.668 kg/m³ and 1.893 kg/m³. Since the density of air at the same conditions is 1.225 kg/m³ it can already be assumed that the propane will go more easily into the downwind area of the fuel nozzle and therefore potentially have better resistance to flame extinction.

- Flammability range

The flammable range is defined by an upper flammable limit (LS) and a lower flammable limit (LI). Below the lower limit, the gas is not concentrated enough to ignite, although an ignition can produce a fuel-combustion reaction, the reaction does not spread within the mixture. Above the upper limit, on the other hand, the atmosphere is rich in gas but low in the oxidizer.

The values of the fuels used in this work are given in the following table 3.6, where the value in a volume percentage of fuel over the whole mixture is indicated.

Table 3.6. Upper and lower limits for the fuel tested.

Fuel	LI	LS
Methane	5%	15%
Propane	2%	9%

- Laminar combustion speed

This is the speed at which the flame front propagates in a mixture of fuel and oxidizer.

It is an intrinsic characteristic of fuel and the main parameters affecting it are temperature, pressure, equivalence ratio. By flame front, we mean the boundary between the fraction of combusted and unburned gases. It is defined as laminar because if there is a certain amount of turbulence in the mixture this speed can increase by up to two orders of magnitude.

Methane and propane near stoichiometric dosing have approximately the same laminar combustion velocity, which at $p=1$ bar and $T=300$ K is around 0.37 m/s for methane and 0.38 m/s for propane. It should be noted, however, that in a poor environment the combustion speed of propane decreases much faster than that of methane.

- Calorific value

Calorific value is the energy that can be obtained by fully converting a unit mass of an energy carrier under standard conditions. In normal combustion, the products of combustion are released at a higher temperature than the reference temperature of the fuel. Thus, some of the theoretically available heat is 'lost' by heating the flue gases and, above all, by the vaporization of the water produced by combustion. This is why the Lower Heating Value (LHV) is used, which does not take into account the latent heat of vaporization of the water generated during combustion.

For methane and propane, this results in 50 MJ/kg and 46.4 MJ/kg respectively.

Comparison of extinction limits with d nozzle 10 mm

By placing the flame extinction limits of both fuels on the same graph, it is possible to observe some very important aspects:

- 1) Propane flames proved to be much more stable in the tests, especially at very low flow rates or equivalently low fuel spillage rates. It was possible to evaluate the extinction of flames even with exit velocities below 0.05 m/s, a limit below which it was impossible to go for

methane. A practical limit for propane velocities was found to be around 0.01 m/s. Higher velocities are very similar between the two fuels.

- 2) Raising the air nozzle relative to the fuel outlet section shows that methane lowers its extinguishing limit very little, compared to propane which is much more sensitive to this change. As can be seen from the squares and triangles in the figure, the propane region for $z=1$ or $z=2$ in which the flame occurs is much larger than the respective methane conditions. The flame extinction limits for methane at $z=5$ mm have similar velocities to the propane limits at $z=4$ mm.

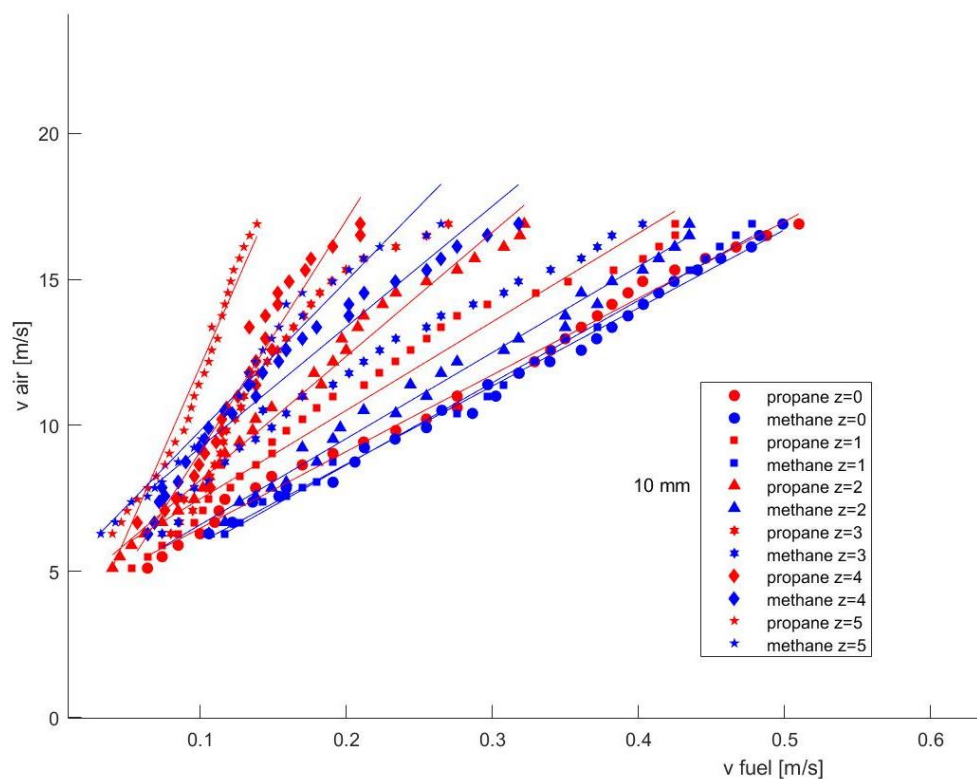


Figure 3.29. Comparison of propane and methane blow-out limits d outlet fuel 10mm.

Experimental data show that propane and methane behave in the same way when the air jet is at $z=0$, i.e. when the airstrikes the flame transversely at its base. When a gap is created, the propane is better able to cope with the jet, an explanation for this phenomenon may lie in the lower density of propane and also in the lower flammability limit of about 3 % compared to CH_4 . The lower density allows the propane to move more easily into the area where the airflow field is lower because the fuel nozzle acts as a shield.

The data for the 15 mm and 20 mm diameters are presented in Figures 3.30 and 3.31.

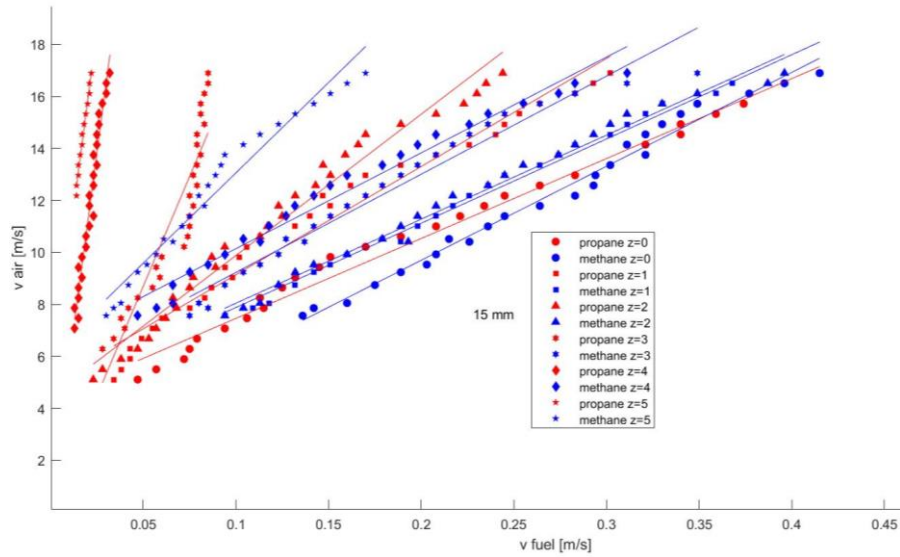


Figure 3.30. Comparison of propane and methane blow-out limits d outlet fuel 15mm.

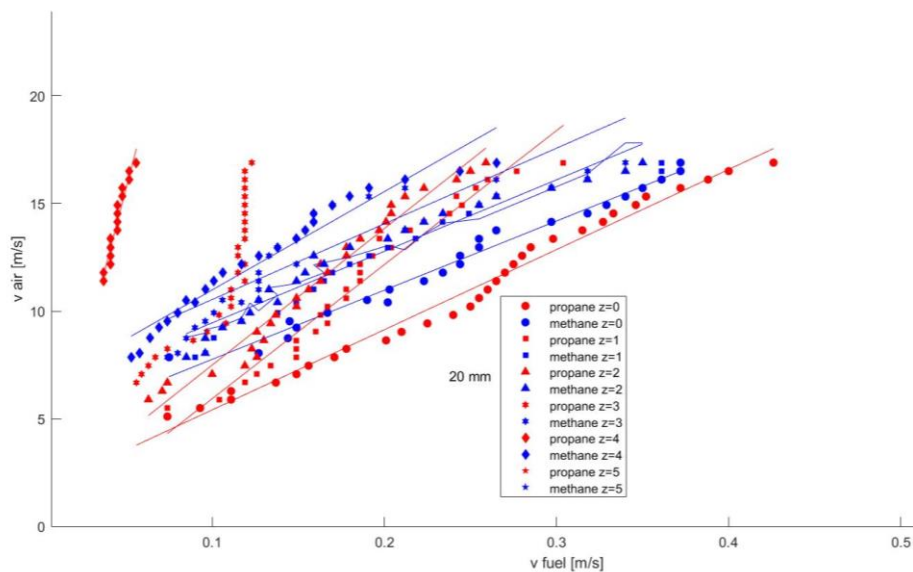


Figure 3.31. Comparison of propane and methane blow-out limits d outlet fuel 20 mm.

Even if the diameter of the nozzle outlet section is increased, the differences between the two fuels are obvious. Propane can guarantee combustion at the same flow rate even with a transverse air jet with a higher velocity. Only at high z values ($z=3$, $z=4$, $z=5$) does this difference become noticeably more pronounced, much more so than in the case of d 10 mm.

It is worth remembering that in this work the 10 mm diameter is the case that comes closest to uniform crosswind conditions, precisely because the air jet, having reached a minimum exit

velocity, is sufficiently large to cover the entire fuel exit section, albeit with a turbulent field of motion (as seen previously in the analysis of the airflow doped with oil particles). A larger area of the fuel nozzle is affected by the air jet in a much less uniform manner. Experimental data showed that propane is better able to adapt to these conditions, bringing its blow-out limit to more powerful air jets than methane.

Chapter 4. SCALING OF GRAPHS WITH FLAME EXTINCTION LIMITS AND COMPARISON WITH BLOWOUT CAUSED BY A UNIFORM CROSSWIND

4.1. SCALING OF BLOWOUT LIMITS

In this section, the blowout limits of the various cases analyzed in chapter 3 are shown, using dimensionless numbers that allow condensing in a few diagrams all the main characteristics of the flame extinction phenomenon through a transversal air point jet, in a quasi-turbulent and completely turbulent regime.

The description of the points is done through:

- Reynolds number

The Reynolds number (Re) helps predict flow patterns in different fluid flow situations. At low Reynolds numbers, flows tend to be dominated by laminar (sheet-like) flow, while at high Reynolds numbers flows tend to be turbulent. The turbulence results from differences in the fluid's speed and direction, which may sometimes intersect or even move counter to the overall direction of the flow (eddy currents).

The Reynolds number is the ratio of inertial forces to viscous forces within a fluid that is subjected to relative internal movement due to different fluid velocities. A region where these forces change behavior is known as a boundary layer, such as the bounding surface in the interior of a pipe. A similar effect is created by the introduction of a stream of high-velocity fluid into a low-velocity fluid, such as the hot gases emitted from a flame in the air. This relative movement generates fluid friction, which is a factor in developing turbulent flow. Counteracting this effect is the viscosity of the fluid, which tends to inhibit turbulence. The Reynolds number quantifies the relative importance of these two types of forces for given flow conditions and is a guide to when the turbulent flow will occur in a particular situation. Concerning laminar and turbulent flow regimes:

- 1) laminar flow occurs at low Reynolds numbers, where viscous forces are dominant, and is characterized by smooth, constant fluid motion;
- 2) turbulent flow occurs at high Reynolds numbers and is dominated by inertial forces, which tend to produce chaotic eddies, vortices, and other flow instabilities.

The Reynolds number is defined as:

$$Re = \frac{uL}{\nu} = \frac{\rho uL}{\mu}, \quad (1)$$

where:

ρ is the density of the fluid [kg/m³]

u is the flow speed [m/s]

L is a characteristic linear dimension [m], in this work the diameter of air and fuel nozzles

μ is the dynamic viscosity of the fluid [Pa·s]

ν is the kinematic viscosity of the fluid [m²/s].

- Dynamic viscosity

In the context of transport phenomena, viscosity is a physical quantity that measures the resistance of a fluid to flow. In other words, it is the momentum exchange coefficient. From a microscopic point of view, viscosity is linked to the friction between the fluid molecules. When the fluid is flowing inside a pipe, the particles that make up the fluid generally move faster along the axis of the pipe and slower near its walls; for this reason, a strain, which translates into a pressure difference, is necessary to counteract the friction between the layers of particles and set the fluid in motion. The effort felt by the fluid is proportional to its viscosity.

The dynamic viscosity of a fluid is a measure of its resistance to flow when tangential stress is applied. The cause of this resistance is due to adjacent layers of fluid moving at different speeds. The definition is given in the case of a laminar regime. The ideal situation is to have a homogeneous fluid between two equal horizontal flat surfaces, one fixed and the other moving. If the velocity of the moving plane is small, and in addition, the fluid particles move in a direction parallel to the moving plane with a velocity that varies linearly from zero on the fixed plane to u on the moving plane, in this case, the dynamic viscosity is simply given by:

$$\mu = \frac{Fd}{Su} = \tau \frac{d}{u}, \quad (2)$$

where:

F is the force applied to the moving plane [N]

d is the distance between the two planes [m]

u is the constant velocity of the moving plane [m/s]

S is the area of each floor [m²]

τ is the shear stress [Pa]

- Momentum flux ratio

$$J = \frac{\rho_f V_f^2}{\rho_a U_a^2}, \quad (3)$$

where:

ρ is the density

V and U are velocities, and subscripts f and a denote the fuel jet and air jets respectively.

Table 4.1 shows the typical values for the physical parameters Re and J for air, methane, and propane.

Table 4.1. Data fluids at pressure 1 atm and temperature 20 °C.

Fluid	Density [kg/m ³]	Dynamic Viscosity [Pa s]	Diameter [m]
Air	1.225	1.81×10^{-5}	0.003
Methane	0.668	1.03×10^{-5}	0.01, 0.015, 0.02
Propane	1.893	0.82×10^{-5}	0.01, 0.015, 0.02

4.1.1. Diagramma Re_{air}/Re_{fuel} diameter fuel nozzle 10 mm

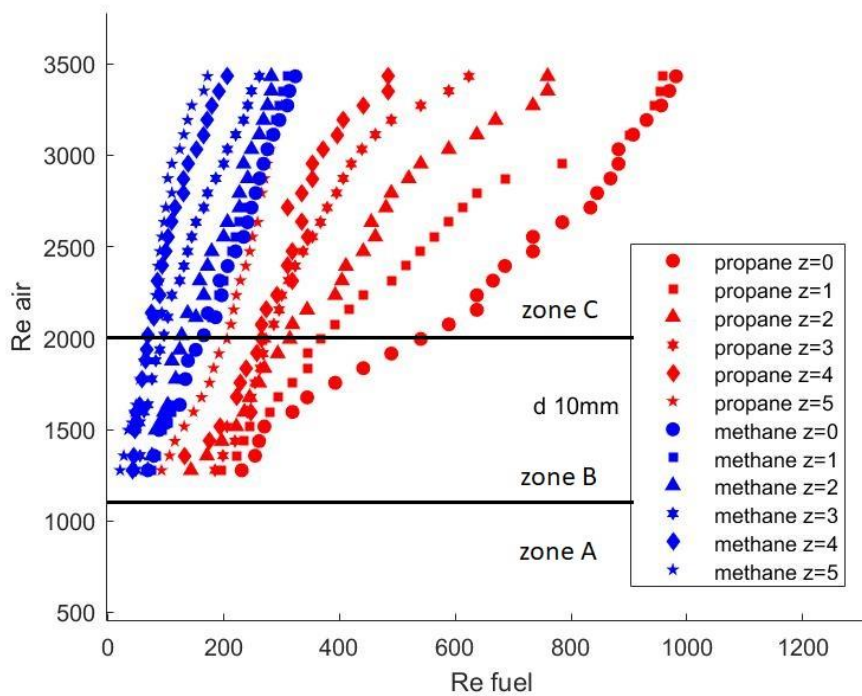


Figure 4.1. Blowout limits for propane and methane flames with Reynolds number.

Fig. 4.1 shows the blowout limits of propane and methane flames for different values of z and with a fuel outlet section diameter of 10 mm. However, the points are plotted through the respective Reynolds number values of air and fuel. Note that:

- 1) The air jets have a Reynolds number between 1250 and 3500 and combining these results with those obtained from the analysis of the jet with the Phantom v611 camera, it can be said that a fully developed turbulent regime in this configuration is obtained for $Re > 2300$. Given the enormous difficulty in analyzing even analytically the laminar/turbulent transition region, this Reynolds value is indicative and closely related to all the boundary conditions of the experiment carried out in this work.
- 2) On the other hand, the very low Reynolds numbers for methane and propane fuels indicate that the escape of fuel occurs in a fully laminar regime. The flame turbulence observed before extinction is caused by the combined effect of air and fuel jets, as indicated by the Damköhler model explained above. Due to the different physical characteristics of the two fuels, it is observed that methane has much lower Reynolds values than propane, and especially when z varies it has little variation. We obtain $50 < Re_{methane} > 320$ and $100 < Re_{propane} > 1000$. This difference is due to the combination of dynamic viscosity and density, which are very different between the two fuels.
- 3) The black lines in Fig. 4.1 separate zones A, B, C are illustrated in chapter 3. It should be noted that, as specified before, the blowout limits of zone A have been cut.

4.1.2. Diagramma R/J

A series of diagrams representing the blowout limits with the parameters jet-to-crossflow velocity ratio R , Equation (8) in Chapter 3, on the y-axis, and the momentum flux ratios J (3) on the x-axis are now shown. These two dimensionless quantities are characteristic of flame configurations hit by a transverse air jet.

Now we start by representing the blowout points of the methane flame for different values of z and fuel diameter 10 mm. Gradually the graphs will be filled with data for other conditions.

- Graph R/J methane flame and d 10 mm

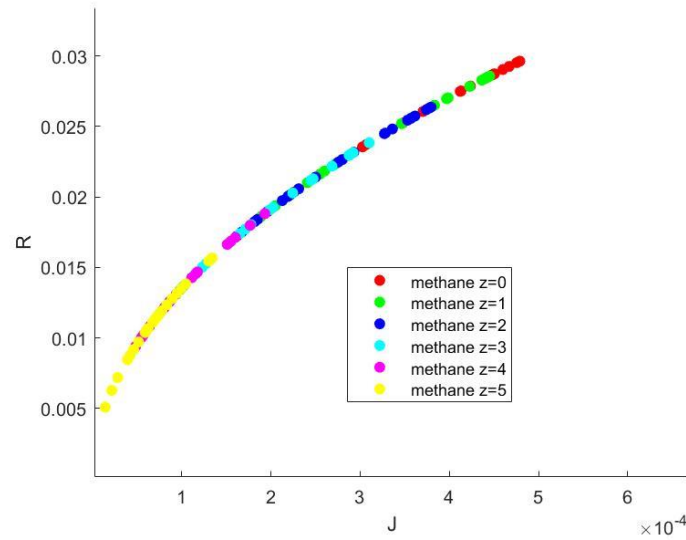


Figure 4.2. Methane flame blowout limit for different values of z and d 10 mm.

Fig. 4.2 shows that the extinction limits of the methane flame collapse on a parabola with a vertex in the origin of the Cartesian plane. It can be seen that as the distance z increases we move to the lower left of the curve, i.e. to lower J and R values. This phenomenon is because the extinction limits for high z occur at lower fuel/air ratios (R). The importance of momentum flux ratios J lies in norm the fluid densities. The trend of shifting points in the lower left-hand corner as z increases is repeated both for propane and for different values of fuel spill diameter. For this reason, we do not report similar graphs but prefer instead to include other information in the following graphs to have a general picture of the blowout phenomenon with point transverse air jet.

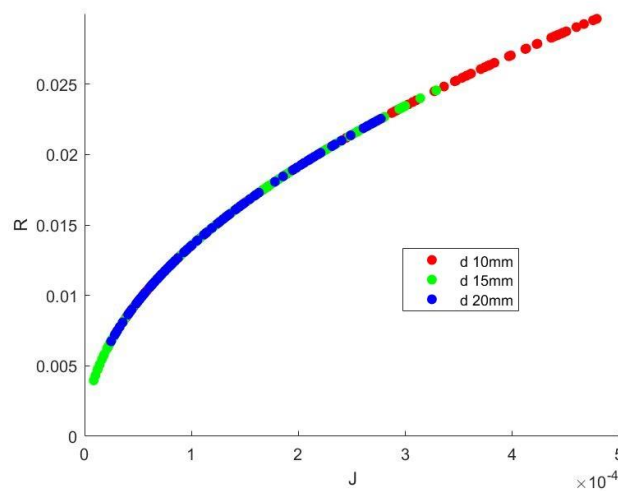


Figure 4.3. Methane flame blowout limit for different values of z and d 10, 15, 20 mm.

Fig. 4.3 shows the blowout limits of the propane flame for different values all z values and diameters evaluated in this work. It can be observed that the points collapse on the same parabola that was also described in Fig. 4.2. the points evaluated for each diameter of the fuel spill section are positioned in a certain order it can be observed that the blowout limits move to the left of the parabola as the diameter increases. It is also true that the last points on the lower-left belong to the 15 mm diameter, which also has a high extension in R and J .

- Graph R/J methane and propane flame with d 10, 15, 20 mm

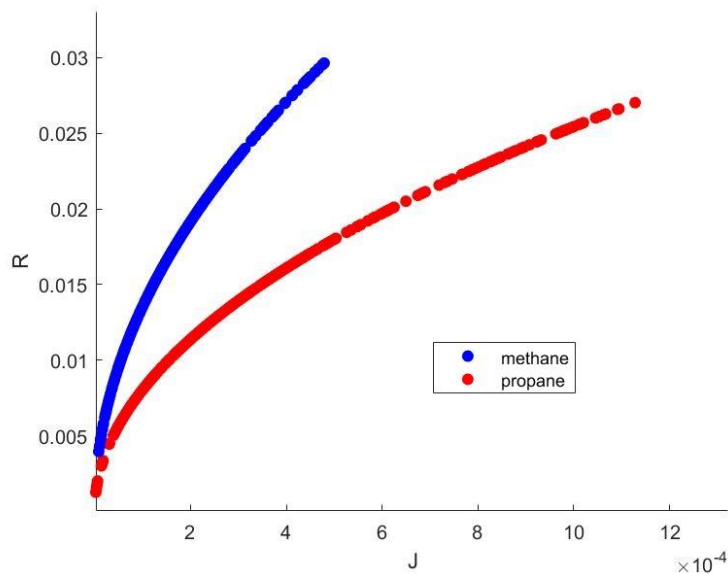


Figure 4.4. Methane and propane flame blowout limit for different values of z and diameters.

Fig. 4.4 compares the flame extinction limits for $z=0, z=1, z=2, z=3, z=4, z=5$ of propane and methane for diameters of 10, 15, and 20 mm. It can be seen that propane also collapses its points into a parabola with a vertex in the Cartesian plane, which however has a smaller aperture. Propane develops for greater J . It should be remembered that propane has a higher density than air, whereas methane has a lower density. The range of R is slightly lower than for methane, this is due to the better resistance to the transverse air jet.

For propane, as the diameter varies, there is a good correlation between the diameter of the fuel outlet section and the position of the blowout limits on the parabola; as the diameter increases, the points move to lower J and R values.

The scaling granted by the parameters R and J allows a good comparison between different fuels or different dilution percentages for future work. It is also possible to characterize the parabola of

each fuel by expressing a form of the empirical relationship between the number of carbon atoms in the fuel and the characteristics of the respective parabola, for example.

4.2. COMPARISON OF FLAME EXTINCTION WITH LOCAL AND CROSS JETS

Over the years, the flame extinction limit has been the subject of research under a wide variety of conditions. There are numerous studies in which the stability of the flame, its main characteristics such as length, inclination, quality, and many others are investigated, precisely because combustion now involves so many human activities and is the basis of many instruments or means that man uses.

Researchers Rengel and Palacios in their work 'Analysis of experimental blowout velocities of jet flames', have found a non-dimensional equation, able to determine the blowout limit velocity of jet flames with multiple gaseous fuels, gas mixtures, orifice diameters, gas velocities, wind conditions, flow regimes, and orientations. This was done by analyzing a large database of jet flame tests. The strength of this research lies in the fact that this equation is generic to flames in different configurations: quiescent air, cross-flow, and co-flow.

In this part of the present work, we try to understand if this equation is also valid for extinguishing points obtained with a local air jet, and where these points are positioned in the diagram that Rengel and Palacios have configured. First, however, the steps to arrive at a single equation that is valid for such a wide range of blow-out cases are briefly described.

On the basis of work by other researchers [28], Rengel and Palacios started from Froude's number which is defined as the square root of the ratio between the force of inertia and the force of weight, i.e.:

$$Fr = \frac{V_0}{\sqrt{gL_0}} \quad , \quad (1)$$

where:

L_0 is a reference length [m]

V_0 is the modulus of a reference speed [m/s]

g is the modulus of the acceleration of gravity [m/s²]

Using the Froude number it is possible to normalise flame heights under different conditions. In order to understand whether it is a sonic or supersonic flow we define Q^* [29]:

$$Q^* = \frac{\dot{Q}}{\rho_\infty c_p T_\infty D^2 \sqrt{gD}} \quad , \quad (2)$$

being the parameters:

\dot{Q} è il heat release rate HRR [W]

D diameter of fuel nprice[m]

ρ_{∞} is the density of air [kg/m³]

c_p is the specific heat at constant fuel pressure [J/kgK]

T_{∞} is the ambient air temperature [K]

g is the gravitational acceleration [m/s²]

If $Q^{*2/5} < 100$ the flow regime of the flame is subsonic if instead $Q^{*2/5} > 100$ the regime is to be considered supersonic.

Given the significant differences in the experimental conditions for jet flames reported in the work they considered, it was necessary to define new dimensionless quantities for the fuel mass flow rate and also for the wind speed:

$$m^* = \frac{\dot{m}''}{\rho_{\infty} \sqrt{gD}} , \quad (3)$$

where is the mass flow rate of fuel per unit area,

$$u^* = \frac{u_w}{\sqrt[3]{g \dot{m}'' \frac{D}{\rho_{\infty}}}} , \quad (4)$$

where u_w is the wind speed. In its absence, the parameter u^* can be taken as 1.

The parameters m^*u^* are used in their study, as these take into account most of the essential parameters governing the development of jet flames: mass flow rate, nozzle area, ambient conditions and wind speed. They were used for comparison with $Q^{*2/5}$, which identifies the jet flow regime at which blowout conditions are realised.

Assuming that the combustion of methane and propane is ideal, the following is found \dot{Q} as:

$$\dot{Q} = HRR = \dot{m} \cdot \Delta H^{\circ} c . \quad (5)$$

It is now possible to evaluate the points of the blowout limits with the new dimensionless quantities and compare them with the general empirical equation.

The following table shows the quantities required to assess the limits with $m^*u^* e Q^{*2/5}$.

Table 4.2. Fluid data.

Fluid	Specific heat at constant pressure [kJ/kgK]	Lower heating value [MJ/kg]
Methane	1.6794	50
Propane	2.2537	46.4

Figure 4.5 shows the jet flame conditions under which the burst velocity is achieved for a wide range of subsonic and sonic turbulent jet flames. The data are shown as indicated in the original work. The blowout and flame regions are indicated for better understanding by the reader. As seen, the higher the Q^* number, the higher the m^*u^* required to reach blowout conditions. The following linear correlation taken from the figure can provide reasonable estimates of the blowout conditions.

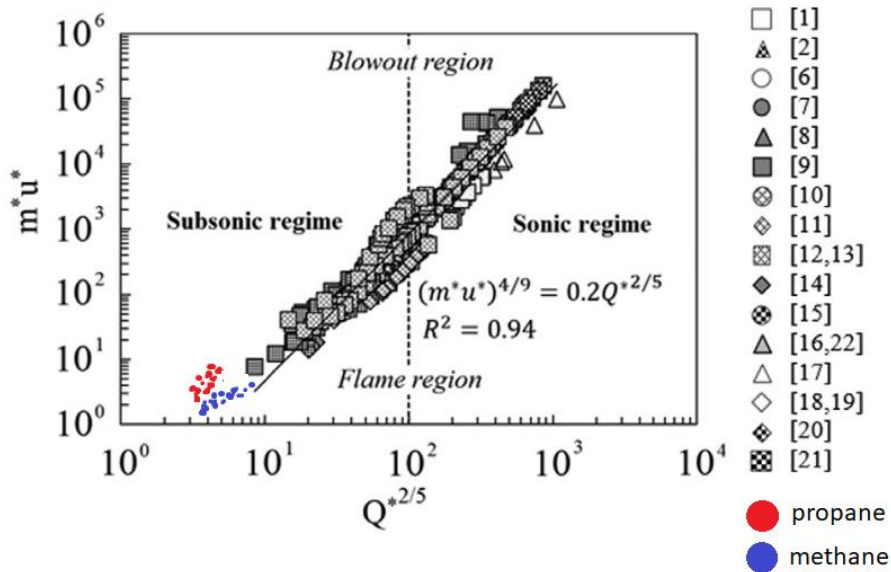


Figure 4.5. Blowout limits under different conditions [5].

It is worth mentioning that the blowout limits evaluated in this work are in the lower-left region of the graph where there are very low values of m^*u^* and Q^* . Methane follows the empirical relationship better than propane, but with another linear slope in the $(m^*u^*, Q^{*2/5})$ -plane. The fluid velocities used resulted in unlifted diffusive flames. In the following, Table 3 is given in which the main quantities of the compared points are shown in Figure 4.5 [5].

Table 4.3. Data is presented in Figure 5.

Ref.	Fuel	u_w (m/s)	D (mm)
[1]	C ₂ H ₄ , C ₂ H ₆ , H ₂	0.0	1.0–16.0
[2]	CH ₄	0.0	3.5
[6]	CH ₄ , C ₃ H ₈	0.0	3.0–8.0
[7]	H ₂	0.0	2.0
[8]	CH ₄ , C ₃ H ₈	0.0	5.0
[9]	CH ₄ , C ₃ H ₈ , H ₂	0.0	2.5–5.0
[10]	CH ₄ , C ₃ H ₈ , C ₄ H ₁₀ , C ₂ H ₄	0.0	1.0–8.0
[11]	H ₂	0.0	2.0
[12]	CH ₄ , C ₃ H ₈ , C ₂ H ₂ , C ₂ H ₄ , H ₂	0.0	0.2–12.0
[13]	C ₃ H ₈	3.0 - 8.0	2.5–5.0
[14]	CH ₄	0.0	3.5–150.0
[15]	CH ₄	0.0	7.0
[16,22]	CH ₄	0.0	11.0–27.0
[17]	H ₂	0.0	0.34–0.75
[18]	C ₃ H ₈	0.0	0.8–4.0
[19]	C ₃ H ₈	0.8–3.2	3.0–8.0
[20]	CH ₄	0.0	78–160
[21]	CH ₄	0.0–11.4	6.–30.0

It should be noted that the diagram in Fig. 4.5 is of the *log/log* type. A standard deviation value of 0.94 is given, and given the nature of the diagram, it means that the equation approximating the points is very coarse indeed and cannot be used in all cases.

Chapter 5. CONCLUSIONS AND FUTURE WORK

5.1. CONCLUSIONS

In this work, the extinction of a diffusion flame using an air jet perpendicular to the flame has been studied. Specifically, an analysis has been carried out on the influence of 3 parameters: (i) distance of the air jet concerning the fuel nozzle outlet, (ii) fuel nozzle diameter, (iii) fuel type.

About the distance of the jet to the fuel nozzle outlet, a linear trend has been observed for both fuels in which the regions where flame exists and where the flame is extinguished are separated (see figure 7, chapter 3). In addition, it has been observed that the areas where the airflow has a laminar (L), transient (TR), and turbulent (TU) regime. These regime changes strongly affect the value of the linear slope. By moving the air nozzle vertically away from the outlet section of the fuel nozzle the blowout limits become lower, and this tendency grows exponentially because the turbulent airflow loses its influence on the volume in which the flame develops especially when it is moved away by a distance equal to its linear diameter. It has been observed that with an air nozzle diameter of 3mm there is no point in studying blowout beyond a height of 6 mm.

About the nozzle diameter, as the value increases, the linear slope increases progressively, i.e. more airflow is needed to extinguish the flame. Data supporting this fact is included in Table 2 of chapter 3. In addition, a discontinuity phenomenon has been observed in the linear slope when moving from Zone A (L) to Zone B (TR, TU). This discontinuity may be associated with hysteresis phenomena that have not been studied in this work. All other things being equal, a larger fuel outlet cross-section diameter results in a flame that is more resistant to extinction, as well as having better resistance to tilting when struck by air.

If we turn our attention to fuel switching, we have observed that propane requires more airflow to extinguish than methane. This statement is evident from the drastic increase in the linear slope when comparing the graph delimiting the flame and non-flame zones under the same conditions of nozzle diameter and distance from the air jet.

Finally, very useful information has been reported in chapter 4 by dimensioning the plots in a (J , R) plane, the parameter R is the square root of the aspect ratio between the convective fluxes of fuel and oxidant (parameter J). In this case, all data of different heights and diameters collapse

for the same fuel in a parabolic fashion. Furthermore, it has been compared with the dimensionless trend of additional mass flow m^*u^* versus a dimensionless flow Q^* and an excellent agreement has been found for propane concerning the slope in the general law already published [5]. The blowout limits evaluated in this work are all in the subsonic regime. However, a disagreement in the slope change for m^*u^* of order unity has been found for propane (see Figure 5, chapter 4).

5.2. FUTURE WORK

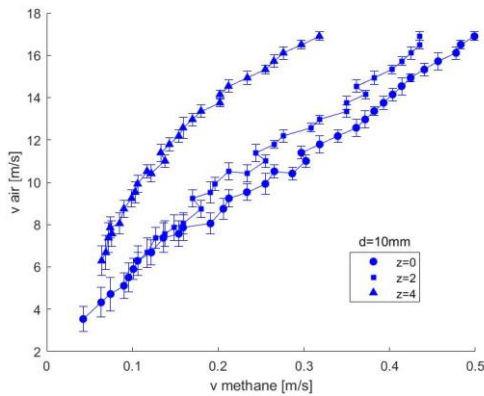
A detailed experimental study in the area of the transition region between zones A and B where a discontinuity appears will be conducted to know if the hysteresis phenomenon exists.

Numerical simulations will be performed to study numerically some turbulent cases of transient extinction using URANS or LES techniques. The analysis of these simulations will help to understand the physical mechanisms of the extinction thanks to the value of the velocity field.

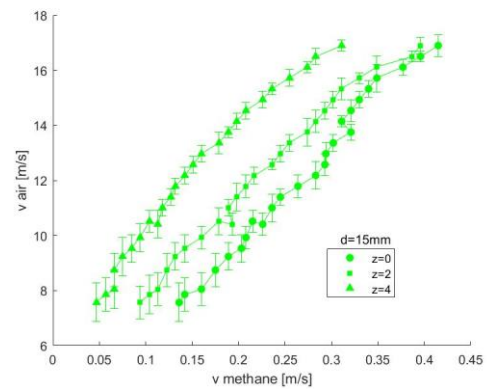
It would be very interesting to test other fuels or methane and propane with the addition of inert substances such as nitrogen and to derive the characteristic parabolas.

Data points with a higher flow rate could be collected to better understand the change of slope of the law reported in [5] in the m^*u^* unit domain.

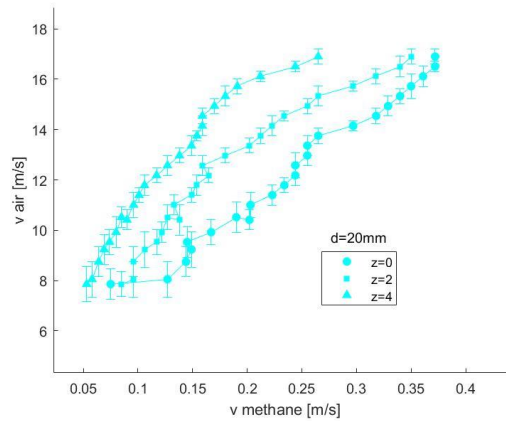
APPENDIX 1. Display of the error of each blowout point of methane



(a)



(b)



(c)

Figure A1. Position error of blowout limits methane: d 10 mm(a); d 15 mm (b), d 20 mm (c).

As indicated above, each test for the evaluation of flame extinction was repeated three times for each point. In the graphs of Figure A1, the Matlab command 'errorbar' indicates the position error of each point. There are no particular differences when the diameter of the outlet section of the fuel nozzle varies, but the error is greater for small air flows, i.e. when the air jet is in the laminar regime (L) or in a turbulent regime (TU) that is not fully developed. In zone A there is an average error of 0.7 m/s on the speed of the transverse air jet, while for zone B there is 0.3 m/s and for zone C 0.2 m/s. The graphs show the data for $z=0$, $z=2$, and $z=4$. In order not to make the diagram too heavy, no further points have been added, also because no particular connection between the evaluation error and the distance z has been noted.

APPENDIX 2. Display of the error of each blowout point of propane

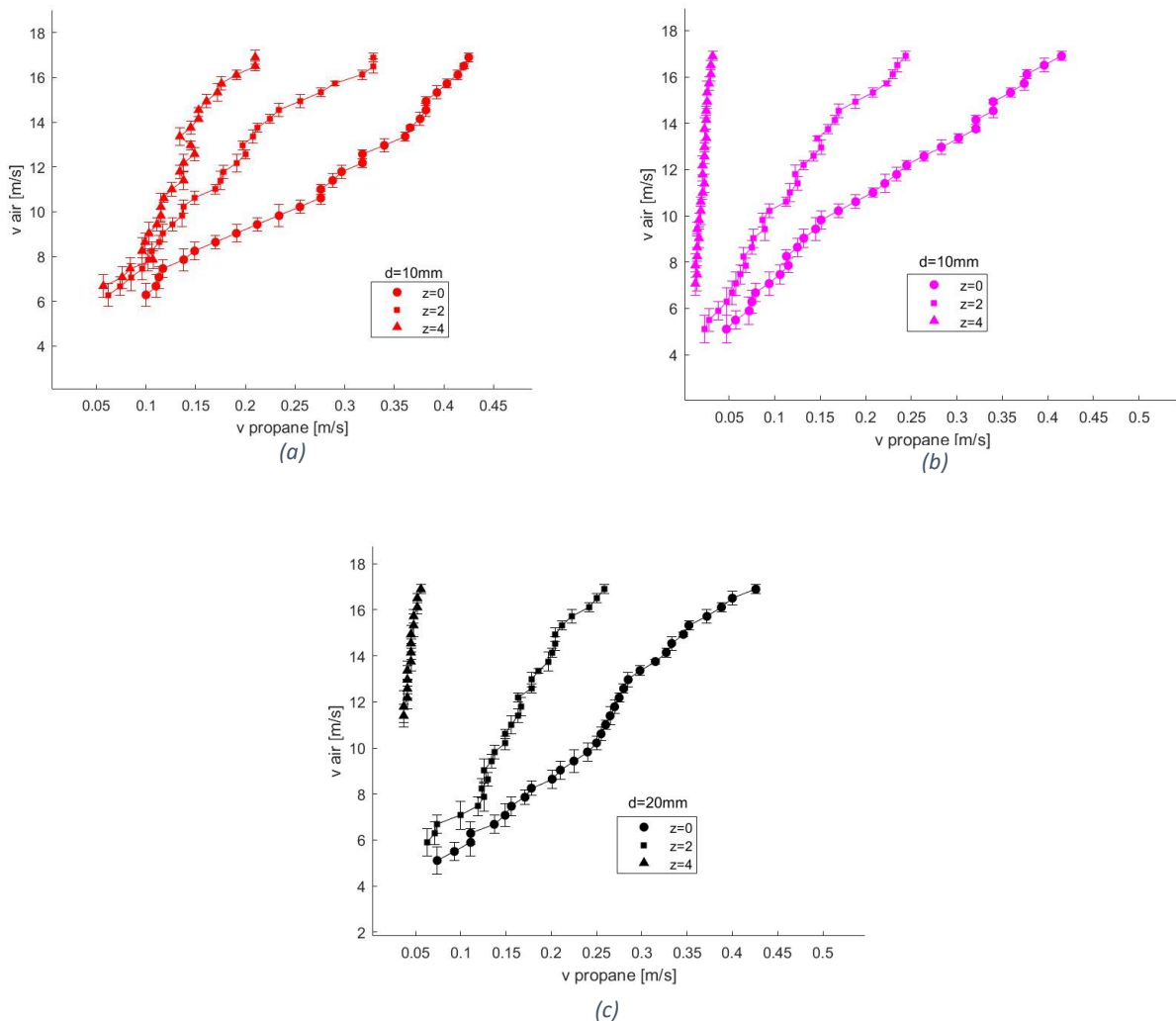


Figure A2. Position error of blowout limits propane: d 10 mm(a); d 15 mm (b), d 20 mm (c).

As with methane, the position error is reported for propane blowout limits. It is immediately apparent that the error is slightly lower than for methane, as will be discussed in the next section propane is more stable to the cross air-jet and therefore the blowout limit evaluation is more repetitive. The absolute errors shown in Figure A2 are independent of the height of the air nozzle, but even here a lower error is noted when there is a turbulent transverse air jet. The average errors are: 0.6 m/s air for zone A, 0.2 m/s for zone B and 0.2 m/s for zone C. This is one more reason why zone A was not evaluated.

REFERENCES

- [1] I. Glassman e R. A. Yetter, *Combustion*, Elsevier, 2008.
- [2] A Linan, and F. A. Williams, “Fundamental Aspects of Combustion” Oxford University Press, Oxford, 1995.
- [3] A. J. Majeski, “Size and Shape of Low Momentum Jet Diffusion Flames in Cross Blow”, Edmonton, Alberta, 2000
- [4] Q. Wanga, L. Hua, S. H. Yoon, S. Lua, M. Delichatsios, S. Ho Chung, “Blow-out limits of non-premixed turbulent jet flames in a cross-flow at atmospheric and sub-atmospheric pressures”, *Combustion and Flame*, Volume 162, Issue 10, Pages 3562-3568, October 2015.
- [5] B. Rengel, A. Palacios, “Analysis of experimental blowout velocities of jet flames”, *Combustion and Flame*, Volume 213, Pages 237-239, March 2020.
- [6] J. Fang, C. Jiang, J. Wang, J. Guan, Y. Zhang, “Oscillation frequency of buoyant diffusion flame in cross-wind”, *Fuel*, Volume 184, Pages 856-863, 15 November 2016.
- [7] C. Liu, L. Huang, T. Deng, S. Zhou, X. Liu, J. Deng, Z. Luo, “On the influence of nozzle geometry on jet diffusion flames under cross-wind”, *Fuel*, Volume 263, 116549, 1 March 2020.
- [8] C. Liu, L. Huang, T. Deng, H. Jiang, P. Wu, B. Liu, J. Deng, Z. Luo, “Influence of bottom wall on characteristics of jet diffusion flames under cross-wind”, *Fuel*, Volume 288, 119661, 15 March 2021.
- [9] L. Bernard; E. Guenther von, *Combustion, ‘Flames and Explosions of Gases’*, Elsevier, 2012.
- [10] P. Norbert, ‘Turbulent combustion’, Cambridge University, 2000.
- [11] M. R. Johnson, L. W. Kostiuik, “Efficiencies of Low-Momentum Jet Diffusion Flames in Crosswinds”, Canada, 2000.
- [12] Ann R. Karagozian, “Transverse jets and their control”, *Progress in Energy and Combustion Science* 36 531–553, 2010.
- [13] Huang, R. F., Chang, “The stability and visualized flame and flow structures of a combusting jet in the crossflow”, *Combustion and Flame*, 98(3), 267- 278, 1994.
- [14] Vanquickenborne, L., and van Tigglen, A., *Combust. Flame* 10:59-69, 1966.
- [15] Broadwell, J. E., Dahm, W. J. A., and Mungal, M. G., Twentieth Symposium (International) on Combustion, The Combustion Institute, Pittsburgh, p. 303, 1984.
- [16] Broadwell JE, Dahm WJA, Mungal MG. *Proc Combust Inst* 20:303–10, 1984.
- [17] Kalghatgi GT. *Combustion Science Technology*, 26:233–9, 1981.
- [18] M. R. Johnson, D. J. Wilson, L. W. Kostiuik, “A fuel stripping mechanism for wake-stabilized jet diffusion flames in crossflow”, *Combustion Science and Technology*, 169(1):155-174, 2001.

- [19] A computational study of turbulent non-premixed methane jet flames in a cross-wind, G. Chamberlain, D. Bradley, P. H. Gaskell, X. J. Gu, and D. R. Emerson, Shell Global Solutions, UK, 2009.
- [20] EL-FLOW® Select Series Thermal Mass Flow Meters and Controllers, Instruction Manual, Bronkhorst®, Doc. no.: 9.17.099 rev. I, Date: 09-11-2020.
- [21] <https://www.digitus.info/en/products/computer-and-office-accessories/computer-accessories/usb-components-and-accessories/interface-adapter/da-70155-1/>
- [22] González Marrero F. E., “Diseño, montaje y puesta a punto de dispositivos experimentales para procesos de combustión”, Escuela técnica superior de ingenieros industriales, Malaga, 2012.
- [23] Gutkowski A. N., Parra-Santos T., ‘Quenching Distance and Quenching Diameter Ratio for Flames Propagating In Propane/Air Mixtures’, Proceedings of the International Conference on Heat Transfer and Fluid Flow, Prague, 2014.
- [24] S. Muppidi, K. Mahesh, J. ‘Study of trajectories of jets in crossflow using direct numerical simulations’, Fluid Mech. 530, 81–100, 2005.
- [25] E.F. Hasselbrink Jr., M.G. Mungal, J. ‘Transverse jets and jet flames. Part 1. Scaling laws for strong transverse jets’ Fluid Mech. 443, 1–25, 2001.
- [26] C.J. Montgomery, C.R. Kaplan, E.S. Oran, ‘The effect of coflow velocity on a lifted methane-air jet diffusion flame’, Proc. Combust. Inst. 27 (1), 1175–1182, 1998.
- [27] E.F. Hasselbrink Jr., M.G. Mungal, J. ‘Lifted flames in laminar jets of propane in coflow air’, Fluid Mech. 443, 27–68, 2001.
- [28] B.J. McCaffrey, Flame height, in: P.J. DiNenno (Ed.), SFPE Handbook of Fire Protection Engineering, pp. 298–305, 1988.
- [29] D. Bradley, P.H. Gaskell, X. Gu, A. ‘Palacios, Jet flame heights, lift-off distances, and mean flame surface density for extensive ranges of fuels and flow rates’, Combust. Flame 164, 400–409, 2016.